UNIVERSITÀ
DEGLI STUDI
DI PADOVA

Dipartimento di Tecnica e Gestione dei Sistemi Industriali

Corso di Laurea Magistrale in Ingegneria Gestionale

Tesi di Laurea

Wear tests on Metal Matrix Composites for applications in Electric Vehicles

A sustainability analysis of the change from cast iron to aluminium metal matrix composites brake discs.

Relatore
Prof. Franco Bonollo

Correlatore
Prof. Anders W. Jarfors

Laureando
Riccardo Paccagnella

2022/2023

Questa tesi ha come obiettivo studiare il comportamento a usura di diversi tipi di materiale impiegati per la costruzione dei freni a disco per le auto elettriche. I materiali a disposizione sono una ghisa grigia (GCI), un aluminum metal matrix composite (AMMC) composto da una matrice ipoeutetica di alluminio (Al) e silicio (Si) e rinforzata con particelle di carburo di silicio (SiC) denominato successivamente AMMC1, e un AMMC, denominato successivamente AMMC2, che presenta le stesse caratteristiche dell'AMMC1 ma con una matrice composta interamente da Al ririclato. Il primo materiale analizzato è una ghisa lamellare con la grafite che assume una forma allungata senza una direzione preferenziale di sviluppo. La percentuale di grafite sulla superficie è dell'8,74%. È presente una struttura interamente perlitica composta da lamelle alternate di ferrite e cementite. La presenza di elementi come Cu, Ni, Mn, Sn favoriscono la formazione di perlite, in quanto elementi perlitizzanti. Per AMMC1 e AMMC2, è stata calcolata la percentuale di rinforzo di SiC sulla superficie dei due materiali con il software LAS X acquisendo un totale di 25 immagini. Nel primo caso, si è ottenuta una percentuale del 20,95 % e nel secondo caso una percentuale di circa il 22,28 % calcolata su diversi punti del materiale. Anche la dimensione media delle particelle del rinforzo è stata calcolata nei due casi con lo stesso software per avere una visione più generale. Per AMMC1 c'è una dimensione media delle particelle di SiC di 8,56 μm mentre per AMMC2 c'è una distribuzione di circa 10 μm. Sono state contate un totale di 490 particelle per eseguire la media. La matrice in entrambi i casi è una lega ipoeutetica di Al-Si composta 9 wt.% Si, 0,15 wt.% titanio (Ti) and 0,6 wt.% magnesio (Mg).

L'obiettivo di questo lavoro di tesi è capire quale materiale è il più adatto ad essere utilizzato per la produzione di freni a disco. L'impianto frenante è uno dei sistemi fondamentali dell'automobile e svolge diverse funzioni, tra cui le più importanti sono la riduzione della velocità durante la marcia, l'arresto completo del veicolo, il mantenimento del veicolo fermo quando desiderato e la prevenzione di accelerazioni indesiderate. Il sistema frenante è composto da diversi elementi, ma in questo lavoro di tesi verrà trattata solo la parte riguardante i dischi freno. I dischi freno per il settore automobilistico sono prodotti tipicamente in ghisa grigia (GCI). La ghisa grigia viene utilizzata perché può offrire molte proprietà utili per il sistema frenante tra cui una discreta conducibilità termica (40 W/mK a 70 W/mK a temperatura ambiente) buona resistenza all'usura, bassi costi di produzione, si adatta bene alla produzione di massa, ha una buona capacità di smorzare le vibrazioni e una buona colabilità. Queste proprietà soddisfano i requisiti dei freni a disco; questi ultimi devono mantenere temperature elevate per un lungo periodo, devono avere una buona resistenza all'usura e un'eccellente capacità di trasferimento del calore. Inoltre, i freni a disco devono avere

bassi costi di produzione, in modo da poter essere utilizzati per la produzione di massa e richiedono anche buone proprietà di riduzione delle vibrazioni e del suono. Questo permette di capire perché il GCI è un materiale che soddisfa i requisiti per la produzione di freni a disco. D'altra parte, la ghisa grigia nasconde diversi problemi in termini di durata e di emissioni. La ghisa grigia ha una bassa resistenza alla corrosione, essenziale per un sistema frenante; un'alta densità (7,83 g/cm^3) che può portare a un aumento complessivo del peso dell'auto con conseguente aumento del consumo di carburante e una bassa conducibilità termica se confrontata con altri elementi come Al o il rame (Cu) (237 W/mK per Al e 395 W/mKper Cu). Un altro probelma da affrontare riguarda la creazione di polveri sottili durante la frenata. Più la resistenza all'usura del materiale è bassa, più polvere sottili vengono generate e immesse nell'atmosfera. La ricerca di materiali innovativi quindi è volta al ridurre i problemi creati dall'impiego del GCI. Un fenomeno che si sta sviluppando negli ultimi anni è quello delle auto elettriche; si stima infatti che nel 2030 le auto elettriche copriranno una percentuale che va dal 11 al 63 %, arrivando al 2050 in cui si stima che quasi la totalità delle auto sarà elettriche. Da queste analisi è possibile affermare che è un fenomeno irreversibile che deve essere analizzato da un punto di vista ingegneristico. Le auto elettriche sono dotate di un sistema di frenata leggermente diverso, chiamato sistema rigenerativo. Questo sistema consente di immagazzinare l'energia della frenata e di utilizzarla per caricare la batteria. Quando si guida un veicolo con questo tipo di sistema e si preme l'acceleratore, il motore elettrico assorbe l'energia dalla batteria per far girare le ruote, creando l'energia cinetica necessaria per muoversi. Tuttavia, quando si frena, il processo passa alla modalità inversa. L'energia cinetica utilizzata inizialmente per spingere il veicolo fa girare il motore elettrico nella direzione opposta, trasformandolo in un generatore. Poiché il recupero dell'energia di frenata converte l'energia cinetica del veicolo in elettricità, è anche in grado di rallentare il veicolo, proprio come fanno i freni idraulici con l'attrito. Nella maggior parte dei casi, il generatore elettrico fornisce una potenza di frenata sufficiente a rallentare il veicolo. Tuttavia, quando si viaggia a velocità molto elevate o molto basse, quando la batteria è completamente carica o il motore elettrico da solo non è in grado di fornire una frenata sufficiente, sarà necessario il supporto di un sistema frenante idraulico. Il sistema idraulico viene quindi utilizzato meno e questo potrebbe sembrare un vantaggio, ma purtroppo nasconde alcuni problemi. Uno dei problemi principali riguarda la corrosione; essendo utilizzati meno, i freni a disco possono soffrire di problemi di corrosione e sporcizia, peggiorando le prestazioni del disco, dei cuscinetti e della frenata in generale. Un altro problema è il peso di questo sistema, molto influente a causa della batteria, ed è quindi necessario trovare un modo per risparmiare peso. È

quindi essenziale trovare un materiale che possa offrire almeno le stesse prestazioni del GCI, ma che allo stesso tempo sia leggero e resistente alla corrosione a causa dei problemi riscontrati con il sistema rigenerativo. Una soluzione è stata trovata nell'utlizzo degli Aluminium Metal Matrix Composites (AMMC). Il motivo del loro utilizzo rispetto ai materiali tradizionali è che migliorano le proprietà dei materiali di base e sono applicabili in molte situazioni. Gli AMMC si trovano in molti settori di mercato, ad esempio quello aerospaziale, del trasporto ferroviario, dell'imballaggio e automobilistico. Il costituente presente in maggiore quantità e in forma continua è chiamato matrice (Al in questo caso) e in genere, è l'elemento che compone la matrice che deve essere rinforzato. Questi materiali offrono delle caratteristiche che combinano le proprietà delle leghe di aluminio, come bassa densità (2,7 g/cm^3), un'elevata conducibilità termica, la riciclabilità con le proprietà apportate andando a rafforzare quelli che sono i punti deboli del materiale, legati alla bassa temperatura di fusione, alla fatica e all'usura, che possono essere superati rinforzando la matrice. In questo lavoro di tesi si useranno delle particelle di carburo di silicio (SiC) come rinforzo per la matrice ipoetutica di Al-Si.

Per studiare la forza di attrito (F_f) e in particolare il coefficiente di attrito (COF) in modo più dettagliato tra le pastiglie dei freni e il rotore, è ricorrente l'uso di un particolare tipo di test chiamato test di usura Pin-on-Plate (PoP) o Pin-on-Disc (PoD). In questa tesi si è usata la configurazione PoP. La prova di usura PoP è un metodo sperimentale ampiamente utilizzato per valutare le proprietà di attrito e usura dei materiali in condizioni di contatto strisciante. In questa prova, un provino a forma di cilindro viene premuto contro una piastra applicando un carico normale. Il movimento relativo tra il cilindro e la piastra genera forze di attrito e induce l'usura sulle superfici a contatto. In questo lavoro di tesi, le prove PoP sono state condotte a temperatura ambiente per una durata complessiva di un'ora. La velocità di scorrimento è rimasta costante durante tutte le prove ed è stata fissata a 0,05 m/s, mentre il carico è stato fatto variare utilizzando prima un carico di 108 N e successivamente un carico di 50 N. Sono state eseguite delle operazioni preliminari prima di eseguire i test di usura con una configurazione Pin on Plate. È stata utilizzata una macchina, chiamata Tegramin 30, per ottenere circa la stessa rugosità superficiale su tutti i campioni, in modo da poter eseguire il test di usura con le stesse condizioni iniziali. È stato utilizzato successivamente il microscopio ottico Olympus per indagare la rugosità superficiale espressa dal parametro Sa. In particolare, sono stati presi almeno tre valori in posizioni casuali per verificare se la rugosità superficiale fosse uniforme su tutta la superficie del campione. Una volta verificato che la distribuzione di questi valori fosse simile, senza variazioni particolarmente elevate, i campioni in questione sono stati pesati. Sono state

effettuate cinque misurazioni per ottenere un risultato il più preciso possibile e poi è stata eseguita la media aritmetica. Dopo aver eseguito il test di usura sui campioni ritenuti necessari, sono stati nuovamente raccolti i dati relativi al peso e alla rugosità superficiale per confrontare la situazione del test pre usura con quella del test post usura. È stato misurato anche un altro parametro che esprime la rugosità, ovvero il parametro Ra. Questo parametro, a differenza di quello precedente, esprime la rugosità lungo un profilo rettilineo e non su una superficie. Come si vedrà in seguito, per il caso del GCI è stata misurata anche la superficie asportata per ciascuno dei profili di rugosità, evidenziando le perdite di materiale.

Sono state eseguite 3 configurazioni tramite metodologia PoP. La configurazione 1 ha come input un carico di 108 N con una pressione di contatto di 2 MPa, eseguita a temperatura ambiente. Il pin cilindrico è costituito da un materiale per fare le pastiglie dei freni denominato Brake Pad (BP) mentre per la piastra sono stati utilizzati due materiali, GCI e AMMC1. La seconda prova, denominata configurazione 2, utilizza gli stessi input e materiali della precedente, l'unico elemento che è variato è il carico applicato. In questo caso, è stato utilizzato un carico di 50 N con una pressione di contatto relativa di 1 MPa. Lo scopo di questa configurazione era analizzare il coefficiente di attrito in funzione di una variazione del carico. L'ultima configurazione, chiamata configurazione 3, prevede un carico di 108 N e una pressione di contatto di 2 MPa. A cambiare sono i materiali utilizzati per i pin e le piastre. In particolare, la piastra è composta da BP, mentre i pin sono composti rispettivamente da GCI, AMMC1 e AMMC2. Lo scopo di questo test era quello di tracciare il COF anche per l'AMMC2 e confrontarlo con gli altri materiali utilizzati in precedenza. Una volta ottenuti i dati sulla forza di attrito per ogni prova, il COF è stata calcolato dividendo la forza di attrito per la forza peso applicata. I dati del COF, messi in valori assoluto, sono stati poi rapportati al tempo di prova in secondi. Inoltre, per ogni prova è stato calcolato un COF medio, calcolando la media aritmetica di tutti i valori raccolti durante la prova. Oltre al valore medio, è stato riportato anche il valore massimo assunto dal COF per ogni configurazione. Questo per fornire un'analisi più completa. È stato inoltre calcolato il tasso di usura specifico (K). I campioni utilizzati per le prove vengono direttamente dai freni a disco prodotti dall'azienda AC Floby.

È stata eseguita inoltre un'analisi di sostenibilità utilizzando la funzione Eco-Audit del software Ansys Granta. Lo scopo di questa analisi è quello di valutare l'energia utilizzata e la CO_2 prodotta per la costruzione di freni a disco successivamente montati su un'auto elettrica. Sono state analizzate tutte le fasi del ciclo di vita del prodotto utilizzando come materiali il GCI, AMMC1 e AMMC2. L'azienda AC Floby sostiene che la durata dei freni a disco in AMMC1 e AMMC2 sia tre volte superiore rispetto a quella

dei freni in GCI, per questo motivo, al fine di condurre un'analisi comparativa, è stata impostata una vita utile dei freni a disco in AMMC1 e AMMC2 di 1/3 rispetto a quella del GCI nella fase di utilizzo. Sono stati fatti variare anche alcuni parametri come: chilometri percorsi al giorno, giorni di utilizzo all'anno e paese di utilizzo.
Passando all'analisi dei risultati, i parametri di rugosità Ra e Sa sono stati rilevati prima e dopo la prova e messi a confronto. Nella configurazione 1, nel caso del GCI usato come piattino, sia per i parametri Ra ed Sa non è avvenuto alcun cambiamento nella rugosità nel campione (il valore di Sa è passato da 0,259 μm a 0,247 μm). Al contrario, nel caso dell'AMMC1 entrambi questi parametri risultano essere più che dimezzati (si è passati da un valore di Sa di 0,401 μm a un valore di 0,183 μm). Si è deciso di calcolare inoltre la superficie asportata nel caso del GCI, perché come si vedrà in seguito, ci sono state delle perdite in peso. Si può notare come la maggiore asportazione sia avvenuta al centro del campione (13828 μm^2) mentre ai bordi del campione l'asportazione di materiale risulta minore (6575 μm^2). Non è stata rimossa superficie nel caso del AMMC1. Le perdite in peso del GCI sono di almeno un ordine di grandezza superiore di quelle dell'AMMC1 (0,00312 g per il GCI e 0,00004 g per AMMC1). Nel caso del GCI, il pin in BP ha scavato nel materiale, andando a rimuovere superficie e creando più perdite in peso. Nel caso del AMMC1 invece il pin in BP ha ridotto le creste di rugosità. La configurazione 2 prevede sempre l'utilizzo del GCI e dell' AMMC1 come piattini e il BP come pin, soltanto che in questa configurazione il carico applicato è di 50 N con una relativa pressione di contatto di un 1 MPa. Sono state eseguite le stesse analisi precedentemente effetuate al fine di confrontare i materiali. Nel caso del GCI, al contrario della configurazione precedente, entrambi i parametri di rugosità si sono ridotti notevolmente (da 0,47 μm a 0,046 μm per il parametro Sa). Nel caso invece dell'AMMC1, è presente lo stesso risultato ottenuto precedentemente; la rugosità risulta essere dimezzata. In entrambi i casi non c'è stata asportazione superficiale di materiale. Riducendo il carico nel caso del GCI, le perdite in peso si sono ridotte di un ordine di grandezza. Questo è confermato dal fatto che non c'è stata asportazione di materiale e che non si sono collezionati detriti. Per quanto riguarda AMMC1, diminuendo il carico da 108 a 50 N le perdite in peso sono aumentate di un ordine di grandezza rispetto alla configurazione precedente. Nella Configurazione 3 è stato applicato un carico di 108 N esattamente come nella Configurazione 1. Ora, però, i materiali di cui sono fatti i piattini e i pin sono invertiti. Per i piatti si usa il BP, mentre per i pin si usano AMMC1, AMMC2 e GCI. La rugosità del GCI si è rimasta invariata, mentre per AMMC1 la rugosità si è più che dimezzata. Entrambi questi risultati confermano i risultati ottenuti con la Configurazione 1. AMMC2 presenta lo stesso comportamento dell'AMMC1, la rugosità risulta essere dimezzata anche in questo caso

(da 1,303 μm a 0,727 μm per Sa). Si può notare, esattamente come nella Configurazione 1, le perdire in peso del GCI risultino essere un ordine di grandezza superiore rispetto a quelle dell'AMMC1. AMMC2 risulta avere le perdite in peso più ridotte all'interno della Configurazione 3 (0,00002 g), rimanendo però all'interno dello stesso ordine di grandezza dell' AMMC1 (0,00006 g). Non si riscontrano quindi particolari differenze tra AMMC1 e AMMC2 in termini di rugosità e perdite in peso. Entrambi i materiali risultano essere migliori del GCI, in particolar modo per la prova a 108 N.

Il COF dell'AMMC1 risulta essere inferiore rispetto a quello del GCI sia per le prove a 50 N che per le prove a 108 N. In particolare per la configurazione 1 il COF del GCI risulta essere 0,15 mentre quello dell'AMMC1 risulta essere 0,11. La forza di attrito che viene esercitata sul GCI risulta essere quindi superiore rispetto a quella dell'AMMC1. Il tasso di usura specifico, che quantifica l'usura del materiale, risulta essere due ordini di grandezza inferiore per AMMC1 (8,84 E^{-7}) rispetto al GCI (2,73 E^{-5}) per la prova a 108 N. Questa differenza si riduce abbassando il carico. Per quanto riguarda AMMC2, sia per il COF che per il tasso di usura specifico, non si notano particolari differenze rispettto all'AMMC1, confermando così che la matrice composta da materiale riciclato non presenta caratteristiche all'usura inferiori rispetto a una matrice non riciclata. L'analisi è proseguita analizzando il tipo di usura che si è verificata durante i test nei diversi materiali. A tal fine, è stato utilizzato il microscopio SEM per rilevare le tracce di usura e il software Pathfinder per comprendere la composizione chimica di un eventuale trasferimento di materiale tra pin e piatti. Tutte le prove effettuate precedentemente sono state condotte in regimi di usura mite. Nonostante i carichi elevati che potrebbero portare a un'usura di tipo severo, la bassa velocità di scorrimento vincola l'usura a un regime mite.

Partendo con la configurazione 1 e analizzando la composizione chimica della superficie usurata del GCI, è possibile rilevare una forte presenza di O che non era presente prima del test. Ciò porta ad affermare che l'ossidazione ha giocato un ruolo importante durante il processo di usura. Questo processo porta alla formazione di uno strato di ossido sulla superficie dei provini. Come analizzato in precedenza, si è verificata un'asportazione di materiale sulla superficie e una perdita di peso. Questi indicatori fanno pensare a un'usura di tipo abrasivo. Le scaglie di grafite sulla matrice potrebbero aver causato un'usura abrasiva a corpo unico. Anche la presenza di scanalature parallele, è un indicatore della presenza di microtagli tipici dell'usura abrasiva. Un tipico meccanismo di usura presente negli AMMC in condizioni di regime mite è l'usura da delaminazione. Questo meccanismo è spesso presente, soprattutto in condizioni di rotolamento o scorrimento dei corpi a contatto. Dopo ripetuti carichi ciclici, si osserva una cricca sulla sottosuperficie. Le cricche sottosuperficiali si

propagano, si collegano con altre cricche, raggiungono la superficie e generano particelle di usura. La presenza di sole cricche però non è un fattore sufficiente per poter parlare di usura per delaminazione. La presenza di scanalature parallele porta all'assunzione che si sia verificata un'usura di tipo abrasivo. Entrambi i tipi di meccanismi sono tra i possibili tipi di usura per un AMMC1 in condizioni di regime di usura mite.

Nella configurazione 2 si notano gli stessi meccanismi di usura sia per GCI che per AMMC1, soltano in maniera meno accentuata. Le dimensioni della cricche per AMMC1 nella prove a 50 N sembrano essere più piccole di quelle ottenute con il carico di 108 N. Si è quindi verificato lo stesso tipo di usura, con la formazione di cricche sulla superficie usurata, solo che queste appaiono di dimensioni minori rispetto alla configurazione precedente.

Nel caso dell'AMMC2 per un carico di 108 N, si è verificata un'usura diversa. Il materiale sulla traccia di usura risultava essere spalmato. Questo potrebbe essere dovuto alla diversa configurazione. In tutte le configurazioni a 108 N è avvenuto trasferimento di materiale da il BP a GCI, AMMC1 e AMMC2. In particolare sulle tracce di usura si possono riscontrare elementi tipici del BP come il bario (Ba) il calcio (Ca), rilevate con il software Pathfinder. Diminuendo il carico a 50 N invece, le tracce di usura sono prive di questi elementi, lasciando intendere che non è avvenuto alcun tipo di trasferimento di materiale. Solo per le prove a 108 N sono stati raccolti e analizzati i detriti rilasciati dopo la prova. I detriti nel caso del GCI sono composti da elementi provenienti sia dal GCI come carbonio (C) e ferro (Fe), ma anche da elementi provenienti dal BP come Ba, Ca e zolfo (S). Nel caso dell'AMMC1 invece i detriti sono composti da elementi provenienti solo dal BP. Con il GCI quindi, c'è stato un consumo reciproco sia da parte del piattino che da parte del pin, nel caso dell'AMMC1 invece, si è consumato solo il BP lasciando intatta la superficie del piattino. Questo è confermato anche dal fatto che le perdite in peso dell'AMMC sono praticamente nulle.

Per ogni fase del ciclo di vita del prodotto riguardante l'analisi di sostenibilità si riportano l'energia consumata (MJ) e le emissioni generate (kg). L'energia utilizzata per la fase di estrazione del materiale risulta essere superiore per AMMC1 (2779 MJ) rispetto a quella del GCI (1130 MJ). Questo risultato è dovuto al fatto che il processo di produzione dell'alluminio è più dispendioso in termini energetici rispetto a quello del GCI. Grazie alla matrice interamente riciclato di aluminio, l'AMMC2 è più conveniente in termini energetici (555 MJ) rispetto all'AMMC1. È stata fissata una percentuale di riciclaggio dell'80%, che costituisce la parte della matrice di alluminio. Il restante 20% è costituito dal rinforzo in SiC. Lo stesso ragionamento può essere applicato anche al consumo di CO_2. La differenza tra GCI e AMMC1 e AMMC2 è ancora più marcata nella

fase di utilizzo. In questa fase sono stati variati parametri come il paese di utilizzo e i chilometri percorsi durante l'anno con un'auto elettrica di medie dimensioni. Si può notare che il GCI è il più svantaggiato in termini di energia consumata (21100 MJ in Europa), evidenziando ancora una volta i vantaggi di AMMC1 e AMMC2 (2100 MJ in Europa). Anche per l'analisi di sostenibilità, AMMC1 e AMMC2 sono i materiali più adatti per la produzione di freni a disco. Le analisi hanno dimostrato che AMMC1 è vantaggioso rispetto a GCI solo per la fase di utilizzo. AMMC2, invece, è adatto in termini di sostenibilità sia nella fase di utilizzo che in quella di estrazione del materiale, grazie alla sua matrice a base di alluminio completamente riciclato. L'AMMC2 si dimostra quindi il più adatto alla produzione di freni in termini di impatto ambientale. In conclusione, AMMC1 risulta più adatto per la produzione dei freni a disco rispetto al GCI sia per quanto riguarda i test tribologici, sia per quanto riguarda l'analisi di sostenibilità. Dall'altra parte però, AMMC2 risulta essere ancora più conveniente per quanto riguarda l'analisi di sostenibilità grazie alla matrice interamente riciclata e non presenta caratteristiche tribologiche particolarmente diverse rispetto all'AMMC1. L'utilizzare una matrice interamente riciclata, non porta ad avere caratteristiche tribologiche peggiori rispetto a una matrice non riciclata.

Abstract

According to the forecasts, the demand for electric vehicles and aluminium (Al) alloys is increasing rapidly. Lightweight design is searching for lightweight materials that can offer at the same time durability, strength, and corrosion protection, and aluminium metal matrix composites (AMMC) can offer the right combination of these aspects. The new Euro 7 regulations will enter into force from the first of July 2025. They will cover the non-exhaust pollution coming from wheels and brake discs, in addition to the exhaust pollution, also for electric vehicles. For these reasons it is fundamental to find a material that can be sustainable for mass production like the one for electric vehicles, but at the same time excellent for mechanical and thermal properties. This master thesis work focuses on automotive brake discs of passenger vehicles, in particular, the thesis covers a sustainability study from grey cast iron (GCI) to AMMC with secondary Al matrix brake discs. Wear tests were conducted using a Pin-on Plate configuration with a linear speed of 50 mm/s, a duration of 1 h, and a variable load of 108 N and 50 N at room temperature. The materials used in the tests were GCI, a grey cast iron with pearlitic structure, AMMC1 and AMMC2, both with a matrix consisting of a hypoeutectic Al-Si alloy composed of 9 wt.% silicon (Si), 0.15 wt.% titanium (Ti) and 0.6 wt.% magnesium (Mg) and reinforced with silicon carbide (SiC) particles. AMMC2, unlike AMMC1, features a matrix composed entirely of recycled Al. The GCI has a graphite percentage of 8,74%, while the SiC percentages for the AMMC1 and AMMC2 are 20,95 % and 22,28 % respectively. The SiC particle sizes in terms of equivalent diameter are 8,56 μm for the former and 10 μm for the latter. The aim is to compare the roughness, weight loss, wear type, material transfer, and coefficient of friction (COF) before and after the tests to understand which material is more suitable to be used in the construction of disc brakes. The materials provided for wear tests were supplied by the company AC Floby, claiming that the product life of AMMC1 disc brakes is three times longer than that of ordinary GCI disc brakes. An LCA analysis was also conducted using the eco-audit function of the Ansys Granta software to show the differences between the materials in terms of energy consumed and CO2 emitted. All phases of the product life cycle were analyzed using the disc brake as the functional unit. The wear tests showed that AMMC1 exhibits lower weight loss than GCI, and the wear rate is smaller for AMMC1 than for GCI. The behavior of AMMC2 was very similar to that of AMMC1, emphasizing the fact that the recycled aluminium matrix did not negatively affect the wear tests. Regarding to LCA study, the most critical phases in terms of energy consumed and CO_2 produced were the material extraction and the use

phase. AMMC1 was found to be acceptable only in the use phase compared to GCI, while AMMC2 due to both its longer product life and high recycling content was found to be the most suitable for the production of disc brakes.

Keywords

Aluminium metal matrix composites, cast iron, LCA, brake discs, electric vehicles, wear tests.

Acknowledgements

As the author of this thesis, I would like to express my sincere appreciation to my supervisors, Professor Anders W. Jarfors and Professor Franco Bonollo. I am thankful for the opportunity and support given to me during this experience at Jönköping University. Their extensive knowledge was an essential input for this thesis work.

I am extremely grateful to AC Floby, in particular to Samuel Awe for the samples and support he provided to me during the experimental part. Without his contribution, this project could not have reached its goal.

I would also like to show gratitude to Postdoctoral Researcher Lucia Lattanzi. Thanks to her teaching and dedication, I was able to do this thesis work to the best of my ability. Her contribution proved essential in carrying out the experiments.

Thanks should also go to Ph.D. student Dharmateja Chalasani for the time and efforts he dedicated to assisting me during my thesis project.

I would like to extend my sincere thanks to my family, who have always supported me during my time at university and especially during my time abroad.

Riccardo Paccagnella

Contents

1. Introduction

This project aims to evaluate aluminium metal matrix composites (AMMC) for electric vehicles' brake discs in a sustainable way. The brake system is a fundamental part of the car, and it requires a lot of parameters to work safely for people driving.
For these reasons, it is fundamental to know how the brake discs work and how they are made. The next paragraph will present the two main types of brake discs, to know what the fundamental parameters a brake system requires.
Before moving to the research question, it is important to understand why brake discs are currently made in grey cast iron (GCI) and why it is difficult, but necessary, changing course. More details on the cast iron manufacturing process can be found in the literature in Chapter 2.

1.1 The braking system

The braking system is one of the fundamental systems in the car. It performs several functions, among which the most important are reducing speed during travel, stopping the vehicle completely, keeping the vehicle stationary when desired, and preventing unwanted acceleration [1]. All this is done by transforming the car's kinetic energy into thermal energy that goes to heat the brakes. The main parts of the braking system are listed below [2]:

- Brake pedal
- Master cylinder
- Brake fluid: it is a fundamental part of the braking system. It is used to amplify the foot force a person put on the brake pedal. Without this, stopping the car by pressing one pedal would be impossible.
- Transmission fluid: Another type of fluid you cannot confront with the brake fluid. It helps to maintain lubricated the metal parts inside the gearbox.
- Pads: They use friction to convert kinetic energy into thermal energy. They are composed of many different kinds of material, the most used are steel wool, natural graphite, resin, carbon black and ceramic fiber [3]. Brake pads must not damage the disc, must resist heat and, as we will see later in Chapter 2, must also generate as little no-exhaust emissions as possible according to the new Euro 7 restrictions.
- Drum brakes or brake discs

There are two main types of brakes. The first system is the one shown in Figure 1 and consists of drum brakes. Drum brakes were the first type of brakes to come onto the market and are still used today due to their low production costs and the fact that they allow little contamination from the outside as they are sealed.

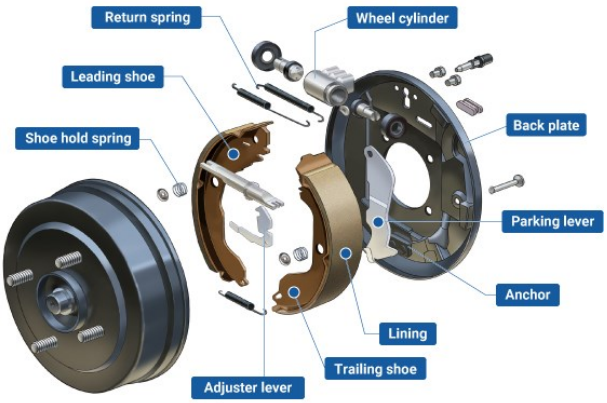

Figure 1- Components of a drum brake system [4].

Their functioning is quite simple; according to [5] a key part is played by the brake shoes, which are only found in this type of brake, and simultaneously by the wheel cylinder. The operation of car brake shoes, also called brake pads, is uncomplicated. When the brake pedal is pushed, oil pressure is applied, which activates the hydraulic cylinders that push the shoes against the side of the drum. In this way, friction is created between the shoes and the drum brakes of the wheels, then the car begins to decelerate. At the end of braking, special springs, called return springs, pull the brake shoes back to their initial position and allow the wheels to turn freely.
The second system, on which this thesis work will mainly focus, is called brake discs. In Figure 2 are visible the main parts of a brake disc system.

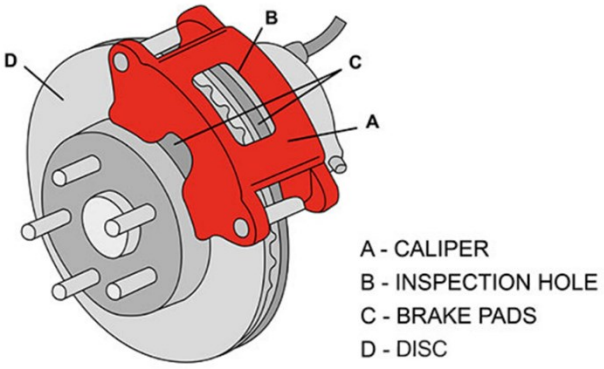

Figure 2- Components of a brake disc system [6].

The main components that make up a brake disc are [7]:

- Caliper: the caliper is an essential component in modern cars and its main function is to push the brake pads against the rotors to create friction that can stop the vehicle. This is possible due to pistons and hydraulic brake.
- Pads: As discussed before, pads can be made up of different kinds of materials, the choice of the materials depends on a lot of factors among which type of vehicle, size of the vehicle, and maximum velocity. The extreme conditions in which they work make pads one of the most sensitive parts of the brake system.
- Disc/rotor: this is the largest part in the brake disc system. As we can see in the next paragraph, the rotor is traditionally made up of CGI. The reasons behind this choice will be presented later. Due to the high temperature, heat must be dissipated as soon as possible, and for this reason, a lot of type of rotor has been created. It is possible to find different types of rotors with different characteristics, for example: slotted, drilled and vented rotors as shown in Figure 3 [8]. Starting with the slotted rotor, it has 2 or 3-mm deep slots. It was created to improve the cooling rate and the cleaning of the disc.

  Another type of disc is the drilled rotor, also called cross-drilled rotor. Each hole can create another surface area that allows a better cooling rate and heat dissipation. For this reason, it can offer better braking conditions.The last one is the vented rotors. It has channels connecting the front with the back part. These channels help to dissipate heat faster.

Figure 3 shows the three types of rotors explained before. It is also possible to find a drilled and slotted rotor that can offer excellent cooling performance.

(a) (b) (c)

Figure 3 – Examples of brake rotor: a) slotted rotor, b) drilled rotor, c) vented rotor [8].

Once, four drum brakes were fitted on all wheels, but now they have been replaced almost completely by disc brakes. There are cases where is possible to find situations with two discs in the front and two drum brakes in the back; this situation is not studied here as we will only focus on the use of four disc brakes.

There are several reasons for the replacement of drum brakes with disc brakes, in

particular the latter offer better braking performance, dissipates heat better, especially in the event of sudden or emergency braking, and finally the fact that the system is not sealed allows easy inspection of its parts in the event of wear. The disc brake is therefore more accessible for inspection. Despite the higher production costs, it remains the best solution to install in the braking system and for this reason, the entire thesis work will focus on brake discs and not drum brakes.
The next section presents the main characteristics of GCI, the most used material to produce brake discs. It also presents its proprieties and why it is an excellent material for brake discs production.

1.2 Grey cast iron brake disc

Conventionally brake discs for the automotive sector are made with GCI. Grey cast iron is an alloy of iron that contains 2 to 4 percent of carbon (C), along with varying amounts of silicon (Si) and manganese (Mn) and traces of impurities such as sulfur (S) and phosphorus (P) [9]; it is produced by reducing iron ore in a blast furnace. Grey cast iron is used because it can offer a lot of useful proprieties for the braking system. Listed below are some fundamental properties [10]:

- Good thermal conductivity: from 40 W/mK to 70 W/mK at room temperature.
- Good castability
- Good wear resistance
- Low production costs
- Easy to produce for mass production
- Fatigue resistance
- The capacity of damping vibrations

These properties meet the requirements of disc brakes in particular: they need to maintain high temperatures over a long period, they require good wear resistance, and they need excellent heat transfer capability. In addition, disc brakes must have low production costs so that they can be used for mass production, and they also require good vibration and sound reduction properties. This allows us to understand why GCI is an excellent material for producing disc brakes. On the other hand, grey cast iron hides several issues in terms of durability and emission. Grey cast iron has low corrosion resistance, which is essential for a braking system; high density, which can lead to an overall increase in the weight of the car resulting in higher fuel consumption; and finally, it generates several hazardous emissions that are no longer acceptable under European regulations. To overcome these problems, studies have been conducted on new types of materials to be used to replace GCI. To change material,

however, the fundamental characteristics of brake discs must be respected, and the change of material must also be consistent with market and demand trends.

1.3 Electric Vehicles and the regenerative braking system

The demand for electric cars is increasing and with this new type of car comes new performance parameters. In particular, the demand for low-density materials has become crucial, as they can provide a lighter solution that leads to reduce weight, which is fundamental for an Electric Vehicle's performance. Electric cars are equipped with a slightly different braking system, which is called a regenerative system. Figure 4 shows how a regenerative system works. This system allows energy to be stored from braking and used to charge the battery. While driving a vehicle with this type of system and pressing the accelerator, the electric motor absorbs energy from the battery to turn the wheels, creating the kinetic energy it needs to move. However, when you brake, the process switches to the reverse mode. The kinetic energy that was initially used to propel the vehicle turns the electric motor in the opposite direction, turning it into a generator. Instead of consuming electricity, the generator starts producing it, using the vehicle's kinetic energy. The electrical energy is then stored in a high-voltage battery (400 V). Since braking energy recovery converts the vehicle's kinetic energy into electricity, it is also able to slow it down, just as hydraulic brakes do with friction. In most cases, the electric generator will provide sufficient braking power to slow the vehicle. However, when traveling at very high or very low speeds, when the battery is fully charged or the electric motor alone cannot provide sufficient braking, will need the support of a hydraulic braking system. The hydraulic system is therefore used less and this might seem an advantage, but unfortunately, it hides some problems. One of the main problems relates to corrosion; being used less, disc brakes can suffer from corrosion and dirt problems, worsening the performance of the disc, bearings and braking in general [11]. Another problem is the weight of this system; it is very influential due to the battery, and it is, therefore, necessary to find a way to save weight. It is therefore essential to find a material that can offer at least the same performance as GCI, but at the same time is light and corrosion resistant due to the problems seen with the regenerative system.

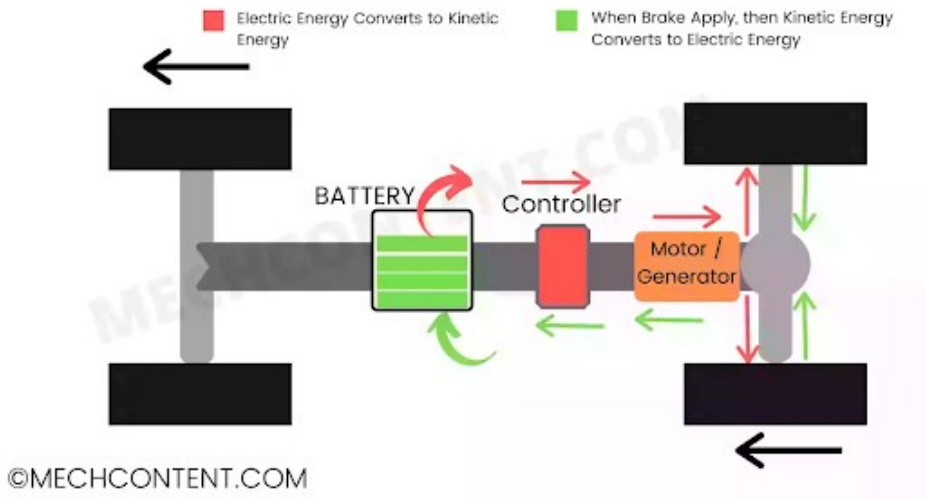

Figure 4- Regenerative system in EV [12].

One material that can be compared with these characteristics is aluminium (Al), a non-ferrous metal with a density of 2.7 g/cm^3, which is approximately one-third of cast iron having 7.83 g/cm^3 [13]. Other characteristics of aluminium alloys are:

- Good corrosion and oxidation resistance. In particular, 5000 series alloys composed of Al and magnesium (Mg) and 6000 series alloys composed of Al, Si, Mg [14].

- High thermal conductivity (237 W/mK)

- Easy to cast

- Recyclability

-High electrical conductivity (3.5*10^7 S/m)

This type of metal, when combined with other elements, can offer optimum characteristics and performance for the braking system. Some elements that can be added to aluminium can be Mn, copper (Cu), nickel (Ni), zinc (Zn) and Si. Pure aluminium, i.e., an alloy containing 99 % of Al [15] is used very little compared to other alloys; this allows us to understand how important the addition of these elements is with this metal. Figure 5 shows the main aluminium alloys as mentioned by Davis et al. [13]. In particular, the alloy that will be studied in the experimental activities is an hypoeutectic alloy with 9 wt.% of Si. The reasons behind Si are several, the main ones being:

- Pure Al has a melting temperature of 660 °C while that of Si is about 1414 °C. This means that adding Si increases the melting temperature of Al.

- Si has a lower density than Al (as shown before, Al density is 2.7 g/cm^3 Si, instead, has a density of 2.33 g/cm^3); therefore, adding Si lowers the density of the alloy.
- Increases fluidity.
- Increases hardness.

Although only 9 wt.% Si is used in this discussion, maximum Si values of around 20-22 wt.% can be achieved in practice. Going beyond these values risks having material that is too hard and brittle. An Al-Si alloy as a matrix supported by silicon carbide (SiC) reinforcement will be discussed, which, as a methodology for strengthening the matrix, increases the mechanical properties of the alloy. In Chapter 2, the aluminium production processes and AMMCs will be studied in detail to test the latter's mechanical properties. The aim, therefore, is to understand whether AMMC is a material that meets the required performance and at the same time is sustainable for mass production.

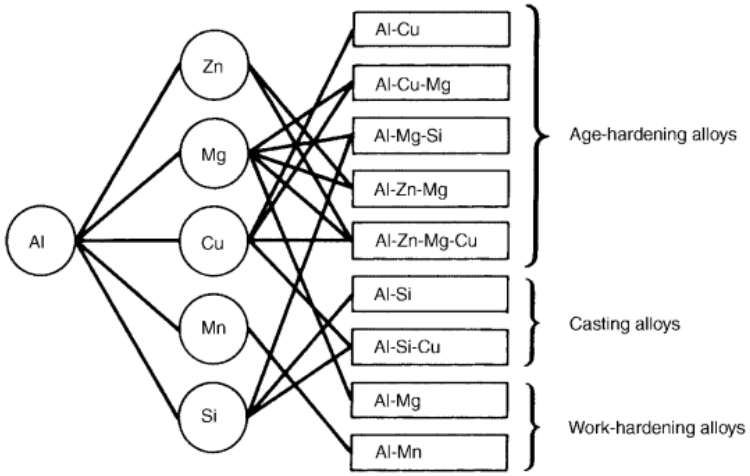

Figure 5- The main types of Al alloys [16].

2. Theoretical background

This chapter will delve into the production aspects of GCI, aluminium, and metal matrix composites (AMMC). We will then look at the wear tests performed on these materials and the type of behavior they have following the tests. However, it is necessary to start with an analysis of the trends in aluminium and electric cars, to define the type of development trajectory that these phenomena have, and to provide an overview of the market situation.

2.1 Market demand and global trends

According to [17], megatrends are the major forces of social development that are likely to influence the future in all sectors over the next 10-15 years. A megatrend is also understood to be a major social, economic, political, environmental, or technological change that forms slowly. Once in place, megatrends influence a wide range of activities, processes and perceptions, both in government and society, probably for decades. It is the underlying forces that drive the trends. Two parameters that can describe megatrends are:

- Reversibility or irreversibility: In this discussion, all trends we will analyze are irreversible. By this term, we mean changes that lead to a no longer modifiable evolution of society and the economy.
- Unclear development trajectory: Another key parameter of megatrends is the type of development trajectory. When we speak of a clear development trajectory, it means that the megatrend in question can be easily studied and analyzed with forecasts ranging from 10 to 15 years.

Now analyze the three main megatrends that are influencing the market. The first is the electrification of vehicles; in this section, we will examine the demand for medium-sized electric cars and, linked to this, also the demand for aluminium, which is in high demand for the construction of these vehicles. The second megatrend is the reduction of pollution, we will discuss Euro regulations to reduce car pollution. Finally, to conclude the trend analysis, we will talk about the circular economy.

2.1.1 Electrification

According to [18], an EV is defined as a vehicle that can be powered by an electric motor that draws electricity from a battery and is capable of being charged from an external source. An EV includes both a vehicle that can only be powered by an electric motor that draws electricity from a battery (all-electric vehicle) and a vehicle that can be powered by an electric motor that draws electricity from a battery and by an internal combustion engine (plug-in hybrid electric vehicle). This thesis aims to study the first

type of car, an all-electric vehicle. Before turning to a study of the demand for these vehicles, it is important to ask why this need is born.

Briefly, some factors that may influence the market for electric cars:

1. One of the most important factors that may influence the electric car market is the constant need to reduce air pollution from car emissions. This aspect will be explored in more detail in the next section when discussing the regulations introduced in Europe.
2. Constant population growth. This influences the size of the market in question. Linked to this is the increasing number of cars per capita, i.e. the number of cars compared to the world population.
3. Europe and China have enacted various regulations to support electric cars, including incentives.

These factors have led to an acceleration in the development of electric cars. Over the years, however, there have also been many barriers to the spread of electric cars that counteract the factors mentioned above. For example: high production costs, the lack of charging stations and high battery charging times.

Starting with historical data, it is necessary to analyze the forecasts for the spread of electric cars by 2030. In 2021 EV sales reached 6.6 million vehicles, almost ten percent of the global car market. To illustrate the great growth of this market, EV sales in 2019 were just 2.2 million [19] [20]. It should be noted that China and Europe have the largest market share, also due to the incentives that have been brought forward to drive the sector. According to [19], the penetration of EVs to total passenger car sales in 2030 forecasts ranges from 11 percent to 63 percent. Projections for 2050 range from 31 percent to nearly 100 percent. Significant changes (e.g., in government policy, technology, and cost) would be needed to reach the level of EV penetration necessary for a net zero 2050 trajectory. These predictions make it clear that the electric car phenomenon is becoming more and more widespread. As we mentioned earlier, Al can be a material that, due to its properties, can offer an overall reduction in vehicle weight and at the same time can provide corrosion resistance for disc brakes. For this reason, it is worth pausing to see how the Al market is evolving to see if the two are following the same trend.

The global aluminum market size was estimated at USD 169.8 billion in 2021 and is expected to hit around USD 277.5 billion by 2030, growing at a compound annual growth rate (CAGR) of 5.61 % from 2022 to 2030 [21]. The trend is also visible in Figure 6. So many sectors are demanding the use of aluminium, among the main ones we can find the construction, shipbuilding, automotive, packaging, and electrical sectors due to Al characteristics. Another aspect to keep in mind, is the growth of the

secondary aluminum market, that is, aluminum derived from recycling processes. We will go into more detail in the following paragraphs on how aluminium can be recycled, why it is recycled and what positive aspects it has; for the time being, it is possible to state, that this market is growing at an annual CAGR of 4.90 % [22].

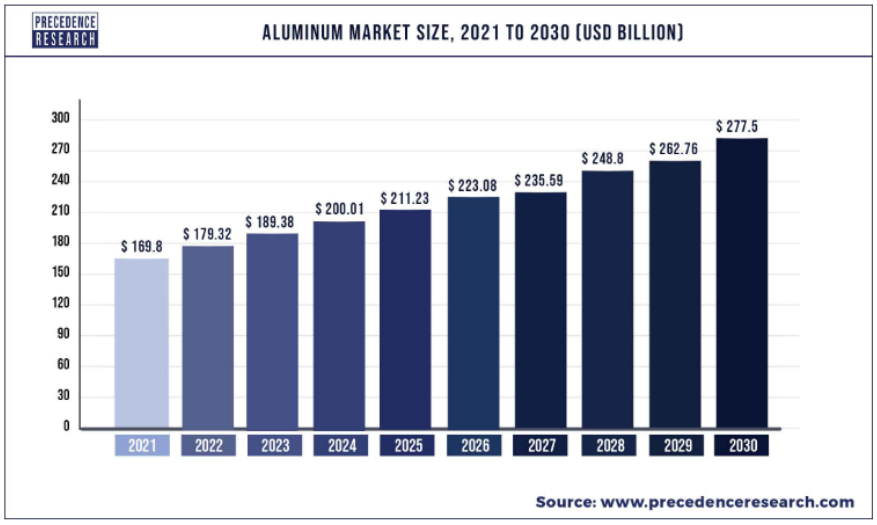

Figure 6- Aluminum market size from 2021 to 2030 [21].

2.1.2 Pollution reduction

Another trend that has become established in recent years and is now irreversible is the increased focus on car emissions. There are two types of emissions that cars can generate. The first type, perhaps the best known, is exhaust emissions. These types of emissions come from car exhausts and are the ones on which most attention is focused. To be precise, car emissions are one of the main causes of pollution in cities; however, at the same time, there is another type of emissions, the so-called non-exhausts emissions. This type of emission mainly concerns fine dust generated by wheels and disc brake pads. These also play an important role in environmental pollution, and research is studying new materials with which to reduce these emissions.

In Figure 7 according to [1] it is possible to observe the exhaust and non-exhaust emission trends from 2000 to 2014. As can be seen, exhaust emissions have fallen dramatically over the years, until reaching a point in 2012 where non-exhaust emissions exceeded the former. This trend is mainly due to European regulations imposing more and more restrictive regulations on this type of emission and to the spread of electric cars, a phenomenon already discussed above.

Especially, the Euro standard was born for this purpose. According to [23], the first European-wide standard, known as Euro 1, was only introduced in 1992, when catalytic converters became mandatory for new cars, effectively standardizing fuel injection.

Since then, a series of Euro emission standards have followed, up to the current Euro 6, introduced in September 2014 for new type approvals and introduced for most vehicle sales and registrations in September 2015. The standards, which are set to become more stringent over time, define acceptable exhaust emission limits for new light vehicles sold in EU and EEA (European Economic Area) member states.
In November 2022, The European Commission proposed a new standard for vehicle emissions called Euro 7 [24]–[26]. This, if finally approved and converted into law by the European Parliament and the European Council, will come into force on 1 July 2025 and will apply to all cars registered for the first time on or after this date; therefore, as the law is not retroactive, nothing will happen to previously registered cars. This standard type will apply to both light- and heavy-duty vehicles, but our focus will be only on light-duty vehicles. One of the main cuts concerns nitric oxide (NOx) emissions, which will have to be reduced by an additional 35 % compared to Euro 6 standards. Another key aspect concerns the reduction of polluting emissions also for brakes and tires; this applies to all types of power supply including electric cars. Brake emissions will have to be reduced to 7 mg/km and then to 3 mg/km in 2035; a total reduction of 27 % compared to the current situation. To date, no previous European legislation had ever addressed brake and tire emissions.
As a result, it is essential to have disc brakes that comply with the current rules and, above all, can remain in competition for the next European regulations. There is an emerging need to increasingly replace the GCI with something that is less polluting.

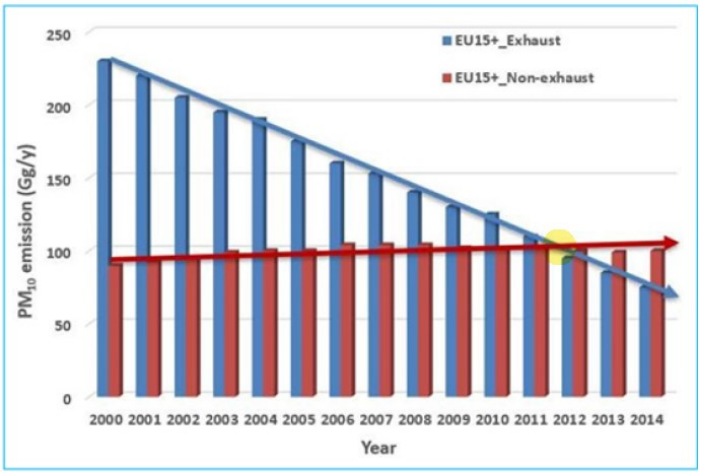

Figure 7- exhaust and non-exhaust trends from 2000 to 2014 [1].

2.1.3 Circular Economy

The last trend discussed, which is also irreversible, concerns the Circular Economy. It is defined "a production and consumption model that involves sharing, reusing, repairing, and recycling existing materials and products for as long as possible. In this

way, the life cycle of products is extended" [27]
In practice, this means minimizing waste. These can be reused productively, thus creating additional value. This is a departure from the traditional, linear economic model, which is based on the 'take, produce, consume and throw' model [28]. This model is based on large quantities of cheap and easily accessible materials and energy. Particularly, this trend is related to the previous trend of pollution, but with a view to recycling materials.
Especially, this thesis will focus on secondary aluminium, i.e. recycled aluminium, which mainly comes from the end-of-life of products. As we will see in the following paragraphs, aluminium is used in many sectors and the waste that can be collected reaches millions of tonnes per year. The possibility of using recycled material also in metallurgy makes it possible to reduce the environmental impact in terms of energy used for production, as the use of recycled material drastically reduces energy and costs. Currently many materials are recycled, and many countries are trying to exploit recycling to reduce environmental impact. Examples are steel, aluminium, titanium, magnesium, and so on. Besides purely environmental and sustainable impact reasons, there are also economic reasons behind recycling. As we will see later, aluminium is an excellent material for recycling, retaining almost all its characteristics. The recycling process is quite simple and consists only in removing the main impurities present in the material using special furnaces with specific functions.
In the following paragraphs, the LCA methodology according to the ISO standard will be explained in detail, before moving on to the actual LCA study in chapter 3 "Experiments". An attempt will be made to assess the environmental impact caused by the production of a disc brake with AMMC.

2.2 Cast iron production

Previously, the main characteristics of cast iron were discussed, highlighting how this material is suitable for the production of brake discs. However, it was pointed out that there are problems mainly related to its high density and pollution due to production. These reasons prompted the search for new materials. However, it is useful to dwell on how cast iron is produced to highlight its consumption in terms of energy and emissions. The cast iron is manufactured by re-melting pig iron with coke; this re-melting is done in a furnace known as the cupola furnace as shown in Figure 8 [29]. It has a cylindrical shape with a 1 m diameter and a height of about 5 m. The raw materials are inserted in the cupola furnace from above and it works intermittently, the opposite of the blast furnace. After the raw materials are placed, the furnace is fired, and a blast of air is forced through tuyeres. The blast of air is cold as the impurities in

pig iron are removed by oxidation. At the end of this process, the molten cast iron is led into molds of the required shapes to form what is known as cast iron castings [29]. It is important to notice that the production of one ton of pig iron from a blast furnace requires approximately 15 to 25 GJ [30].

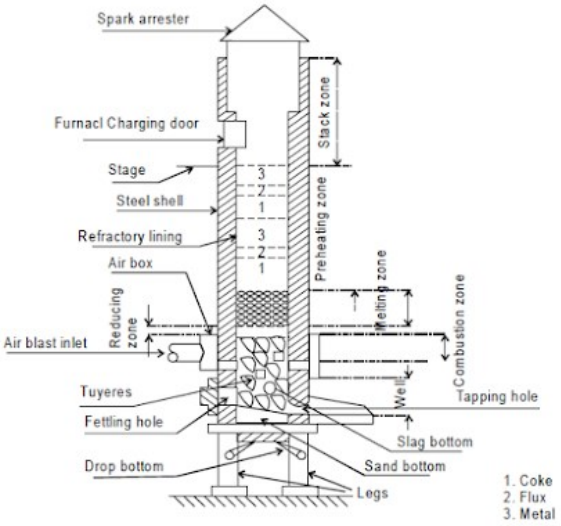

Figure 8-Main parts of the cupola furnace [31].

In the next paragraph, it can be seen that the production of primary aluminium requires even more energy, especially in the latter stages of processing.

There are different types of cast irons, which can be distinguished from one another based on their microstructure. This thesis work focuses on grey-cast irons, in which the carbon is in the form of lamellar graphite. They are the most widely produced due to their low production costs and they are the first to appear on the market. To obtain graphite, one must act on the composition, for example by adding 2 wt.% Si, and on the cooling rate, in particular by slow cooling. These two methods make it possible to obtain a cast iron in which the carbon occurs as graphite and not as cementite (Fe3C), which would lead to the formation of a so-called 'white' cast iron. Grey cast iron has poor mechanical performance due to the elongated shape of the graphite lamellae and the two apexes where cracks are more likely to initiate and propagate. It is worth focusing on the mechanical properties of cast iron EN GJL 150, as it is the one that comes closest to the materials used to conduct wear tests.

- Chemical composition: 3.2-3.5 wt.% C, 1.8-2.4 wt.% Si, 0.5-0.9 wt.% Mn, P ≤ 0.2 wt.%
- Density: 7.1 g/cm^3
- Brinell Hardness: 160-190 HB
- Tensile strength: 150-250 MPa

Note the 2 wt.% Si, which allows the formation of graphite as described above. The

matrix can have a ferritic or pearlitic structure or both. Stable iron at room temperature is called ferrite and ferrite is soft and ductile. Cementite is an iron carbide phase that is very hard and brittle. Pearlite is a lamellar microstructure made of ferrite and cementite. The mechanical properties of pearlite are intermediate between ferrite and cementite [32]. Elements that promote pearlite formation on the matrix are Cu, nickel (Ni), Mn and tin (Sn).

2.3 Aluminium production

The primary process uses bauxite as an input, a mineral found in the earth's crust from which Al can be obtained, while the secondary cycle uses processing waste or end-of-life products as input. There are two main types of aluminium scrap. In the first case, we speak of the new scarp, in the second case we speak of the old scarp. The term new scrap refers to aluminium obtained from processing waste, e.g., from processes such as extrusion, drawing and more, which can generate this type of scrap; it doesn't contain impurities because it was not in contact with other types of materials. It can be remelted and reused for another aim. This type of scrap will not be dealt with here. This thesis work focuses mainly on old scrap, i.e., aluminium waste from end-of-life products. Figure 9 shows where the main bauxite mines are located. Studying how aluminium is produced is useful for understanding which steps are most energy-intensive and which production problems can be addressed. Before moving on to the production of aluminium, however, it is necessary to highlight the essential characteristics of one of the most widely used alloys because of its properties. As mentioned in Chapter 1, many elements can be added to pure aluminium, among them Si. Specifically, in the Al-Si alloy, the eutectic point is at 12,6 wt. % Si and the eutectic temperature is 577 °C. Alloys below this percentage are termed hypoeutectic, while alloys above are termed hypereutectic. The eutectic has a lamellar form consisting of alternating lamellae of phase a and Si. Hypoeutectic alloys are the most used because of the positive characteristics brought by the low Si content, such as better castability and less shrinkage during solidification. In the hypoeutectic Al-Si alloy, the Si content normally varies between 5 and 12 percent by weight and rarely goes below this percentage. During the solidification of a hypoeutectic alloy, the formation of the alpha phase (a-Al), an aluminium-rich phase with a dendritic form, can be observed. The solidification of the alloy continues with the formation of the eutectic Al-Si mixture. In eutectic solidification, the two Al and Si phases precipitate simultaneously from the liquid at a constant temperature. As the amount of Si in the alloy decreases, the dendrites will tend to swell. Hypereutectic alloys, on the other hand, are characterized by having a Si content greater than 12,6 wt.%. These have a high degree of hardness

and brittleness and, apart from a few exceptional cases, never exceed 20 wt.% Si. In the case of hypereutectic alloys, the silicon crystals solidify first in the melt, until the remainder of the melt solidifies as eutectic.

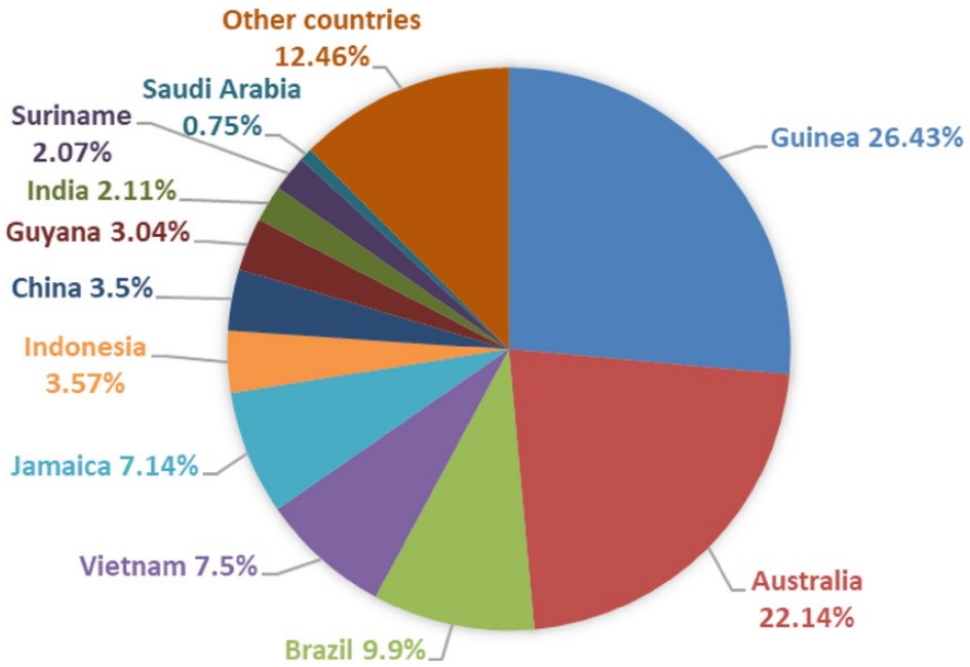

Figure 9- The main bauxite mines in the world 2020 [33].

2.3.1 Primary aluminium production

The starting point is bauxite, a mineral widely present in the earth's crust composed mainly of iron oxides, silicon oxides and aluminium oxides, also called alumina (Al_2O_3). Al_2O_3 is the most interesting element in bauxite, but it is only present in 30-54 wt.%. A process must therefore be used to separate all other oxides from Al_2O_3. To be able to extract it, it is needed the Bayer process, created in 1877 by Karl Bayer. This process has, however, a very low yield; in fact, to obtain one tonne of Al_2O_3, two tonnes of bauxite are needed; and other important aspect that must be considered is that it can only be used on high-quality bauxite with low content of admixtures, especially silicon. The process was born 100 years ago, and it is still used for primary production. The entire Bayer process is based on caustic soda (NaOH): the crystallized aluminium hydrate ($AlOH_3$) inside the bauxite can easily dissolve in NaOH at high temperatures, around 200 °C at a 15-bar pressure; and when the temperature is lowered and the concentration of the solution increases again, aluminium hydrate crystallizes. At the same time, the other elements contained in the bauxite either don't dissolve and settle to the bottom well before aluminium hydrate crystallizes. This means that after

aluminium hydrate gets dissolved in caustic soda the other materials can be easily isolated and removed [34]. Figure 10 shows the main steps of the Bayer process.

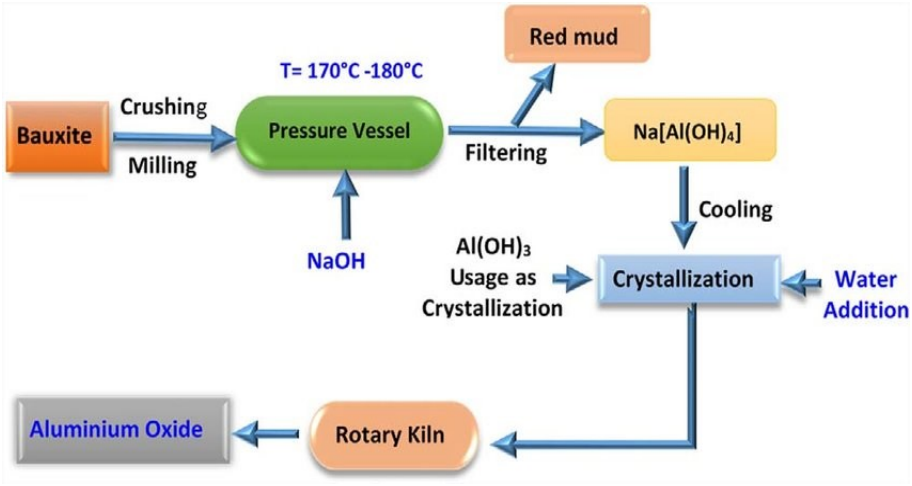

Figure 10- Main steps of the Bayer process [35].

The second step to extract aluminium from aluminium oxide is called the Hall-Héroult process. The Hall-Héroult process is the main technique for producing aluminum. It involves the electrolysis of alumina (Al_2O_3) dissolved in cryolite salt (Na_3AlF_6). During the electrochemical reaction, carbon anodes are constantly consumed while the produced aluminium liquid is accumulated at the bottom of the cell operating as the cathode. A classic cell contains 18 to 40 anodes connected in parallel, sharing a DC current in the order of several hundred kilo-amps [36]. Nowadays this process is considered the most energy and CO2-intensive industrial process, consuming around 1 % of the globally produced electricity. A 'cradle to gate' life cycle assessment suggests that the energy requirement of current primary aluminium production, including mining, manufacturing, and transportation, is 211 MJ/kg Al [37]. The main electricity consumption in the primary aluminium production, approximately 56 MJ/kg of Al, happens in the Hall-Héroult process [38]. Assuming coal-based electricity generation which is the case used in many primary aluminium plants around the world, approximately 170 MJ of energy are consumed for the electrolytic reduction and an additional 14.84 kg of CO2 are indirectly released through coal burning for each kg of aluminium produced in this way [38]. These data show that primary aluminium production has a much higher embodied energy than GCI. For this reason, a series of innovations have been implemented to increase the efficiency of processes, in particular, the Hall-Hèroult process being the most energy-intensive. Another way to reduce the impact in terms of energy consumed and emissions generated is through

the use of recycled materials. By using an aluminium alloy with 100 % recycled material, the energy consumed and CO2 emitted during the material extraction phase tends to be zero.

2.3.2 Secondary aluminium production

As seen above, the circular economy and the reduction of air pollution are two main mega-trends that characterize this historic period. One of the fundamental characteristics of Al, is that recycling does not worsen the intrinsic characteristics of the material, in other words, Al can be recycled without loss of performance for an infinite number of cycles [39]. Reasons for adopting this process include the following:

-Reduction in energy consumption compared to the primary process

-Reduction of production costs

-Reduction of air pollution

-Reduction of bauxite mining activities

-Recovery of material that would otherwise be wasted

The recycling process, therefore, involves collecting all this scrap and taking it to foundries. The aluminium scrap, however, must be cleaned of all impurities in the alloy. Figure 11 shows different Al scrap types.

Table II. Selected Scrap Types Listed in European Aluminum Scrap Standard (EN 13920)[8] and Their Average Scrap Compostion

Part	Scrap Description	Aluminum Metal[a] (%)	Oxides[b] (%)	Foreign Material[b] (%)
3	Wire and cable (new scrap)	98.7	1.3	—
	Wire and cable (old scrap)	97.7	1.8	0.5
4	One single wrought alloy	97.2	1.0	1.8
5	Two or more wrought alloys of the same series	97.2	0.8	2.0
6	Two or more wrought alloys	94.0	0.8	5.2
7	Castings	83.4	6.2	10.4
9	Shredded and density separated scrap	84.5	5.4	10.1
10	Used beverage cans	94.0	0.8	5.2
12	Turnings, one single alloy	95.3	3.7	1.0
13	Mixed turnings, two or more alloys	84.0	3.3	12.8
14	Packaging (coated)	71.5	3.8	24.7
15	Packaging (de-coated)	86.1	12.9	1.0
16	Dross	55.7	44.3	—

[a]Based on empirical data.
[b]According to the definitions of the different EN 13920[8] scrap categories and industry knowledge about scrap composition.

Figure 11-Different aluminium scrap types.

There are preliminary operations that can be done to make aluminium ready for casting. Grinding operations can be performed to remove major impurities, drying, especially for packaging, and magnetic separation to remove iron (Fe). Next comes the melting of scrap in particular furnaces; there are different types depending on the type

of scrap available. It is possible to identify the following types of furnaces:
- Sloping hearth furnaces: mainly used with scrap mixed with Fe. As Al has a lower melting temperature than Fe (660 ˚C for the former and 1538 ˚C for the latter), due to the sloping hearth, it slides to the bottom of the furnace, so that it can be collected.
- Reverberatory furnaces: Used mainly for very clean, unpainted scrap. They can bear a weight of up to 100t and require very careful preliminary quality control.
- Induction furnaces: particularly expensive and with little capacity in terms of weight support. They are suitable for particularly fine scraps.
- Rotative furnaces: For low-grade scrap. It has a weight capacity of around 20 tons. The furnace continues to rotate itself around a horizontal axis while the burner melts the metal.

It is important to notice, secondary aluminium production contributes to cutting off high energy demand by around 90-95 % by remelting both new and old scraps [40].

2.4 Tribological properties

In the previous paragraphs, it has been discussed how particulate emissions are an aspect that can no longer be neglected. To study the friction force (F_f) and in particular the coefficient of friction (COF) in more detail between brake pads and the rotor, it is recurrent to use a particular type of test called Pin-on-Plate (PoP) or Pin-on-Disc (PoD) wear tests. The choice between these tests depends on the specific application. The PoP wear test is a widely used experimental method for evaluating the friction and wear properties of materials under sliding contact conditions. In this test, a pin-shaped specimen is pressed against a plate while applying a normal load. The relative motion between the pin and the plate generates frictional forces and induces wear on the contacting surfaces. In Chapter 3, the PoP configuration will be used for the experiments, as the available samples on which to carry out the tests are plates. A scheme of the PoP setup is shown in Figure 12.

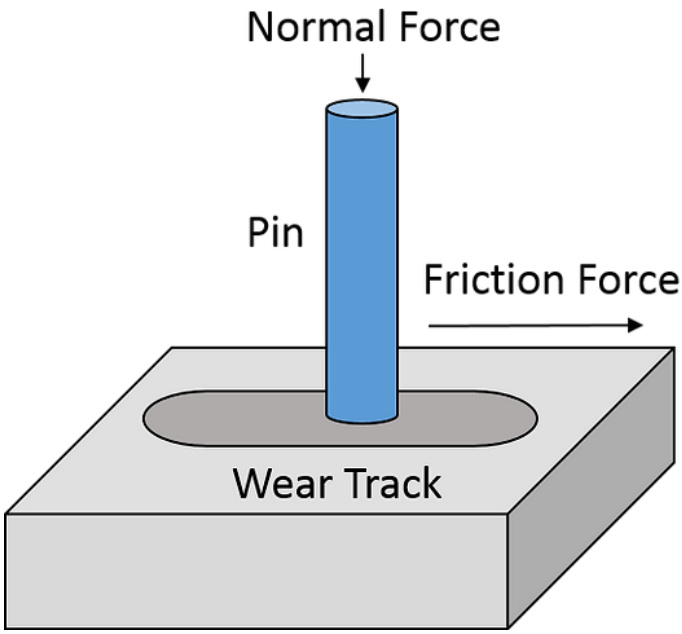

Figure 12- Representation of PoP configuration. The normal force is applied through a load measured by a load cell. Once obtained the friction force it is possible to calculate the COF [41].

Before performing the wear tests, it is necessary to evaluate some essential aspects:

- The compositions of materials and their mechanical properties. In this part, it is necessary to ensure that all test specimens have approximately the same roughness, so that all tests are carried out under the same initial conditions. To verify that the surfaces to be tested have approximately the same surface roughness, a parameter called Sa (μm) defined by Equation 1 is calculated, where A is the observed surface. The Sa parameter is calculated by averaging the absolute values of these height deviations from the mean line, which represents the average height of the surface profile [42]. Another important parameter to note is the Ra parameter (μm), defined by Equation 2, where L is the length of the profile. Ra (average roughness) measures the deviation of a surface from a mean height [43]. The substantial difference between the two parameters is that the former is a measurement on a surface, while the latter is along a profile. These two data combined offer a detailed view of the roughness of the material.

$$Sa = \frac{1}{A}\iint_A |Z(x,y)|\, dxdy \tag{1}$$

$$Ra = \frac{1}{L}\int_0^L |Z(x)|\, dx \tag{2}$$

- Weight evaluation. Before starting the test, it is good practice to weigh the available samples to measure the subsequent weight loss at the end of the experiments.
- The use or non-use of lubricants. In some cases, lubricants are used between contact surfaces to test the materials' properties, in other cases dry sliding friction is used without the use of lubricants. The configuration without lubricants will be the one used in Chapter 3.
- The evaluation of the applied load in Newtons. This measurement is carried out using a load cell. Different tests can be performed by changing the load to evaluate different friction forces. Sometimes it is possible to refer to the applied pressure p (MPa) instead of the applied load. The relationship linking the pressure to the applied load is described by Equation 3 below where F_n is the applied force in Newton and A is the contact surface measured in mm^2:

$$p = \frac{F_n}{A} \tag{3}$$

- The time configuration is typically expressed in hours. Before setting up the test, the number of hours or cycles to be performed must be determined. This is also a parameter that can be changed to achieve different results.
- Once the friction force has been derived, it is useful to derive the COF to relate the different material behaviors. In particular, the COF is derived using Equation 4 where F_f is the friction force and F_n is the applied load, both expressed in Newton:

$$COF = \frac{F_f}{F_n} \tag{4}$$

- The operating temperature is measured by thermocouples.
- The stroke length (S_L). This is the length of the wear track as shown in Figure 12. Once set, the entire distance traveled during the entire wear test can be easily calculated by multiplying S_L by the number of cycles traveled during the test.
- The linear speed (L_S). It represents the speed at which the test is carried out, typically expressed in mm/s or m/s.

These are the preliminary aspects to take into account before performing a wear test, regardless of whether it is performed on a PoP or PoD. Once the tests have been performed, the weight loss is calculated, the roughness is observed to see how it has changed compared to the initial situation, the COF and Wear rate, Wr, are derived [44]. Another parameter that can be useful to calculate is the specific wear rate K ($mm^3/N{\cdot}m$) expressed by Equation 5 where Δm is the mass loss (g), ρ is the material density (g/cm^3) and s is the total sliding distance (m) [45].

$$K = \frac{\Delta m}{\rho \times s \times F_n} \quad (5)$$

This parameter is useful to calculate as it allows us to compare the wear of different materials. Once calculated, it can be compared with the COF of the individual materials to see whether the relationship of the two is direct or indirect. Two other fundamental parameters that can be derived are the normalized velocity (V) and normalized pressure (F) described by Equations 6 and 7 respectively. In this case, H_o is the pin hardness (HB), r_o is the pin radius (mm), v is the sliding speed (m/s) and a is the thermal diffusivity (m^2/s) [46]:

$$V = \frac{v\, r_0}{a} \quad (6)$$

$$F = \frac{F_n}{A\ H_0} \quad (7)$$

Through these parameters, it will be possible to understand the type of wear that has occurred in the different materials.

Several experiments were conducted on both GCI and AMMC. In particular, it can be observed how the following parameters can influence the COF and the wear loss in the study of AMMCs. An important aspect to consider is the size of the reinforcement particles and the percentage of reinforcement within the matrix. These two parameters can influence the wear behavior and COF of the material during testing. For example, normalized velocity (V) increases as the percentage of reinforcement increases, while normalized pressure (F) varies as the percentage of reinforcement and particle size change [46]. The homogeneity of the reinforcement distribution is also an element to be taken into account, the more homogeneous the particle dispersion, the higher the microhardness. The presence of clusters or aggregations of particles tends to decrease the efficiency of the composite in terms of mechanical behavior [47].

Regarding the hardness, the matrix hardness exerts a strong influence on the dry sliding wear behavior of the SiC particles reinforced composite, and the composite with the lowest matrix hardness displays the lowest wear rate [48]. Another parameter to be taken into account that can vary the wear rate is the applied load. As the applied normal force increases, the wear rate increases [48]. Finally, a further aspect that influences the coefficient of friction for an AMMC with SiC-based reinforcement is the sliding distance (s) measured in km or m traveled. In Figure 13, it can also be seen that as s increases and as the applied load varies, different behavior occurs between an aluminium alloy without reinforcement and an AMMC with SiC as reinforcement [49].

The reason behind this is because as the sliding distance increases, the temperature between the sliding surface and the rotating disc surface increases. It is possible to note, that with an increase in loads, the value of COF decreases for both aluminium matrix alloy as well as silicon carbide-based aluminium metal matrix composites. Another important aspect regards the volume of wear loss (mm^3). It can be noticed, that the volume of wear loss increases with the increase of the applied load. Furthermore, the volume loss is lower for AMMC with the SiC reinforcement than for the Al2014 aluminium alloy considered [49].

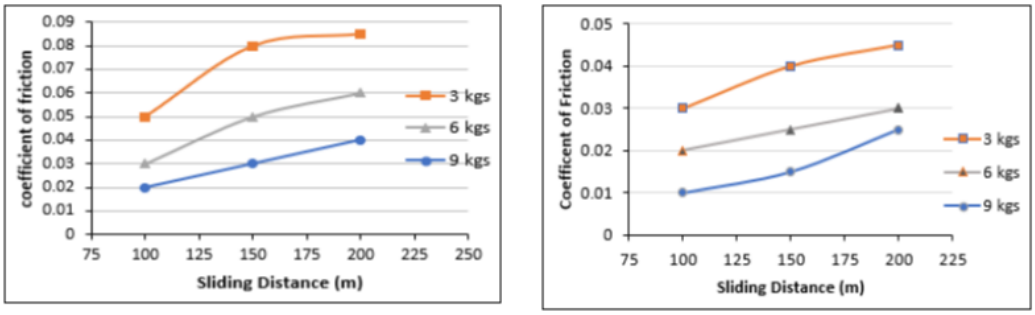

a)Al2014 alloy b)Al-SiC composite

Figure 13- COF as a function of sliding distance: a) for an unreinforced alloy, b) for AMMC with 5 % volume fraction SiC reinforcement [49].

Other experiments were conducted, again through PoD, on different types of GCI. Figure 14 shows that the wear of grey irons decreases as the applied pressure decreases. [50]. According to the literature, again speaking of GCI, it is interesting to note that weight losses increase with increasing test duration and with increasing sliding distance (s). The same phenomenon occurs when increasing the applied load [51]. Adding elements that enhance perlite such as Cu, on the other hand, decreases the weight losses of the material. In particular, by increasing the percentage of Cu from 0.00 wt.% up to 3.5 wt.%, a decrease of up to 30% in weight losses due to the pearlitic cast iron structure can be observed [51].

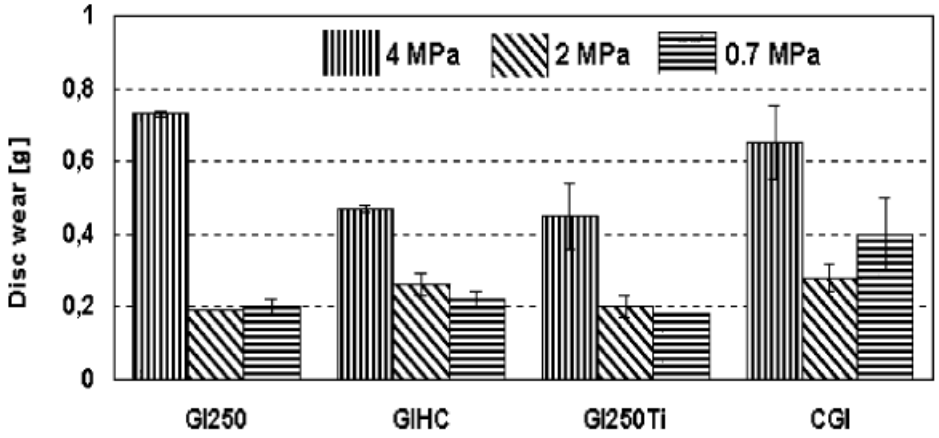

Figure 14- Different types of grey iron compared to compact graphite iron (CGI). When the applied pressure decreases, the grey iron wear also decreases [50].

Currently, however, there is no study performed on AMMCs with a secondary aluminium matrix in the literature. As will be seen later in Chapter 3, through microstructural characterization it is possible to observe a different arrangement of the SiC reinforcement between AMMCs with primary aluminium and AMMCs with secondary aluminium. As mentioned above, the reinforcement distribution and the volume fraction can cause different behaviors concerning friction force and friction coefficient.

2.5 Aluminium metal matrix composites

After discussing the properties and production methods of aluminium, it is necessary to focus on AMMCs, as they are the key element of this thesis work. It is necessary to start by defining a compound; a composite material is defined as a combination of two or more materials with different physical and chemical properties [52]. The constituents, also called phases, are chemically distinguishable on a microscopic scale, presenting separate and distinguishable interfaces [53]. When these materials are combined, they can create a material that is specialized to do a specific task. The reason for their use over traditional materials is that they improve the properties of their base materials and are applicable in many situations. AMMCs can be found in many market sectors, for example, aerospace, rail transport, packaging and automotive. The constituent that is present in the greatest quantity and has a continuous form is called the matrix; typically, it is the element that makes up the matrix that needs to be reinforced. As mentioned above, aluminium has very good qualities to replace cast-iron disc brakes, but at the same time, it presents problems related to low melting temperature, fatigue, and wear that can be overcome by reinforcing the matrix. The

other material that makes up AMMC is defined as the reinforcement phase, and it is this that goes to give the required characteristics to the matrix. Typically, this phase is harder and stronger than the matrix and gives it the required characteristics. In some cases, it is possible to find silicon carbide (SiC) or alumina (Al_2O_3) as reinforcement. These reinforcements may appear in the form of fibers or particles with different sizes occupying an ever-changing percentage of the surface area concerning the matrix.
The major improvements in the properties of AMMCs are represented in the form of greater strength and improved stiffness, reduced density (for example, SiC has a density of 3,21 g/cm^3), improved both abrasion and wear resistance, improved high-temperature properties, better heat management [54]. For example, the elastic modulus of pure aluminium can be enhanced from 70 to 240 GPa by reinforcing with 60 vol.% continuous alumina fiber [53] [55]. In Figure 15 is possible to observe the variation of tensile strength changing the percentage of SiC.

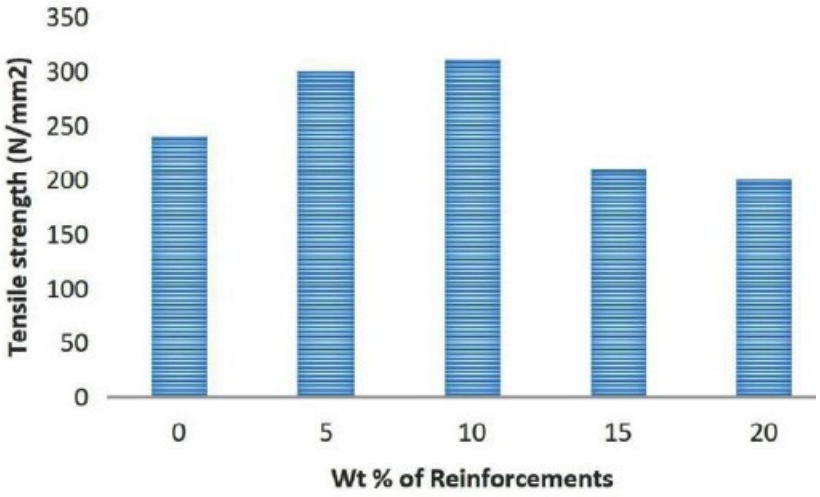

Figure 15- Tensile strength as a function of wt % of reinforcements [54].

A typical example of application can be found in car disc brakes; to be taken into consideration, however, are the production and processing costs which are higher than the production of cast iron disc brakes. Other aspects to consider when using AMMCs, besides those purely related to mechanical performance and thermal, are:

- The increased useful life of the component/product.
- Energy savings, related to the previous point.
- Reduced maintenance costs during the product's lifetime, related to the increased mechanical characteristics.
- Environmental benefits such as reduced emissions.

Before turning to the production methods of AMMCs, it is important to emphasize the number of variables that affect the production process of these materials. There are variables concerning both the matrix, such as composition, mechanical characteristics

and hardness, and the reinforcement. Regarding the reinforcement, as mentioned earlier, parameters such as reinforcement percentage, particle size, type of distribution and composition can influence wear behavior. To these must be added the type of production process, the types of heat treatment if performed [56]. This makes it difficult not only to produce AMMCs but also to study the wear of these materials.
There are many ways to produce AMMCs, in Figure 16 it is possible to see the main production processes.

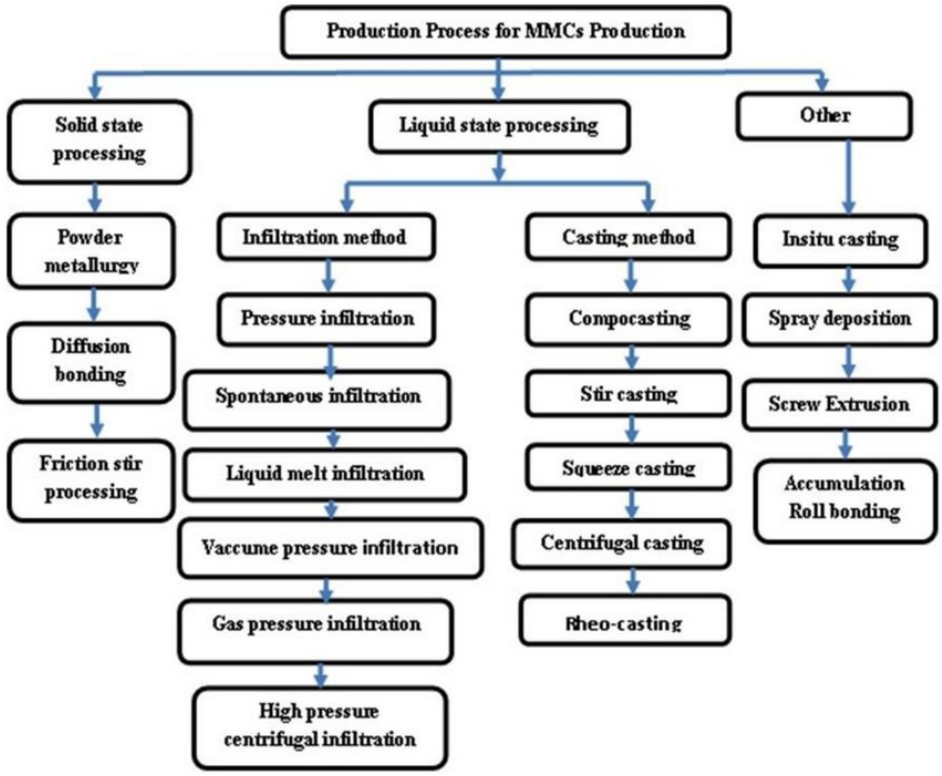

Figure 16- Different types of AMMC production systems [57].

The process known as squeeze casting is worth investigating, as the primary and secondary AMMCs on which wear tests will be performed in the following chapter were produced through this process. This is another method to manufacture AMMC in a liquid state. By using the closed die, metal gets solidification under pressure. Due to the movement of mold parts, pressure is applied over the molten metal, and it penetrates over the dispersed phase. Squeeze Method manufacturing parts have the features of high weldability, high-temperature resistance, good surface finish, high corrosion resistance, and high dimensional accuracy. The major advantage of squeeze casting is that the final products have good grain size with achieved microstructure. Another fundamental characteristic of this technique is the applied pressure during solidification, which avoids the extensive machining process for casted components, usually done in the conventional casting process. Squeeze casting also suits the fabrication of wrought alloys which gains the economic importance of recycled AMMC

[58]. But there are also disadvantages like, the reinforcement is not continuous, only simple shapes are achievable, and high production cost [59].

2.6 Types of wear

Wear is the removal of solid metal from one or both surfaces in contact in the solid state. Wear is quantified by the term 'wear rate', defined as the loss of mass or volume of the removed material considering the duration of the test in terms of time or sliding distance. In some cases, it is possible to speak also of "specific wear rate" (K), if it is necessary to consider the density of the material [60]. Mainly it can be said that wear is characterized by mild and severe wear, except in some cases as will be seen later where there is ultra-mild wear for composite materials such as AMMC with SiC reinforcement [61]. In the first case of mild wear, the worn surfaces are smooth, and the wear debris is small, ranging from 0,01 μm to 1 μm. In the second case, on the other hand, severe wear involves larger wear debris, starting from 20 μm up to 200 μm, visible to the naked eye and with a roughened worn surface. The different types of wear and tear are shown below [60].

Adhesion: In this type of mechanism, there is a transfer of material from one surface to another, leaving as output pits, voids, and cavities on the surface of the treated material. This type of phenomenon typically occurs when the two materials in contact have approximately the same composition or the two surfaces do not have oxide layers. Soft metals exhibit greater adhesion wear than other metals. This is because these have a greater contact surface during testing. The use of lubricants can also increase adhesion.

Abrasion: This type of wear occurs when a hard particle comes into contact with the soft surface of a material. Two main types of wear fall into this category. The first is single-body abrasive wear, in which the wear track only occurs on one surface. The second is two-body abrasive wear, in which the trace of wear is present on both surfaces. One aspect to be taken into consideration here is the hardness of the material. In fact, it has been shown that the hardness of the two materials in contact is inversely proportional to the abrasive wear, the higher the hardness, the lower the wear. On the other hand, it has been shown that it is directly proportional to the applied load [62].

Erosive wear: A type of wear mechanism that occurs between a solid material and a fluid. From a practical point of view, erosive wear is important. However, in some experiments conducted with ceramic surfaces, high-velocity impingement of silicon carbide particles causes localized surface melting.

Delamination wear: It usually occurs in rolling or sliding contact bodies such as bearings. After repeated cyclic loading, a crack is observed on the subsurface. The

subsurface cracks propagate, connect with other cracks, reach the surface and generate wear particles. The crack propagation is influenced by several factors like the relative humidity in the air. The crack propagation speed is directly proportional to the percentage of moisture in the air, which means that in a high-humidity environment, it is easier for this type of wear to propagate.

Corrosive/oxidative wear: This type of wear occurs when sliding between materials takes place in a corrosive or oxidative environment. Oxygen and even other gases in the air can interact with the materials in question. The presence of particular chemicals can also lead to material corrosion during testing.

It is therefore of paramount importance to understand what kind of wear occured in the materials studied. Various empirical maps have been constructed that relate tribological parameters such as load, sliding speed, sliding distance, and wear rate. From these maps, it is therefore possible to define the type of wear that occurs on the material after testing. This is the case of a map for pearlitic grey cast iron with the graphite lamellae oriented without a preferred direction [63]. Figure 17 shows the presence of three types of wear depending on the specific wear rate obtained for different values of sliding speed (m/s) and load (N) during the tests. The ultra-mild wear regime is characterized by the presence of compact layers of iron oxides in the worn surface and the absence of plastic deformation. In the mild regime, the wear rate was controlled mainly by surface oxidation. Starting with low loads and speeds (2N and 0.3 m/s), this oxide layer was thin and of the order of a few microns but increasing these parameters (5N and 2 m/s) the oxide layer increased in size and covered up to 80% of the wear track. In this condition, medium to large debris was formed. Regarding the last type of wear, the severe wear regime, a significant increase in the roughness of both the cast iron and the disc used for the test can be seen, and an evident plastic deformation occurred in the track. In this case, an increase in the micro-hardness of the transferred material can also be observed. This hardness increase can be regarded to be an indication that martensitic hardening might have taken place during the rapid heating and cooling cycles accompanying the material transfer process. It is important to emphasize that the transition from one wear regime to another is characterized by a linear transition using, however, a logarithmic scale for both load and sliding speed [63].

Empirical maps were also constructed to show the different wear patterns for AMMCs, depicted in Figure 18. In this case, an AMMC consisting of an A356 aluminium alloy with 20% SiC particle reinforcement with an average particle size of 13.6 μm was analyzed. [61]. The composite was tested by a Block on Ring test at different loads and sliding speeds and then the wear rate was calculated. This was also carried out against

the Al-Si alloy A356 with a composition of 7 wt.% Si, 0.20 wt.% Mg, 0.11 wt.% Fe, 0.20 wt.% Ti, 0.05 wt.% Mn to compare the different wear regimes appearing in the materials.

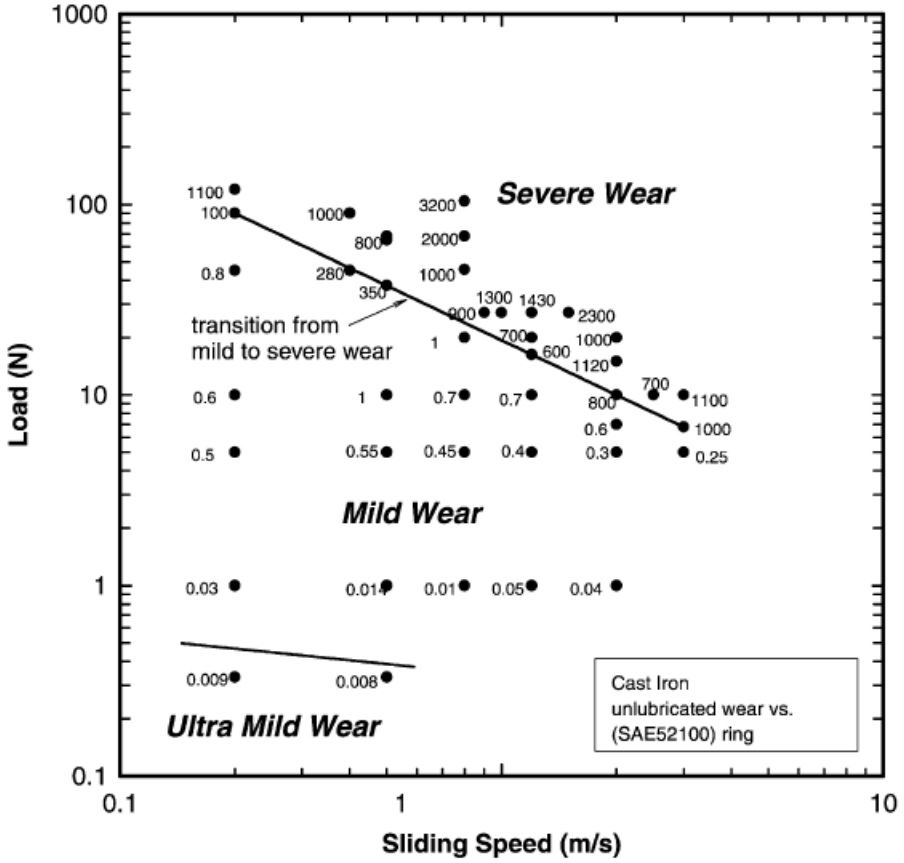

Figure 17- Types of wear mechanism in a pearlitic grey cast iron [63]. The points on the map express the wear rate for different wear regimes. These values should be multiplied by 10^{-3} to get the values in mm^3/m.

The test revealed three wear regimes that characterize AMMC. The first is called the ultra-mild wear regime, and appears only in the composite, characterized by low loads and low sliding speeds (from 0.2 N at 0.2 m/s to 0.3 N at 0.4 m/s). This phenomenon is mainly due to the reinforcement provided by the SiC particles, and an iron oxide layer can also be seen on the surface of the reinforcement due to the counterpart. The second so-called mild wear regime is characterized by two fundamental phenomena: the "mechanical mixing/oxidation" at low loads and speeds and the "delamination" wear at higher speeds. Mechanical mixing/oxidation produces a wear contact surface covered with a compacted layer of debris that is typically a fine powder composed of mixed Al and Fe particles together with amorphous Al and aluminium oxides. The delamination wear arises at greater sliding speeds in the mild wear regime, above 3 m/s at 5 N to 1.0 m/s at 80 N. Debris produced above the critical speed range is plate-

like in morphology and has a shiny metallic appearance. The last type of regime is the severe wear regime. It is characterized by high loads and speeds and the wear rate is one magnitude above the mild wear regime wear rate. Figure 18 shows the main wear mechanism for a AMMC. with 20% SiC as reinforcement [64].

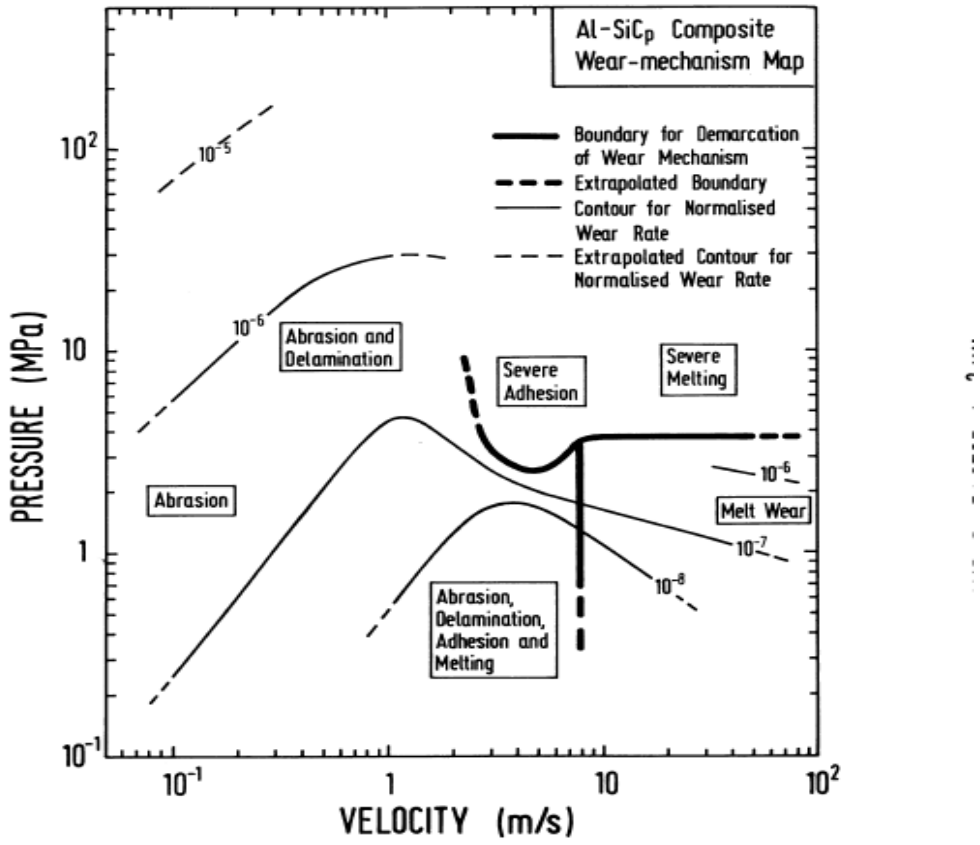

Figure 18-Types of wear mechanism in AMMC with 20% SiC reinforcement [64].

2.7 Life Cycle Assessment

When talking about the circular economy, it is necessary to mention the Life Cycle Assessment methodology, henceforth abbreviated to LCA. It is described in the ISO 14040 standards and can be defined according to [65] as" a process of evaluating the effects that a product has on the environment over the entire period of its life thereby increasing resource-use efficiency and decreasing liabilities. LCA, therefore, is an objective method for assessing the energy loads and related environmental impacts of a product-service system and considers the entire product life cycle. The aim of this approach is to understand what the critical environmental issues are in the phases of a product's life cycle so that measures can be put in place to limit these damages. Optimizing production cycles in terms of the energy consumed also leads to an overall reduction in costs; and this is one of the main strengths of this methodology. The life

cycle phases of a generic product are:

1. Raw material extraction
2. Manufacturing
3. Transport
4. Use
5. Disposal

As well as being applied to the study of a single product, this methodology can also be applied to make comparisons in terms of energy consumed and environmental impact between several similar products and/or services.

The LCA methodology, according to ISO standards, requires the following steps to be followed to obtain an objective and quantifiable result. The following steps have been written based on [66] and [67].

1. Definition of the objective and scope of the study: As mentioned above, the main aims of an LCA study are to assess energy loads and environmental impacts, and to identify the most critical processes within the product life cycle. There are typically two elements to any LCA study: the first concerns the definition of the system, while the second concerns the definition of the functional unit. Concerning the first element, we must conceive of the system to be analyzed as a succession of operations and processes that require certain energy inputs and release emissions and waste in the form of outputs. This allows us to make the system more visual and simplify it. This part also defines the boundaries of the system itself, i.e. what is studied and what is not. As for the other aspect, that of the functional unit, it is defined as the reference to which all the inflows and outflows of our system are linked. When conducting an LCA study, it is important to decide on the functional unit and relate all flows to it. By correctly defining the functional unit and thus having it as a consistent reference, sensitivity analyses can be carried out by analysing different scenarios.
2. Life Cycle Inventory (LCI): this phase defined by the ISO 14041 standard, has to outline all the processes and operations that lead to the realization of the output in question. A flowchart must then be created to make the process diagram as visual as possible. Once the flowchart has been outlined, it is necessary to objectively quantify the energy inputs into the system and the emission outputs generated by the system itself, thus making an inventory of what flows in and out of the flowchart. When speaking of inputs, it should be pointed out, we are not only talking about energy, but we can also refer to flows of water input or auxiliary materials. The same applies to outputs, we are not only talking about atmospheric emissions, but also waste in general, which can be solid, liquid, and gaseous. At the

end of the inventory analysis, therefore, it will be shown, for example, how many kilos of raw materials were used as input and how many kilos of emissions were emitted as output, all concerning the chosen functional unit. There are several ways to collect data useful for this phase. The first method is to collect them directly in the field, by analysing flows and analysing datasets produced by suppliers. The second method is to refer to the literature, a third method is to use specific databases. A key parameter to be considered is the quality of the data; this quality must be properly documented.

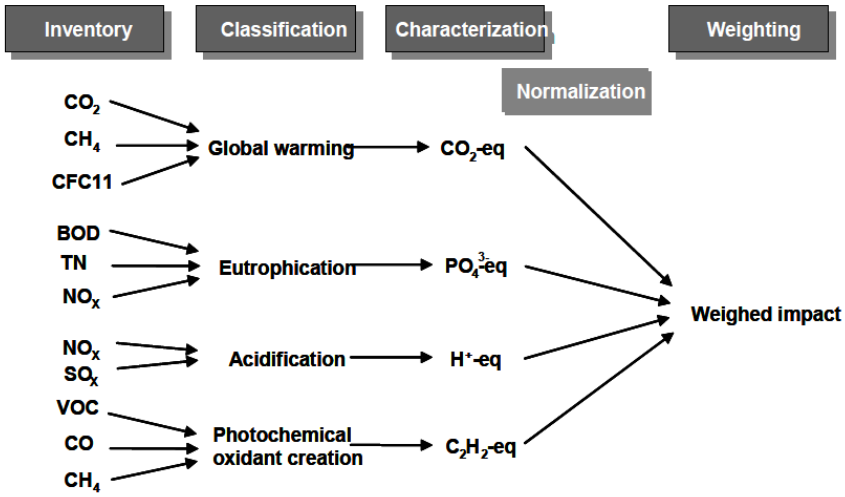

Figure 19- LCIA phases overview [67]

3. Life Cycle Impact Assessment (LCIA): This step is regulated by the ISO 14042 standard and serves to assess the environmental impacts caused by the production of the functional unit using the data obtained from the inventory analysis as input. There are mainly four steps to be followed, the last two of which are considered optional and are: classification, characterization, normalization, and weighting. Figure 19 shows the main steps for the LCIA phase.

Classification: The first step of the LCIA is to use the LCI data on energy consumption and emissions to identify environmental impact categories. The most common impact categories are:

-Global warming

-Ozone depletion

-Acidification

-Human toxicity

-Ecotoxicity

-Solid waste, hazardous and radioactive waste

It is necessary to choose one or more environmental impact categories, and one must

link the LCI parameters with these categories according to a cause-effect relationship. Making this connection is not easy, as the parameters may affect several categories simultaneously. One must therefore consider the possibility of direct, indirect and even multiple effects.

Characterization: this is the last of the mandatory steps and consists of the quantification of environmental impacts. Fundamental to this part is the concept of the characterization factor, which is based on chemical equalization. Each category of environmental impact has its own unit of measurement, for example, Global warming (GWP) is measured in g CO2 eq/g; this means that each inventory parameter that falls under the GWP category will have to be converted, according to chemical equalization, into g CO2 eq/g. This is because even if several substances all fall under the same category, they affect each other differently. The normalization and weighting parts are not compulsory and are outside the scope of the present study, so they will not be examined in this document.

4. Data Evaluation: defined by ISO 14043, this phase concludes the LCA analysis and uses data on environmental impacts as input. The purpose is to communicate, in the form of a report, which elements or phases of the system are critical so that corrective measures can be implemented to limit the damage. Within this phase, if the functional unit is chosen correctly, sensitivity analyses can be performed, varying the boundary conditions of our process. An example of sensitivity analysis is shown in Figure 20. Once the critical phases have been identified, one can then start with the implementation of corrective actions to reduce the environmental impact. As mentioned earlier, reducing the use of energy and the emissions created not only reduces the environmental impact, but also reduces the costs incurred by the company to feed the processes.

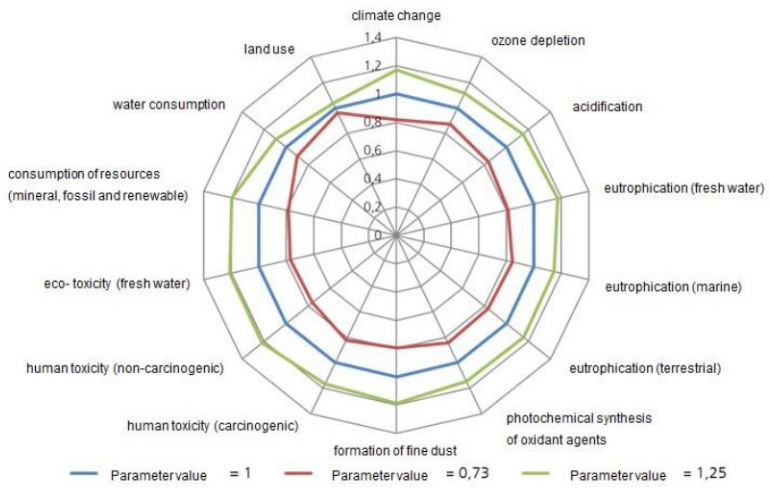

Figure 20- A sensitive analysis after an LCA study [66].

Finally, LCA can also be used during the product development process and not only when the product has already been created. Using LCA during product development provides a real-time view of consumption and emissions, so that a product with a reduced environmental impact can be brought to market.

2.8 Research question

Analysing the present literature, many studies have been done in the field of AMMCs to replace brake discs from cast iron to aluminium. As could be assumed, the mechanical and non-mechanical characteristics offered by this type of material are superior to those of cast iron. Several studies have also been conducted about sustainability, one of the megatrends mentioned above, mainly focusing on LCA analyses of aluminium.

What is not present in the literature currently, however, is a comprehensive study regarding the use of secondary aluminium as a matrix in AMMC. Two main aspects will therefore be studied in the following chapters:

- The durability of different alloys will be tested through the PoP test. In particular, the differences between GCI, AMMC with primary aluminium, and AMMC with secondary aluminium will be analyzed. Several parameters will come into play in these tests, including the duration of the test, the temperature involved, and the load applied. The dimensions of the emissions will then be analyzed and measured.
- An LCA study will be conducted to understand the environmental impact this type of material causes in the production of disc brakes. Critical steps in the production process and possible improvements for the future will then be highlighted.

The aim is, therefore, to find a solution that can link together:

- High performance, both in terms of mechanical characteristics and durability. The brakes that will be fitted four-disc brakes without drum brakes, will have a service life equal to that of a medium-sized car.
- Sustainability. In particular, the production of disc brakes with AMMC with secondary aluminium must be sustainable in terms of environmental impact and suitable for the mass production of electric cars, which according to previously studied trends is increasing. Furthermore, the emissions released from the use of these materials must be acceptable and in compliance with current regulations.

2.9 Delimitations and Problems

The use of AMMC with silicon carbide reinforcement and a secondary aluminium metal matrix could be a solution that offers both high performance and sustainability. Unfortunately, however, even the treatment of secondary aluminium hides problems. Although the treatment of old scrap has reached good levels, there are still some problems, like:

- they are often contaminated with other impurities like Fe, Cu, Zn.
- they require a pre-cleaning process (less costly from a monetary/energy point of view than the production of the primary one, but still a cost to be reckoned with).
- waste is scattered in different places on the planet, and there is no efficient management of waste streams, which could be optimized.

This section also includes some of the topics that will not be covered in the thesis work due to the vastness of the subject. What has not been covered can be used as a starting point for future work. For more details, see Chapter 5 'Future Work'.

The following topics are not covered:

- Only medium-sized electric vehicles such as cars will be dealt with, neglecting heavy vehicles. This is mainly for two main reasons: the European Euro 7 regulations are different in subject matter and entry into force, and the type of demand is different. Whereas cars are mainly for a b2c market, the HGV (Heavy Goods Vehicles) market is mainly B2B, which leads to differences in demand analysis and requirements. In addition, one of the reasons for focusing on medium-sized vehicles is that they require more moderate and restrained braking than heavy trucks, and so less mechanical performance is required from the brakes.
- The present thesis focuses only on the disc/rotor, neglecting other parts of the braking system, mainly neglecting the bearings. Although they are a necessary and fundamental part of the braking system, they are not dealt with because of the following reasons:

· Completely different materials, even if there is a metal composition inside them,

they are mostly ceramic materials, and this is beyond our studies.

- The only brake pads tested are suitable for cast iron brake discs. We don't have brake pads for AMMC brake discs.

3. Experimental procedure

This chapter describes the experiments conducted in this thesis work. As stated in the previous chapter, the aim is to test the durability of different materials, including GCI and an aluminium metal matrix composed of 9 wt.% Si, 0.15 wt.% Ti and 0.6 wt.% Mg with 20 wt.% SiC particles reinforcement with primary aluminium and recycled aluminium as a matrix. This will be done by performing pin-on-plate tests with the different types of materials available and then measuring the effects of friction on them. Before doing this, it is necessary that all available materials, both pin and plate, have the same roughness, to have as homogenous values as possible before starting the tests. To do this, a grinding machine will be used on both pins and plates to obtain homogenous roughness values, which will then be obtained using the Olympus microscope.

The second part of this chapter will concern an LCA study to understand more precisely the emissions generated by the creation of disc brakes with these materials. The same materials as in the pin-on-plate test will be considered, and an attempt will be made to analyze the differences, in terms of emissions and environmental impact, between the different extraction, production and recycling processes.

Before starting with the analysis, however, it is necessary to study the composition of these materials in more detail, through an optical microscope analysis. Through microscopic analysis, it is possible to show the microstructure of these samples, highlighting their composition and microstructural characteristics.

3.1.1 Materials Characterization

The chemical compositions of the different materials used in this thesis work are presented in Table 1. The chemical composition was measured by optical emission spectroscopy and the average values of five measurements were collected.

Table 1 – Chemical composition of GCI and aluminium matrix [wt.%].

	C	Si	Mn	P	S	Cr	Mo	Ni	Cu	Fe
GCI	4.53	1.98	0.71	0.05	0.14	0.10	0.02	0.05	0.17	Bal
	Si	Ti	Mg	Al						
Al matrix	9	0.15	0.6	Bal						

3.1.2 Pre-wear tests

Before moving on to the wear test, however, it was necessary to make some preliminary treatments on the surfaces of the samples. In particular, a grinding machine, called

Tegramin 30, was used to obtain approximately the same surface roughness on all samples, so that the wear test could be performed with the same initial conditions. Starting from the plates, the surface roughness of GCI and primary AMMC was studied. For each of these materials, 3 samples named A, B and C are available. For each sample, there are 4 tracks on which to subsequently perform the wear test. For the GCI plates, a grinding disc called Piano 500 was used, meanwhile, for AMMC1 plates a grinding disc called Piano 220 was used. When referring to the first disc, we speak of a grain size of 30 μm, while when referring to the second, we have a grain size of 68 μm. After using these discs, the Olympus microscope was used to investigate the surface roughness. In particular, at least three values were taken at random positions to see whether the surface roughness was uniform across the surface. From this analysis, the following parameters were noted:

- Average: This parameter indicates the average of at least three values for each track considering the maximum peak on the sample surface. For a better representation, see Figure 21.
- Sa average: This parameter is also the result of at least three values for each track. The Sa parameter is calculated by averaging the absolute values of these height deviations from the mean line, which represents the average height of the surface profile. Sa allows for the comparison of surface roughness among different materials, components, or manufacturing processes. By comparing Sa values, it is possible to determine which surfaces are rougher or smoother [68].

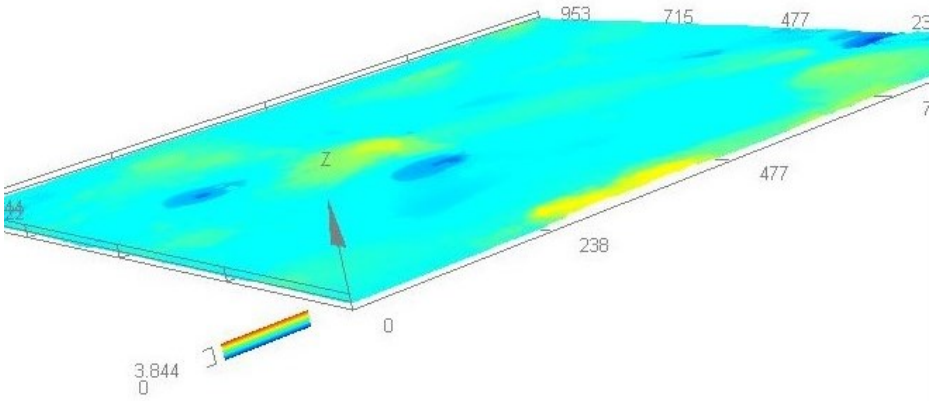

Figure 21- Representation of the peaks and valleys on the CGI plate sample. Sample C track 1, value 4. The surface area is 1mm².

Once it was verified that the distribution of these values was similar without particularly high variances, the samples were weighed. Five measurements were taken to obtain as accurate a result as possible and then the arithmetic mean was performed. The weight measurement is crucial, as weight loss will later be measured after the wear test. For the third material, the brake pad plates, the same methodology as described

above was performed.
The second part concerns the use of pins. Table 2 shows the type of pins, the number of pins available and their nomenclature. Again, the methodology used is similar to that used with plates. While the number of pins is the same for aluminium metal matrix composites with primary aluminium (AMMC1) and for aluminium metal matrix composites with secondary aluminium (AMMC2), when it comes to plates, only AMMC1 is available.

Table 2- Types and number of pins used for the experiments.

Type of pin	Number of pins	Nomenclature
GCI	3	1,2,3
AMMC1	3	A1,A2,A3
AMMC2	3	RA1,RA2,RA3
BP	26	BP1 to BP 26

After performing the wear test on the samples deemed necessary, the weight and surface roughness data will be collected again to compare the pre-wear test and after-wear test situation. To do this, the same methodology used for the pre-wear test will be used.
Another parameter expressing roughness was also measured namely the Ra parameter. This indicator, expressed as a line integral along a profile, unlike the Sa parameter, which is expressed along a surface, was only measured on the GCI and AMMC1 plates before and after the wear tests. Neither the pins nor the BP plates were analyzed. The track was divided into 5 horizontal profiles 5 mm apart and the Ra parameter was measured for each of these profiles. As will be seen later, for the case of the GCI, the surface area removed for each of the profiles was also measured, highlighting the material losses. Graphs were then constructed to relate the Ra value along the length of the analyzed profile. Tests were performed on two lengths. The first is 8 mm and shows the roughness inside the track, while the second is 12.5 mm and includes the parts not involved in the track.

3.1.3 Pin-on-plate wear tests

The first part of the experiments focused on the use of pin-on-plate. In particular, before starting with the experiments, it was of fundamental importance to decide on the configuration and the various variables involved. Table 3 shows the main input used for the PoP wear test.

Table 3- Input for the wear test.

Pin diameter (mm)	8
Plate length (mm)	50 for GCI and AMMC; 45 for BP
Stroke length (mm)	20
Linear speed (mm/s)	50
Time (s)	3600
Use of lubricants	no

Three configurations were performed during the Pin on Plate wear tests. Please note that for each test, both before and after, the Sa and Ra parameters for roughness and relative weight loss were measured.

Configuration 1: This test has as input a load of 108 N with a relative contact pressure of 2 MPa, performed at room temperature. The cylindrical pin consists of BP, while two materials, GCI and AMMC1, were used for the plate.

Configuration 2: This test uses the same inputs and materials as Configuration 1, the only thing that changes is the applied load. In this situation, a load of 50 N with a relative contact pressure of 1 Mpa was used. The purpose of this configuration was to analyse the COF as a function of a change in load.

Configuration 3: In this case, we return to a load of 108N and a contact pressure of 2 Mpa. What is changed are the materials used for the pins and plates. Specifically, the plate is composed of BP, while the pins are composed of GCI, AMMC1, and AMMC2, respectively. The purpose of this test was to plot the COF for AMMC2 as well and compare it with the other materials used previously.

Once the friction force data was obtained for each test, the COF was calculated with Equation 4 and reported with the absolute value. The COF data was then plotted against the test time in seconds. In addition, an average COF was calculated for each test by performing an arithmetic mean taking into account all values collected during the test. Along with the average value, the maximum value assumed by the COF for each configuration was also reported. This was done to provide a more complete analysis. The specific wear rate (K) was also calculated as shown in Equation 5. The value of Δm was obtained by making the difference in weight before and after the test, the value of F_n is given by the configuration, and the value of the sliding distance (s) can be calculated once the number of cycles of the test has been obtained by multiplying this value by the stroke length (S_L). Regarding the density of the materials, the value of cast iron EN GJL 150 is used for the GCI, which has a density of 7,1 g/cm^3, while Equation 8 below was used for the two composites [69]:

$$\rho_c = \rho_m \times V_m + \rho_r \times V_r \quad (8)$$

Where ρ_c is the density of the composite, ρ_m is the density of the matrix (2.7 g/cm^3) and ρ_r is the density of the SiC reinforcement (3.21 g/cm^3). V_m and V_r, on the other hand, represent the volume fractions of the matrix and SiC reinforcement, respectively. These values will later be calculated using the LAS X software for both AMMC1 and AMMC2. The aim is to understand what kind of correlation there is between the COF and the specific wear rate, to understand which material reaches wear faster. Once the test is finished, which will be repeated 3 times for each type of configuration, the size and weight of the emissions generated will be measured.
After the tests, Leica LAS X software was used on the GCI and AMMC1 plates for the following reasons:

- Comparison of roughness parameters: Using the software, the roughness parameters Sa and Ra were recorded to obtain a comparison with previously obtained data. Average values and length-roughness diagrams were reported.
- Obtaining 3-D models: 3-D panoramas were obtained using the software, highlighting the roughness profiles and the part removed from the test.

3.2 LCA analysis

As stated in the previous chapters, conducting an LCA study is necessary to verify the sustainability of disc brake production processes. Having disc brakes made of materials with optimal properties is not enough if the production of these materials is not sustainable for the market. For this reason, it was also necessary to understand the energy consumption and emissions in the mass production of disc brakes by comparing the three types of material also discussed in the previous section, namely GCI, and AMMC with primary and secondary aluminium matrix. The Ansys Granta Selector software was used to do this, in particular, the Eco-Audit function for the following reasons:

- Ease of use: the software allows, through quick training, to create the products under study. In particular, the energy consumed in the various stages of the product life cycle in MJ and the CO2 emitted in kg are returned as output.
- Complete database: The software contains a database with a large amount of data on different materials. This is an aspect that should not be underestimated, as the completeness of the database is a key parameter for a successful LCA study.
- Ease of performing a sensitivity analysis: Conducting a sensitivity analysis is a fundamental part of the LCA study. Varying different parameters to understand how the outputs vary is an essential aspect, and this gives an overall view of the

materials studied.

The materials provided for the wear tests and the data reported thereafter were supplied by AC Floby. Some parameters were fixed during the study, while others were varied. Table 4 below shows the constant parameters for each type of material.

Table 4- Fixed parameters for the LCA study

Parameters/Materials	GCI	AMMC1	AMMC2
Database reference	EN GJL 150	Duralcan Al-20SiC (p) cast F3S20S	Duralcan Al-20SiC (p) cast F3S20S
Mass of one disc (kg)	12,13	3,558	3,558
Recycled content (%)	Typical %	Virgin %	80 %
Primary process	Casting	Casting	Casting
End of life	Recycle	Recycle	Recycle
% recovered	90	70*	70*

For the recycled content, 0 % represents the use of virgin material, where all the feedstock is produced from raw materials. 100 % represents the other extreme, where the material is manufactured entirely from feedstock reclaimed from end-of-life components. Typical % lies between the two extremes and accounts for the level of recycled material incorporated back into the supply chain as standard practice. This applies to materials, such as metals and glasses, where end-of-life recycling has become integrated into the supply chain. This practice leads to standard grades containing significant levels of recycled material. For example, lead alloys generally contain 50–60 % recycled material.

To these data, Transportation must be added as a constant parameter. Specifically, transport is from AC Floby to Volvo Cars Göteborg by truck over a distance of 117 km. The entire study was compared to the energy consumption and emissions of an average-sized electric car. It should be noted that AMMC1 and AMMC2 are practically the same, the only difference being the recycling percentage of aluminium in the matrix.

The parameters that are made to vary are:

- Country of use: depending on the country of use, different results are obtained for both energy consumed, and emissions produced. Continents such as Europe, North America, the Middle East, and Asia were analyzed. When it comes to states, countries such as Italy and Sweden were analyzed.
- Days of use per year

- Kilometers per day
- Product's lifespan

*The recycling rates for AMMC1 and AMMC2 are lower than for GCI. This is due to the problems caused by the SiC reinforcement. Once the matrix of the AMMC has been melted, the separation of the reinforcement particles from the matrix must be carried out. This separation can be done by various methods such as gravity separation. This involves not only additional costs, but also an environmental impact in terms of consumed energy.

4. Results and discussion

4.1 Microstructural characterization

By optical microscope, micrographs of the microstructure were obtained for each material. Figure 22 shows the composition of GCI. It is a lamellar cast iron with the graphite assuming an elongated shape with no preferred direction of development. The percentage of graphite on the surface is 8,74 % with a standard deviation of 1,09, calculated with LAS X image analysis software. In Figure 23, an entirely pearlitic structure composed of alternating ferrite and cementite lamellae can be seen. The presence of elements such as Cu, Ni, Mn, and Sn lead to the formation of perlite, as pearlitising elements as mentioned in the literature. The Brinell hardness obtained is 170 HB.

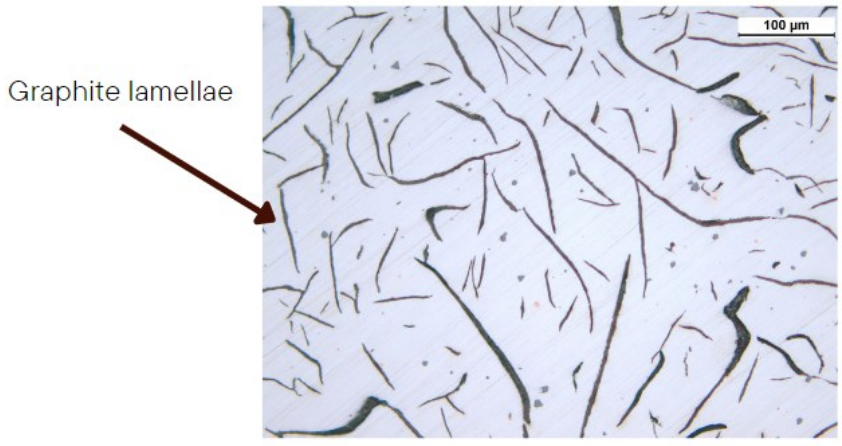

Figure 22- Composition of GCI. Elongated lamellae of graphite can be seen.

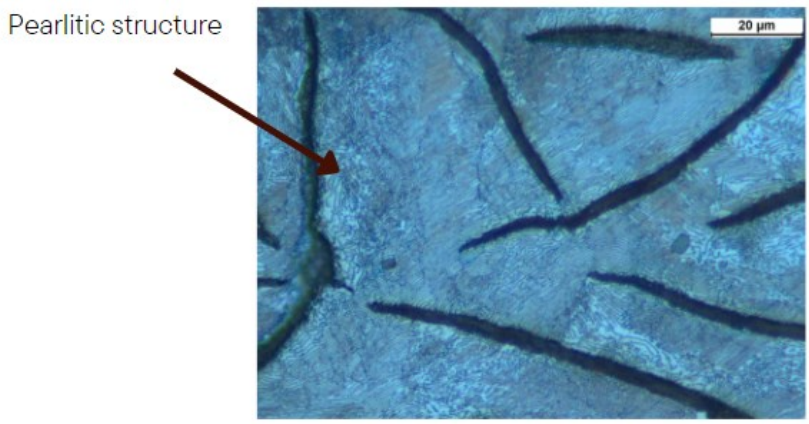

Figure 23- Pearlitic microstructure of GCI.

For AMMC1 and AMMC2, the percentage of reinforcement on the surface of the two materials with LAS X software was calculated. In the first case, it is obtained a percentage of 20,95 % with a standard deviation of 6,33, and in the second case a percentage of around 22,28 % with a standard deviation of 5,04 calculated on several points of the material. In both cases, the mean and standard deviation were calculated by acquiring 25 images. The average particle size of the reinforcement in the two cases was also calculated using the same software to get a more general view. Using the software, regions within the matrix rich in SiC particles were searched for. For these regions, images were taken and the equivalent diameter of the SiC particles was calculated, then averaged and the standard deviation calculated. Initially, the software agglomerated the SiC particles, forming clusters that did not respect the actual particle size, thus increasing the value of the equivalent diameter. For this reason, these clusters were divided using the software's 'image modification' functions to reduce the size of the clusters as much as possible. When the cluster sizes were similar to those of the SiC particles, the equivalent diameter was calculated. For AMMC1 there is an average size of 8,56 µm with a standard deviation of 7,14 while for AMMC2 there is an average size of 10 µm with a standard deviation of 6,51. Figure 24 shows the microstructure of the AMMC1, it is possible to see the reinforcement, the α phase, and the lamellar eutectic composed of Al-Si. Figure 25 instead, shows the microstructure of AMMC2. There is no particular difference between the two materials. 490 particles were counted for the calculation of the equivalent diameter. The particle count as a function of equivalent diameter is shown in Figure 26 for both AMMC1 and AMMC2.

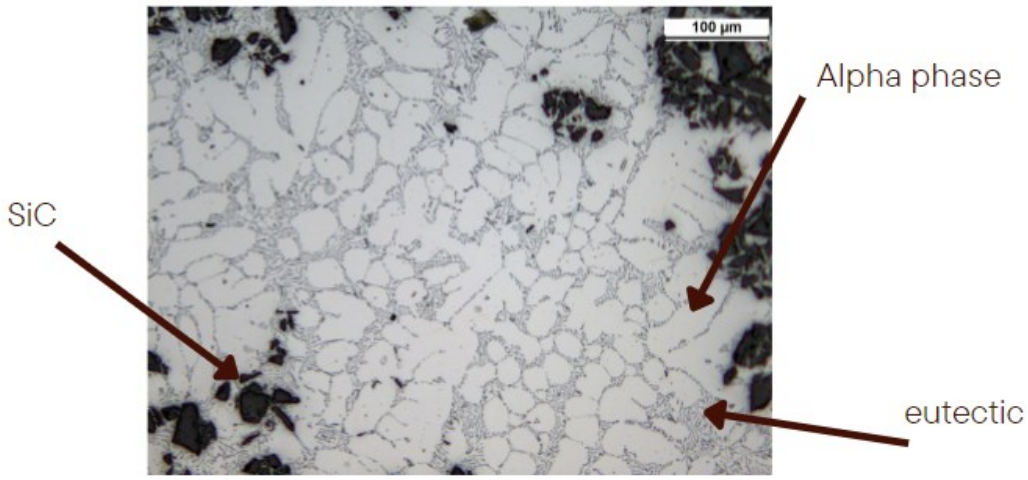

Figure 24- Characterization of AMMC1. The reinforcement percentage is 20,95% and the average particle size is 8,56 µm. Figure shows one of the 25 images taken to calculate the SiC reinforcement percentage.

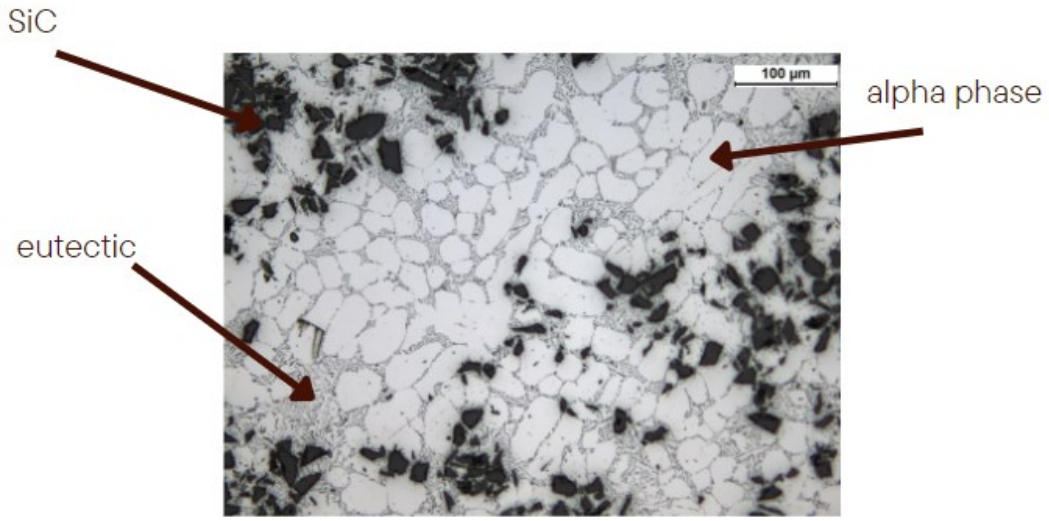

Figure 25- Characterization of AMMC2. The reinforcement percentage is 22,28 % and the average particle size is 10 µm. Figure shows one of the 25 images taken to calculate the SiC reinforcement percentage.

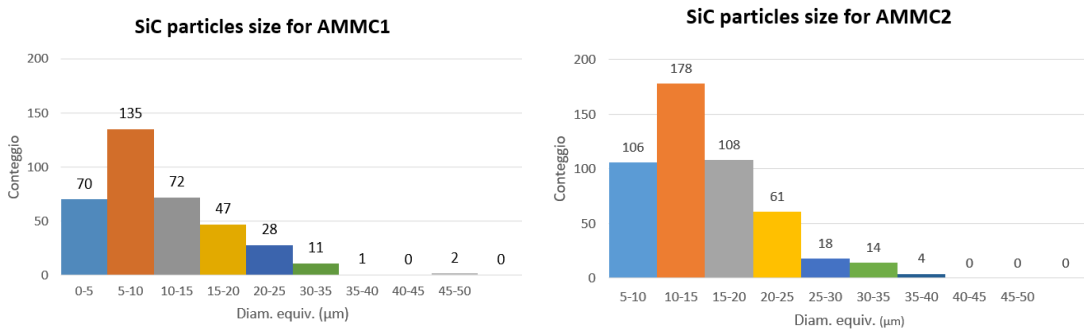

a) b)

Figure 26- Distribution of SiC particle size for: a) AMMC1, b) AMMC2.

4.2 Wear performance

This section analyses the results obtained after the wear test. The following aspects will be examined for each configuration:

- Sa and Ra roughness parameters, analyzing also the removed surface on the plates after the tests for GCI and AMMC1 plates.
- Weight losses.
- The types of wear using SEM microscope and material transfer.
- Average and maximum COF obtained during the tests.

Congifuration 1: Table 5 shows Sa parameter differences for a GCI plate. As can be seen, there was no noticeable change in the surface roughness of the sample. The analysis was continued by dividing the GCI track into 5 profiles equidistant 5 mm from each other as previously written in Chapter 3 Section "Pre Wear Test". The division into profiles allowed the detection of the Ra parameter.

Table 5- Comparisons between Sa parameters before and after wear test for a GCI plate.

Material	Sample	Sa average before the test (µm)	Sa average after the test (µm)
GCI	B	0,2597	0,247
GCI	B	0,264	0,255

Figure 27 relates the Ra parameter on the base material, on the left, and on the track, on the right, for a total length of 8 mm. The Ra value for the base material is 0,259 while the Ra value for the track is 0,237 for the first profile. Also in this case, it can be seen that there was no significant decrease in roughness, yielding a similar result to the previous parameter.

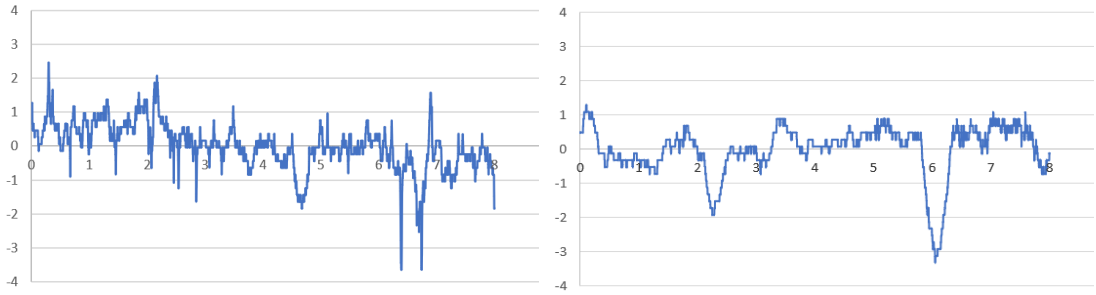

a) b)

Figure 27- Comparison between Ra parameters for a GCI plate: a) base material Ra 0,259, b) on the track, profile number 1 Ra 0,237.

The roughness analysis was continued by detecting the surface area removed for each highlighted profile. Figure 28 shows the surface area removed for several profiles with a total length of 12.5 mm. This length was chosen to include in the analysis both the part of the track, which has a length of 8 mm, and the parts outside the track. The vertical red lines indicate when the track begins and ends. It can be seen that most of the removed surface was found in the center of the track, at profile numbers 2 and 3. Moving towards the ends of the track, the surface area removed is less. Figure 29 instead, shows a 3-D model obtained by Leica software. Only half of the track was analyzed in this situation.

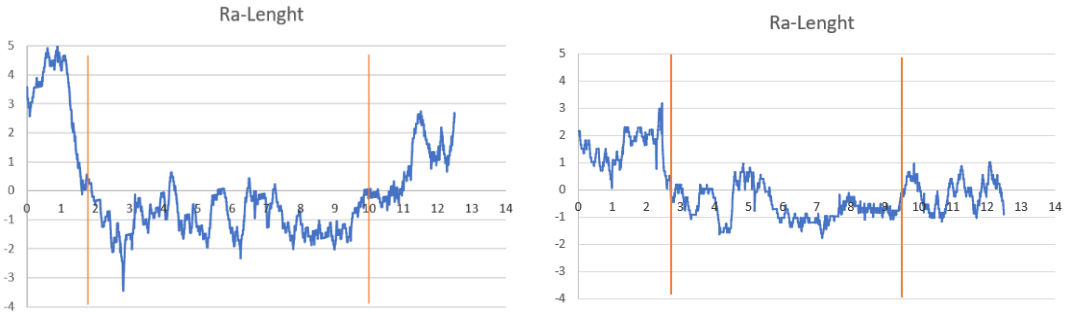

a) b)

Figure 28- Removed surface for different profiles: a) Profile 3 removed surface 13686 μm^2, b) Profile 4 removed surface 92333 μm^2.

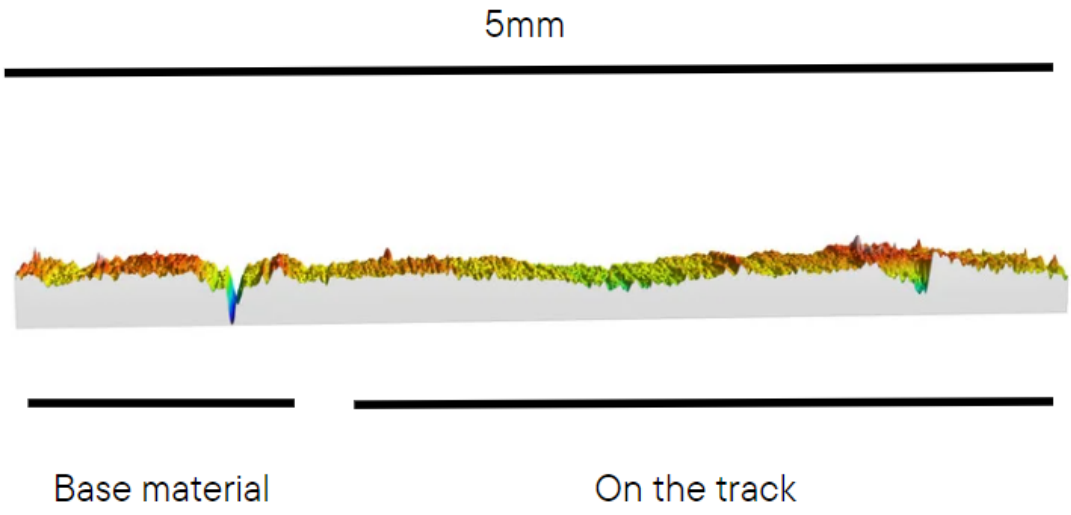

Figure 29- a 3-D model representing the GCI profile. On the left part is possible to see the part not covered by the test, on the right instead, the part covered by Pin on Plate test.

Table 6 shows the weight loss for a GCI plate. This analysis showed that the roughness, both in profile and surface, remained the same. What happened is that during the test, the Pin in BP "dug" into the material. This is confirmed both by the weight loss and debris formation, but also by the fact that material was removed as shown in Figure 28.

Table 6- Weight losses for a GCI plate.

Material	Sample	Weight before (g)	Weight after (g)	Loss (g)
GCI	B track 1	36,88816	36,88504	0,00312
GCI	B track 2	36,88504	36,88144	0,0036
GCI	B track 3	36,88144	36,87768	0,00376

The analysis continued by analyzing the type of wear that occurred during the test in the different materials. For this purpose, the SEM microscope was used to detect the wear tracks, and Pathfinder software was used to understand the material transfer between pins and plates. Figure 30 shows SEM images for a GCI plate on the track. From the tribological parameters used as input, an ultra-mild regime can be excluded, as both the applied load and the sliding speed used for the test turn out to be too high

for this category. The same discussion can also be made for the severe wear regime; this regime also occurs for loads around 108 N but for higher sliding speeds, so this category can also be excluded. It can therefore be said that the test took place under mild regime conditions. As analyzed subsequently, a transfer of material occurred between the BP pin and the GCI plate. Analyzing the chemical composition of the worn surface of the GCI, as shown in Table 8, it is possible to detect a strong presence of O that was not present before the test. This leads to state, that oxidation played an important role during the wear process. It can therefore be stated a wear mechanism appears, namely tribo oxidation wear. This process leads to the formation of an oxide layer on the surface of the test specimens. As analyzed before, material removal occurred on the surface and there was a loss in weight. These factors, together with the fact that the roughness of the material remained the same, describe a type of wear that is not represented by oxidation wear. These indicators lead to the possibility that an abrasive type of wear has occurred. The graphite flakes on the matrix may have caused single-body abrasive wear. The presence of parallel groves, as in Figure 30, is also an indicator that micro-cutting typical of abrasive wear has occurred. In this case, therefore, two main wear phenomena appear namely abrasive and oxidation wear.

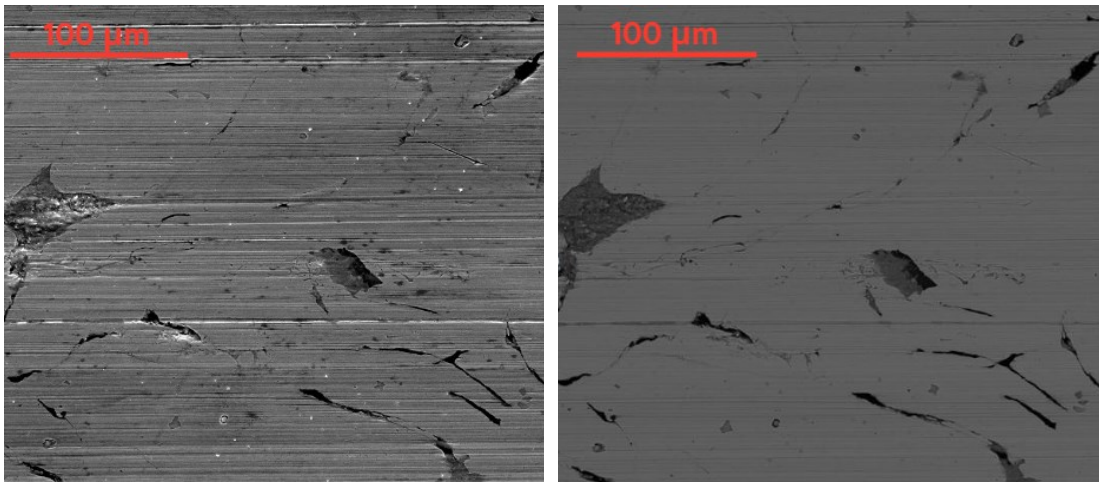

a) b)

Figure 30- SEM images of GCI plate on the track with 1000x magnification: a) SE mode, b) BSE mode.

Pathfinder software was used to understand whether there was material transfer during the test between the pin and the plate. The software reveals the X-rays emitted by the atoms being hit by the electron beam, which allows the chemical composition of the trace to be understood. For the GCI, a point analysis was performed, choosing five

points within the trace to understand its chemical composition. The aim is to understand whether the material that makes up the BP is also present on the plate of GCI and subsequently AMMC1 within this configuration. To do this, SEM images of the BP plate were also collected as shown in Figure 31. Table 7 shows the chemical composition of a BP on the base material. A strong presence of C, O, Si, Ca and Ba is detected. In Table 8 it can be seen the chemical composition of five points measured on the worn surface of the GCI. Material transfer has occurred between the two materials in contact. Point 1 was selected on the matrix, which explains the strong presence of Fe, while point 2 was selected on a graphite lamella, which has a strong presence of C. Points 3, 4 and 5, on the other hand, were chosen on wear traces, in fact in this case, the material transfer is more evident. There are traces of Ba, a typical element used for BP [70] and an increase in Cu. The strong presence of O in the wear traces indicates that oxidation has occurred. As this is a point analysis, an arithmetic mean was not used, as selecting specific points on the material can lead to totally different results. Figure 32 shows the debris collected for the GCI after the test. Again, the Pathfinder software was used to understand the chemical composition of the debris, doing a surface analysis at 4000x magnification. Three detections were carried out and the arithmetic mean of these detections is shown in Table 9. In this case, a strong presence of O can be noticed. It can be seen from Table 9 that the debris is composed of materials from both the GCI such as Fe and C, but also from the BP such as Ba and Ca.

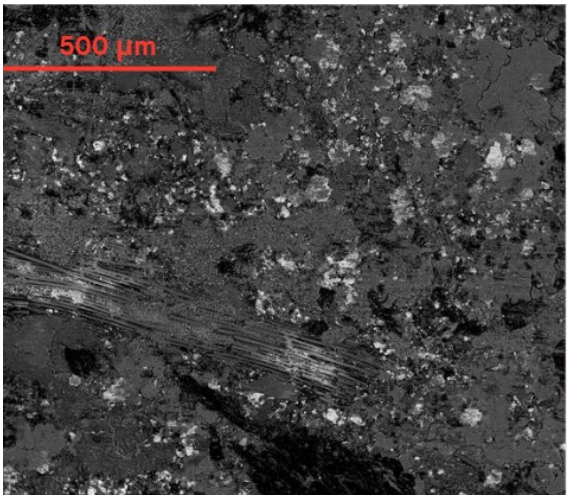

Figure 31- SEM image of a BP plate, base material.

Table 7- Chemical composition of BP base material [wt.%].

	C	O	Mg	Al	Si	S	K	Ca	Fe	Cu	Ba
BP	32,12	33,59	1,91	6,27	6,66	1,75	0,81	3,91	0,97	4,84	7,17

Table 8- Chemical composition of 5 points in GCI plate on the worn surface [wt.%].

	C	O	Mg	Al	Si	S	K	Ca	Fe	Cu	Ba
1	1,41	0,57	-	-	2,11	-	-	-	95,25	-	-
2	34,22	1,24	-	-	1,30	-	-	-	62,47	-	-
3	5,55	31,56	0,63	0,45	2,50	0,91	0,16	0,67	48,49	5,91	2,43
4	3,21	28,03	0,37	0,47	2,10	0,71	-	0,60	59,63	2,32	2,55
5	5,34	27,90	0,64	1,95	2,23	1,15	0,24	0,84	52,44	4,50	2,77

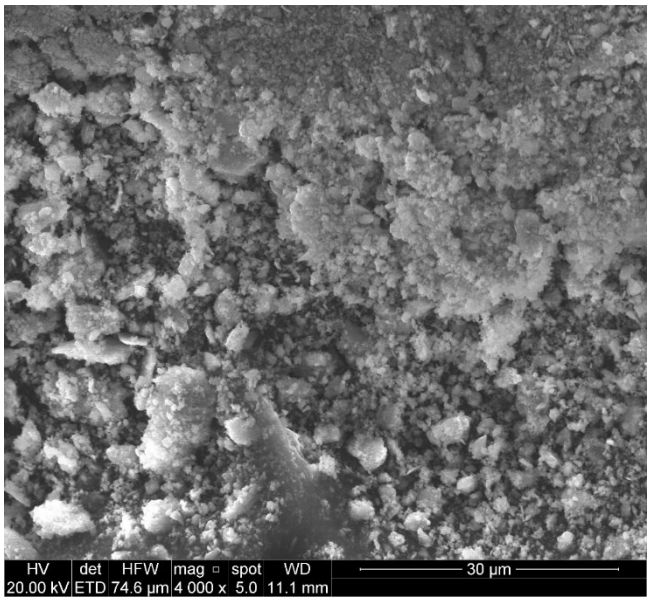

Figure 32- Debris collected at 4000x magnification for GCI.

Table 9- Chemical composition of GCI debris [wt.%].

	C	O	Mg	Al	Si	S	Ca	Fe	Cu	Ba
Average	6,23	26,01	0,75	2,20	3,06	0,99	1,52	48,52	5,78	4,97

The behavior of the AMMC1 is now analyzed within Configuration 1. Table 10 shows the differences in the Sa parameter before and after the test. In this case, it can be seen that this parameter is significantly reduced by half, in contrast to the GCI. In addition, it can also be seen that the starting parameter had much higher values than the GCI.

Table 10- Comparison between Sa parameters before and after wear test for an AMMC1 plate.

Material	Sample	Sa average before the test (μm)	Sa average after the test (μm)
AMMC1	A	0,406	0,183
AMMC1	A	0,683	0,3853

The situation is also similar for the Ra parameter. Using the same profile division for the GCI, it was noted that the roughness of the base material was almost halved after the test. Figure 33 relates Ra for the base material on the left and the track on the right, with a value of 0,571 for the former and 0,251 for the latter, respectively. Figure 34, on the other hand, shows the trend of Ra for a 12.5 mm section covering both the inside and the outside of the track. The Ra value in this case is 0,419 and it is influenced by the base material value on the graph's extremes. In this case, unlike the GCI, there was no surface removed.

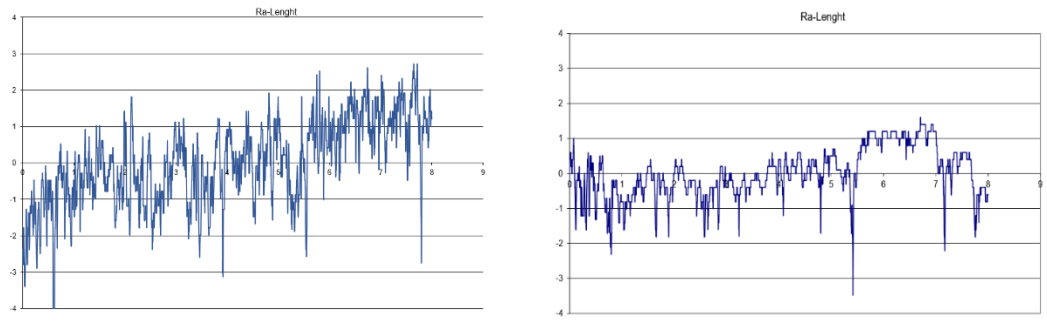

a) b)

Figure 33- Comparison between Ra parameters for an AMMC1 plate: a) base material Ra 0,571, b) on the track Ra 0,251.

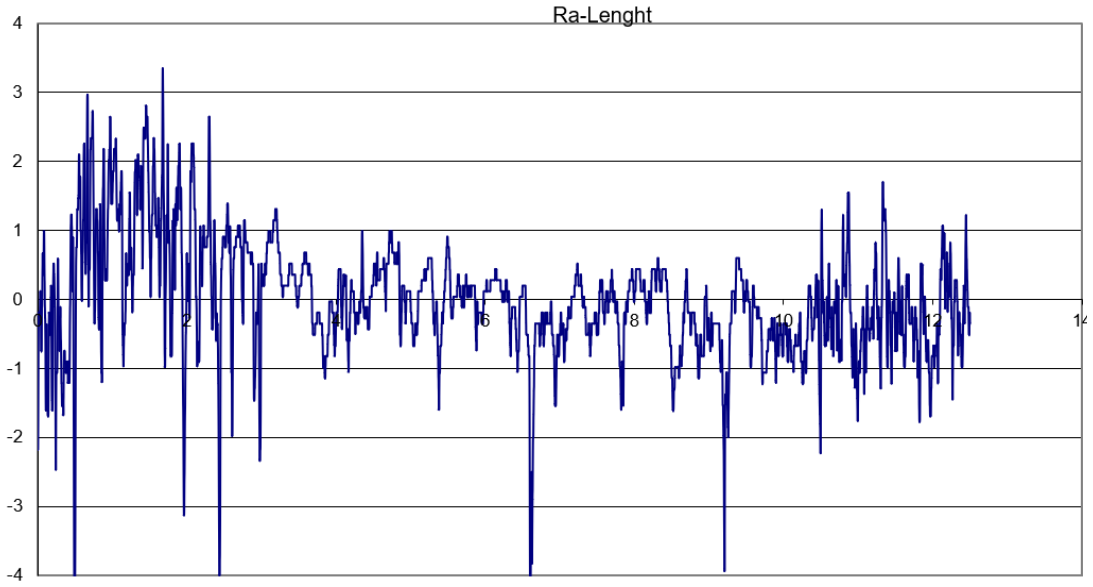

Figure 34- Ra value for an AMMC1 plate. To also cover the parts outside the track, the length was set at 12,5 mm.

Table 11 shows the weight losses of AMMC1. The following considerations emerge from this analysis:

- The weight losses of the AMMC1 plate are at least an order of magnitude lower than those of the GCI.
- In the AMMC1 the roughness was halved, the Pin in BP went to smooth the roughness peaks of the material, making them flatter. On the other hand, in the GCI, the Pin in BP went to "dig" the material, removing the surface and

exporting material.

Table 11- Weight losses for an AMMC1 plate.

Material	Sample	Weight before (g)	Weight after (g)	Loss (g)
AMMC1	A track 1	13,3533	13,35318	0,0001
AMMC1	A track 2	13,35318	13,35316	0,00002
AMMC1	A track 3	13,35316	13,35312	0,00004

Again, SEM and Pathfinder software were used to investigate the type of wear and material transfer. Figure 35 shows the images acquired with the SEM for an AMMC1 plate on the worn surface. It is fundamental to understand what kind of wear regime occurred with the test and the type of wear. From the previous analyses, it was found that there was no surface removal of material, the weight losses were insignificant and the roughness was reduced, smoothing out the peaks of roughness while leaving the valleys untouched. For this reason, it is possible to exclude a severe wear regime, which is characterized by factors that are opposite to those just mentioned. An ultra-mild regime can also be excluded, as the applied load of 108 N is too high for this category. From these conditions, it can be said that the tests took place under mild regime conditions. A typical wear mechanism present in AMMCs under mild regime conditions is delamination wear. This mechanism is often present, especially for conditions of rolling or sliding contact bodies. After repeated cyclic loading, a crack is observed on the subsurface and Figure 36 shows the presence of cracks on the worn surface. The subsurface cracks propagate, connect with other cracks, reach the surface and generate wear particles. Figure 35 shows the presence of irregular pits on the worn surface. As analyzed later, however, a material transfer occurred between the AMMC1 plate and the BP. The presence of parallel grooves may be an indicator of a slight form of abrasive wear. It is therefore possible that two types of wear have occurred simultaneously, delamination wear due to the formation of cracks on the material surface and abrasive wear in lesser form. Both types of mechanisms are among the possible types of wear for an AMMC1 under wear regime conditions. The presence of O on the worn surface was also detected in this case as shown in Table 12. This presence of O, however, appears to be less than that of the GCI obtained previously under the

same conditions. AMMC1 therefore appears to be less oxidised than the GCI.

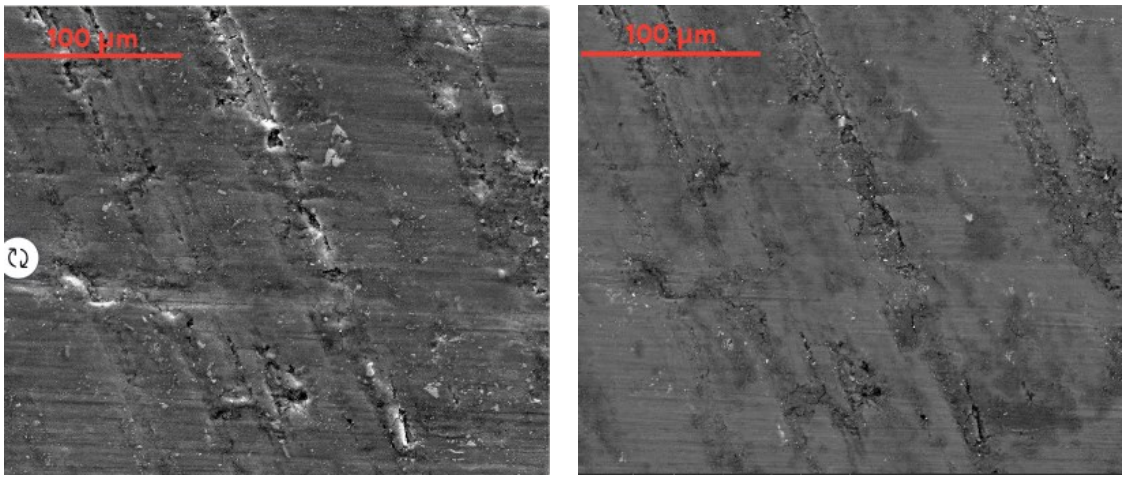

a) b)

Figure 35- SEM images of AMMC1 plate on the track with 1000x magnification: a) SE mode, b) BSE mode.

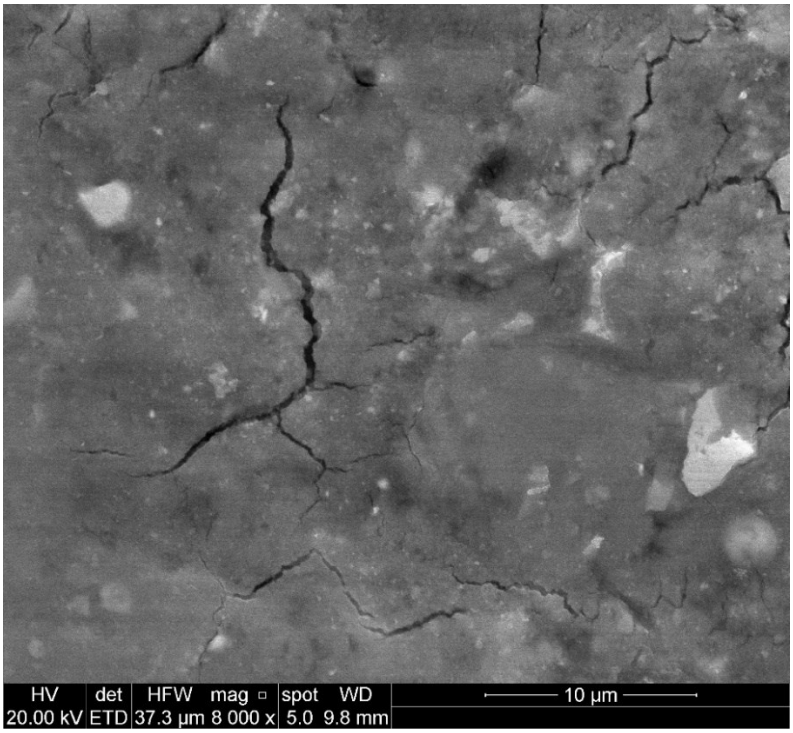

Figure 36- SEM image of AMMC1 plate with 8000x magnification.

Table 12 shows the chemical composition of an AMMC1 plate after a test. For BP, Table 7 previously used for comparison with the GCI is used. In this case, a surface analysis was carried out at 1000x magnification, detecting the composition of three surfaces and calculating the average. Again, a transfer of material took place in particular for elements such as Ba, S and C not originally present in the composition of the AMMC1. These elements were derived from the BP pin used for the test. It is possible to note a lower presence of Ba and Cu and O on the worn surface compared to the GCI. It is possible to state that there is less material transfer for AMMC1 than for GCI. Figure 37 shows the debris of AMMC1 collected after the test and analyzed with the SEM. To compare with the GCI, Pathfinder software was used to understand the chemical composition of the debris. Table 13 shows the average chemical composition of the debris after performing three surface detections at 4000x magnification. Ba and Cu detected on the AMMC1 debris are present in greater quantities than on the GCI debris. The debris in this case could be due more to the decomposition of the BP pin, which released wear particles by wearing against the AMMC1 plate. This can be confirmed by the fact that AMMC1 plate did not suffer any significant weight loss and no surface removal of material was observed. In the case of the GCI, on the other hand, the debris was mainly composed of atoms belonging both to the BP such as Ba, and belonging to the GCI such as Fe. In the case of AMMC1, the collected debris was found to have a higher O content than the GCI debris. Figure 38 shows a scheme of the PoP tool after a test. It is possible to notice wear debris randomly distributed around the surface of the track and on the surface of the plate used.

Table 12- Chemical composition of AMMC1 plate on the worn surface [wt.%].

	C	O	Mg	Al	Si	S	Ca	Cu	Ba
AMMC1	15,31	14,36	0,31	55,11	16,31	0,32	0,34	0,35	0,61

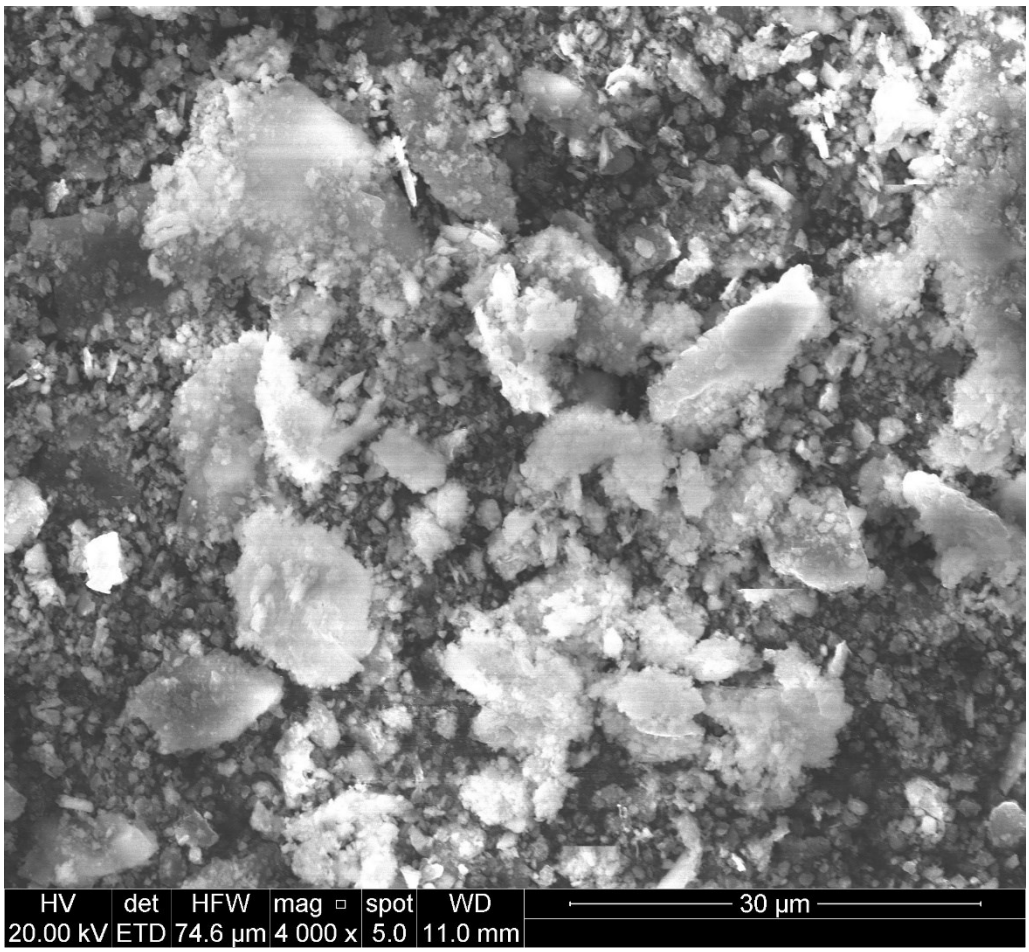

Figure 37- Debris collected at 4000x magnification for AMMC1 plate.

Table 13- Chemical composition of AMMC1 debris [wt.%].

	C	O	F	Mg	Al	Si	S	K	Ca	Cu	Ba
Average	21,51	39,06	2,14	1,53	12,90	3,78	1,78	0,59	2,39	5,77	6,18

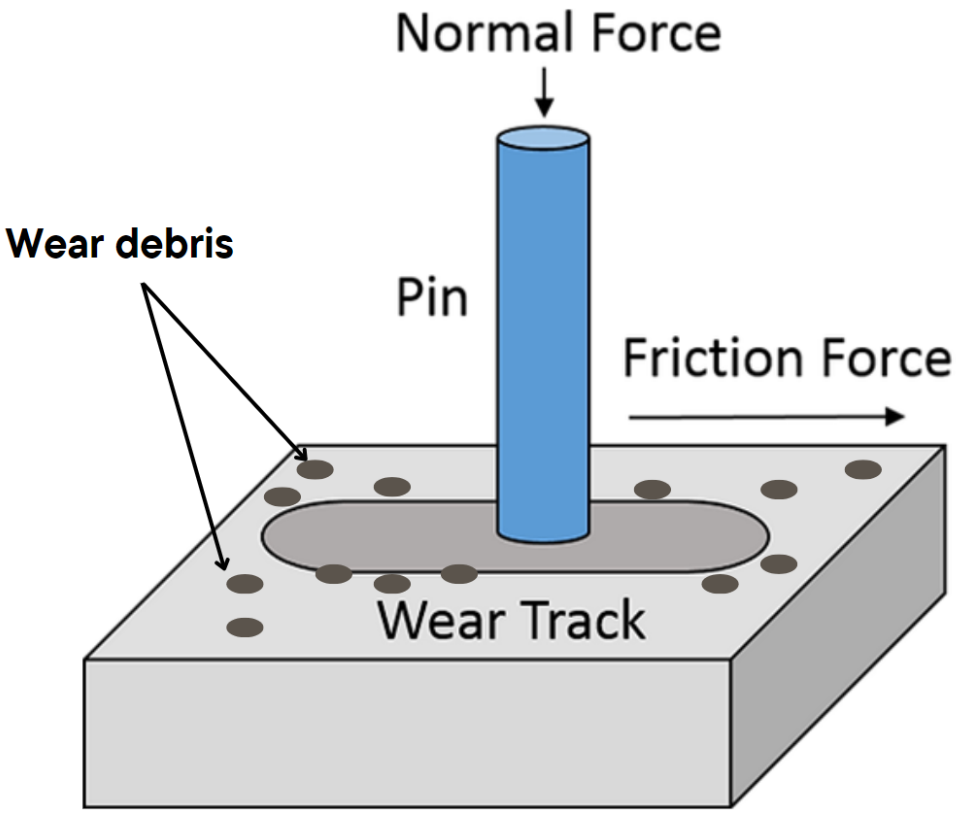

Figure 38- Schematic representation of the Pin on Plate instrument following a test.

Before examining the next configuration, the behavior of the COF during the test must be analyzed. Figure 39 shows COF-Time graphs for AMMC1 plate and GCI plate. The former presents an average COF of 0,111 while the latter of 0,152. Both average COFs were calculated taking into account all the values measured during the test. Not only is the COF of the GCI higher than the COF of the AMMC1, but also the trend in the graphs is different. In the case of the AMMC1, the COF has a linear increasing trend and then stabilizes; in the case of the GCI, on the other hand, this trend is not present, as increasing and decreasing trends follow one another. The maximum value assumed by the function in both cases was also calculated. For AMMC1, a peak value of 0,231 is reported, while the GCI has a maximum value of 0,331. Equation 4 was used to calculate the specific wear rate (K) while Equation 8 was used to calculate the AMMC1 composite density. The value of V_r is 20,95 %, corresponding to the percentage of SiC calculated in the previous paragraph using the LAS X software. Table 14 shows the values used for the calculation of K. AMMC1 turns out to have a K one order of magnitude lower than that of the GCI. This means that, inside the same configuration, AMMC1 turns out to have milder wear than the GCI. Table 15 summarises the COF and

K values obtained for this test.

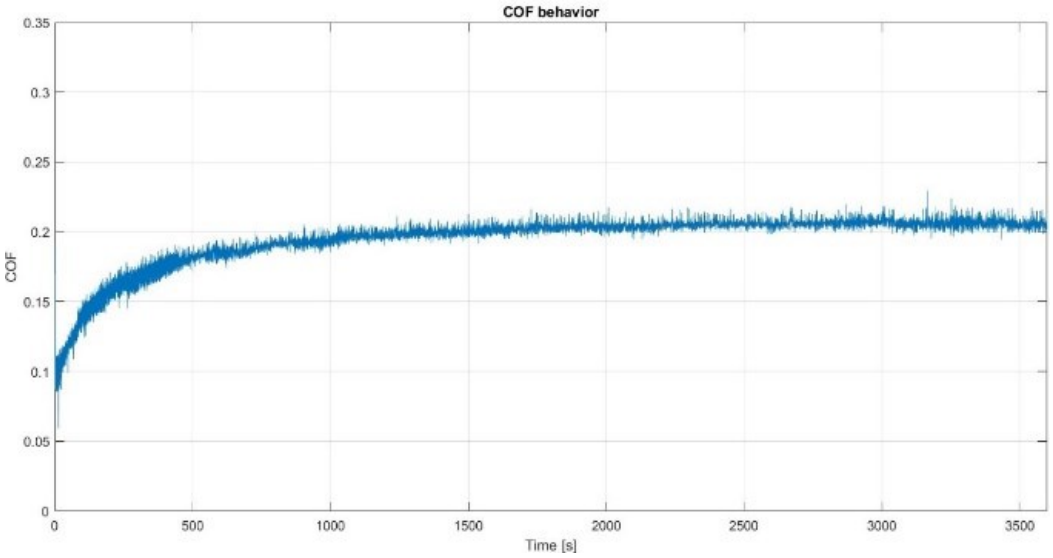

a)

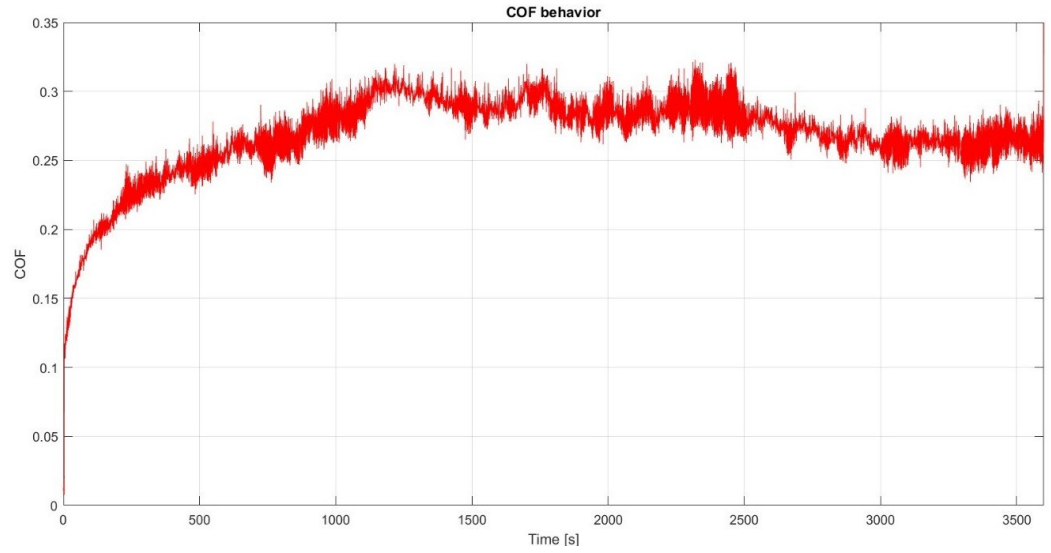

b)

Figure 39- Configuration 1 COF-Time graphs: a) for an AMMC1 plate, b) for a GCI plate.

Table 14- Values used for calculating the specific wear rate (K).

	AMMC1	GCI
Δm (g)	0,0004	0,00312
F_n (N)	108	108
s (m)	149,28	149,28
ρ_r	3,21	-
ρ_m	2,70	7,1
V_r (%)	20,95	-
V_m (%)	79,05	-
ρ_c	2,81	-

Table 15- Comparison between AMMC1 and GCI in terms of COF and specific wear rate (K) at 108 N.

	Average COF	Maximum COF	K
AMMC1	0,111	0,231	$8,84E^{-7}$
GCI	0,152	0,331	$2,73E^{-5}$

Configuration 2: As stated in Chapter 3 “Pin on Plate wear test” Configuration 2 uses the same materials as Configuration 1, the only difference is the applied load and consequently the contact pressure. In this case, the applied load is 50 N instead of 108 N. Starting with the GCI, Table 16 shows the different values assumed by the Sa parameter before and after the test. In this case, unlike the previous configuration, this parameter decreased strongly. The same behavior also occurred for the Ra parameter, thus showing a different behavior to that of the previous configuration. Figure 40 shows the Ra parameter for the base material on the left and the track on the right.

Table 16- Comparisons between Sa parameters with 50 N applied load for a GCI plate.

Material	Sample	Sa average before the test (µm)	Sa average after the test (µm)
GCI	C	0,2545	0,072
GCI	C	0,4773	0,046

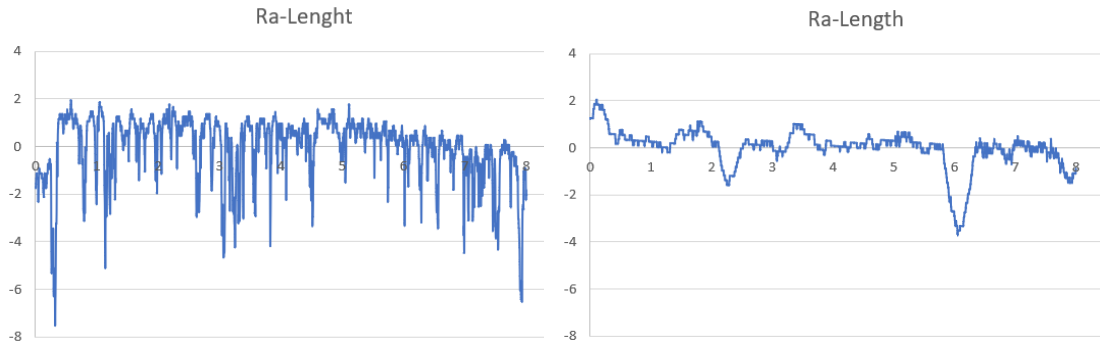

a) b)

Figure 40- Ra parameter comparisons with 50 N applied load for a GCI plate: a) base material Ra 0,637, b) on the track Ra 0,206.

Table 17 shows the weight losses for the GCI plate subjected to a load of 50 N. It can be seen that these losses are an order of magnitude lower than those for Configuration 1. As the applied load decreases, the weight loss decreases, and this is confirmed by the fact that no debris can be collected and no surface is removed. The BP pin, in this case, did not dig into the material as it did previously but simply reduced the roughness peaks. The negative loss value in the table may be due to an error when weighing the samples or it may be due to oxidative phenomena that led to an increase in the weight of the sample after the test.

Table 17- Weight losses for a GCI plate with 50 N as applied load.

Material	Sample	Weight before (g)	Weight after (g)	Loss (g)
GCI	A track 3	38,9088	38,90696	0,0019
GCI	C track 1	37,0304	37,03064	-0,0002
GCI	C track 2	37,03064	37,03006	0,0006

Analyzing the type of wear that has occurred, Figure 41 shows SEM images of GCI with 50 N as applied load. The presence of parallel groves is an indicator that micro-cutting typical of abrasive wear has occurred. The load is still too high to speak of the ultra-mild regime, so mild-regime wear has also occurred in this case. No debris was collected and the weight losses are smaller than in Configuration 1. It is therefore possible that abrasive wear has also occurred in this case, but milder than with a load of 108 N. Lowering the load therefore also reduced the effect of wear on the worn surface. Through analysis with the Pathfinder software, it can be seen that no material transfer occurred. As in the case of the GCI of the previous configuration, a point analysis was carried out on 5 points within the worn surface. It can be seen from Table 18 that elements such as Ba Ca and Al, which were previously present on the worn surface of the GCI, are now absent. These elements, as shown in Table 7, are part of the chemical composition of BP. When analyzing Table 18, the strong presence of O on the trace can be detected. This may indicate that a tribo-oxidation type of wear occurred as in Configuration 1 for the GCI. However, the presence of O is less than previously obtained. It can therefore be said that by lowering the load, the abrasive and tribo-oxidation wear is less severe.

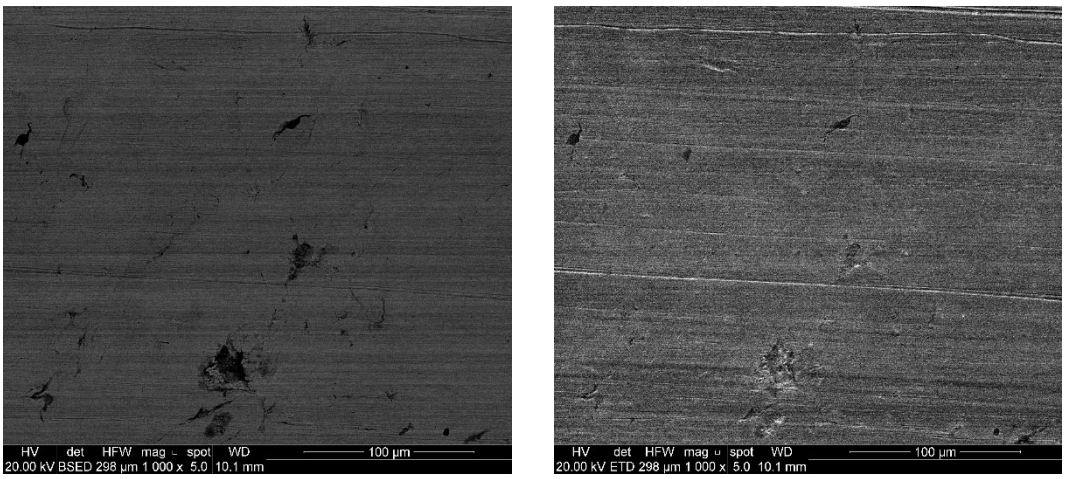

a) b)

Figure 41- SEM images for a GCI plate at 50 N: a) BSE mode, b) SE mode.

Table 18- Chemical composition of 5 points in GCI plate on the worn surface [wt.%].

	C	O	Si	S	Mn	Fe	Cu
1	1,16	23,17	1,21	0,36	-	71,67	2,42
2	13,66	5,68	1,16	-	1,29	71,24	-
3	3,12	27,06	1,38	0,51	-	67,93	-
4	1,73	-	2,00	-	-	96,27	-
5	1,76	2,31	2,09	-	-	93,84	-

Turning to the analysis of the AMMC1, in Table 19 can be seen the differences in the Sa parameter. Again, exactly as in Configuration 1, there was a reduction in this parameter by approximately half. The behavior is similar for the Ra parameter, as shown in Figure 42. The base material has a Ra value of 0,516, on the other hand, the Ra value inside the track is 0,237.

Table 19- Sa parameter comparisons with 50 N applied load for an AMMC1 plate.

Material	Sample	Sa average before the test (μm)	Sa average after the test (μm)
AMMC1	B	0,5453	0,26
AMMC1	B	0,672	0,36

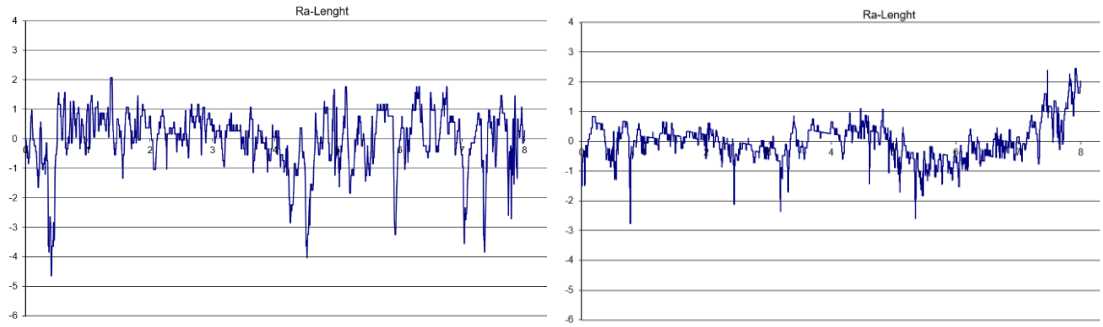

a) b)

Figure 42- Ra comparisons with 50 N applied load for an AMMC1 plate: a) base material Ra 0,516, b) on the track, profile number 1 Ra 0,237

Table 20 shows the weight losses for an AMMC1. By decreasing the load, it can be seen that weight losses increased, in contrast to what happened to the GCI. Again, negative weight loss values may be due to errors with the measuring instrument, or they may be due to oxidative phenomena that affected the material during and after the test.

Table 20- Weight losses for an AMMC1 plate with 50 N applied load.

Material	Sample	Weight before (g)	Weight after (g)	Loss (g)
AMMC1	B track 1	14,4919	14,49288	-0,0010
AMMC1	B track 2	14,49288	14,49264	0,00024
AMMC1	C track 1	13,8759	13,87624	-0,0004

Studying the wear mechanisms, Figure 43 shows the images obtained with the SEM microscope for AMMC1 at 50 N. On the worn surface, pits and voids can be seen, although they are less pronounced than in Configuration 1. Once again, mild-regime

wear occurs as the applied load is still too high to speak of an ultra-mild wear regime. In this case, cracks can be detected on the worn surface, thus establishing that delamination wear has occurred. Figure 44 shows the cracks obtained on the worn surface for AMMC1 at 108 N on the left, and at 50 N on the right, at 120000x magnification. The crack dimension appears to be smaller than that obtained with the 108 N load. The same type of wear therefore occurred, forming cracks on the worn surface, only these appear to be smaller in size than in the previous configuration. The Pathfinder software was used to determine whether material transfer had occurred by performing three surface analyses and calculating the arithmetic mean of the values found. Table 21 shows the results of the analysis. Elements such as Ba and Ca, which are typical for the composition of BP as shown in Table 7, are not present on the worn surface of the AMMC1. For both GCI and AMMC1 at 50 N, therefore, no material transfer occurred, while for the Configuration at 108 N, material transfer occurred in both cases. The O level present in Table 21 is very similar to the O level present in Table 12 with a load of 108 N. By changing the load, therefore, the oxidation level of the material did not change and it is still lower than the GCI with both the 50 N load and the 108 N load.

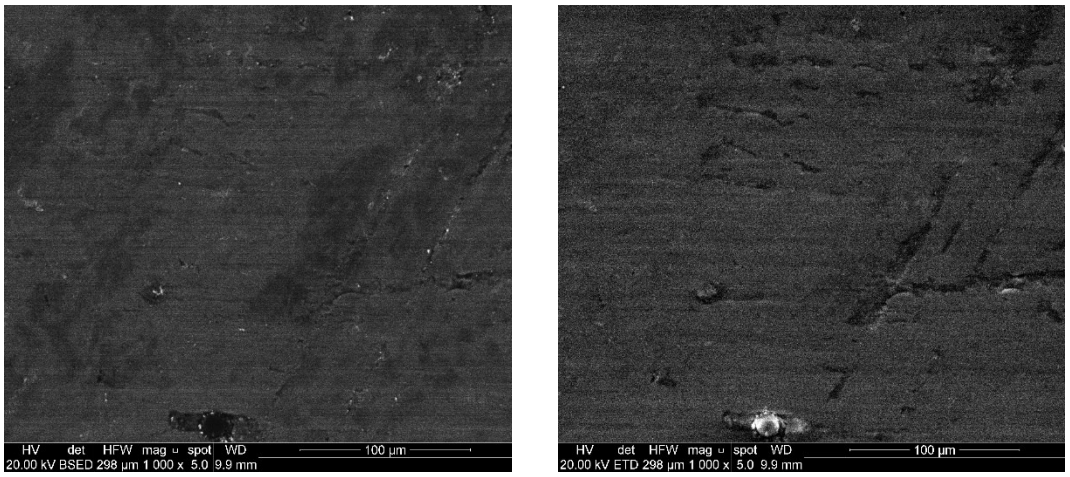

a) b)

Figure 43- SEM images for an AMMC1 plate at 50 N: a) BSE mode, b) SE mode.

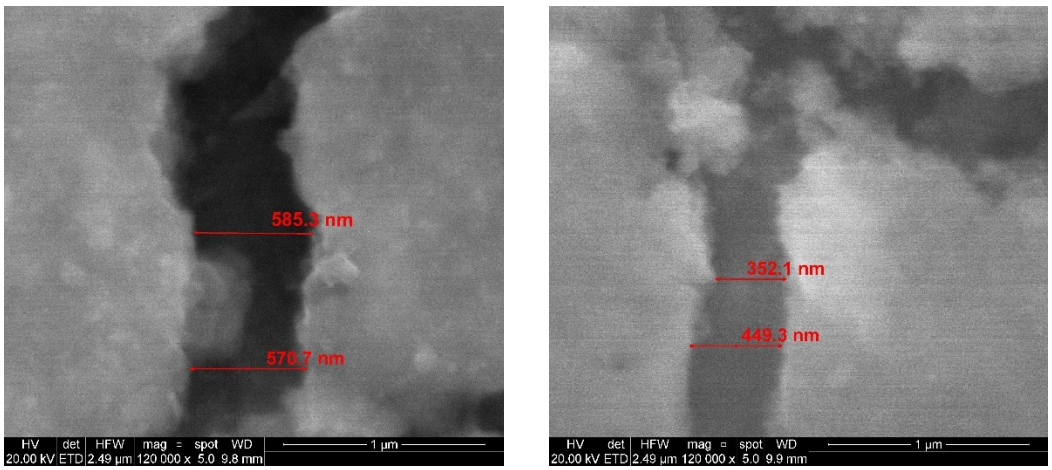

a) b)

Figure 44- Crack length comparisons at 120000x magnification for: a) AMMC1 at 108 N, b) AMMC1 at 50 N.

Table 21- Chemical composition of AMMC1 plate on the worn surface [wt.%].

	C	O	Mg	Al	Si
Average	5,70	14,94	0,50	53,75	25,10

Before moving on to the last configuration, it is necessary to compare the COF to see how the materials responded to a test with a different load. Exactly like Configuration 1, the COF was related to the test time expressed in seconds. Figure 45 shows the COF trend for AMMC1 plate and for a GCI plate. The GCI appears to have a higher average COF than the AMMC1 plate in this case as well. For AMMC1, an average COF of 0,086 was obtained; while for GCI, an average value of 0,115 was obtained. By lowering the load, both materials obtained a decrease in the average COF. Also in this case, the maximum value assumed by the function was calculated. For AMMC1, a maximum value of 0,235 was obtained; for GCI, 0,222. In contrast to the previous test, the maximum values assumed by the functions are very close, with AMMC1 having a higher maximum value than the GCI. Again, the GCI exhibits different behavior from the AMMC1. The former has a non-constant developmental trend, while the latter is characterized by linear growth during the test. For the calculation of K, parameters such as total sliding distance and density remained unchanged. The load changed from

108 N to 50 N, and the weight losses also differed. A weight loss of 0,00024 g was chosen for AMMC1 and 0,0006 g for GCI. Table 22 shows the results obtained for this configuration. In this case, in contrast to Configuration 1, the two specific wear rates are very similar and belong to the same order of magnitude. Thus, by lowering the load, the wear behavior of the materials is more similar than for high loads. For AMMC1, lowering the load lowered the COF, but the specific wear rate increased by almost an order of magnitude.

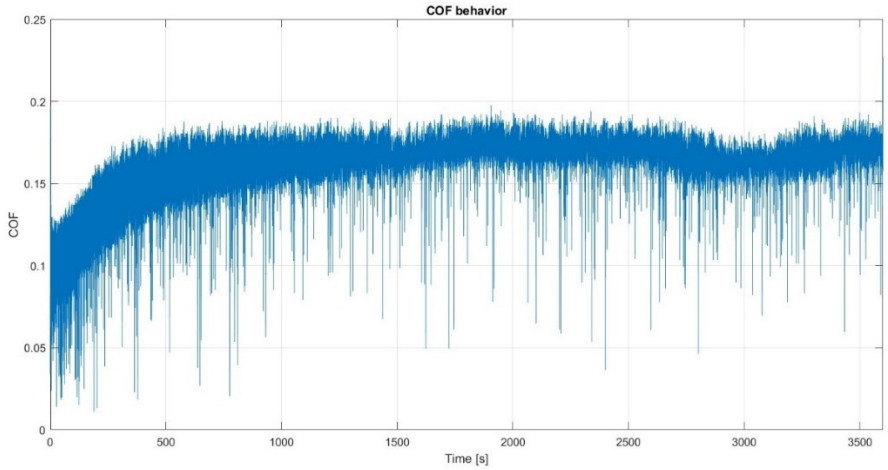

a)

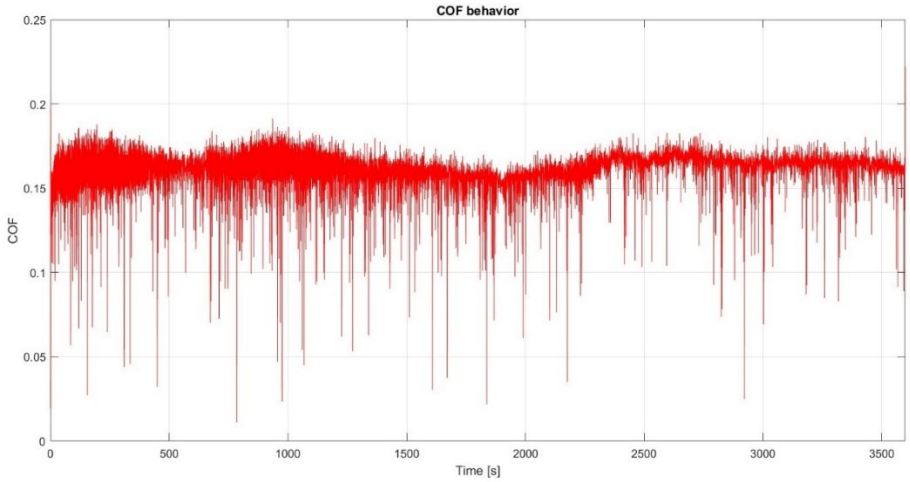

b)

Figure 45- COF comparisons for a 50 N test: a) for an AMMC1 plate, b) for a GCI plate.

Table 22- Comparison between AMMC1 and GCI in terms of COF and specific wear rate (K) at 50 N.

	Average COF	Maximum COF	K
AMMC1	0,086	0,235	1,14 E^{-5}
GCI	0,115	0,222	1,13 E^{-5}

Configuration 3: In this case, a 108 N load was applied exactly as with Configuration 1. Now, however, the materials from which the plates and pins are made are reversed. BP is used for the plates, while AMMC1, AMMC2, and GCI are used for the pins. This configuration, as mentioned in Chapter 3 "Pin on Plate wear test" serves to study the behavior of the AMMC2, which was not present in the previous configurations. Table 23 shows the Sa values for the three metal pins. From this table, it can be seen that the behavior of the Sa parameter before and after the test is similar to that of Configuration 1. In particular, in the AMMC1, the value of Sa is more than halved, while the GCI shows a smaller increase. The behavior of AMMC2, on the other hand, is similar to that of AMMC1. In this case, the Ra parameter was not measured, as it was not possible to profile the roughness on the cylindrical pins.

Table 23- Sa comparisons for different metallic Pins.

Material	Sample	Sa average before the test (μm)	Sa average after the test (μm)
AMMC1	A3	1,544	0,789
AMMC2	RA3	1,303	0,727
GCI	3	0,598	0,603

Table 24, on the other hand, shows the weight losses for the metal pins analyzed. Again, it can be seen that the weight losses for GCI are an order of magnitude higher than those for AMMC1 and AMMC2. Thus, results similar to Configuration 1 were obtained, despite inverted materials.

Table 24- Weight losses for metallic pins.

Material	Sample	Weight before (g)	Weight after (g)	Loss (g)
AMMC1	A3	2,30586	2,3058	0,00006
AMMC2	RA3	2,67966	2,67964	0,00002
GCI	3	6,0535	6,05332	0,0018

Figure 46 shows SEM images for an AMMC2 pin on the worn surface. As in Configuration 1, the test was performed under mild regime conditions. Pathfinder software was used and a surface analysis was performed by averaging over three detections. In this case, a material transfer occurred between the pin of AMMC2 and the BP plate as shown in Table 25. However, no debris was collected as a result of the test and the transferred material was smeared on the worn surface. It can therefore be assumed that smearing wear occurred on the surface. Also in this case there is a presence of O that was not present before the test. This may indicate that tribo oxidation wear has occurred. Using the same BP composition as in Table 7, Table 25 shows the chemical composition of an AMMC2 pin on the worn surface. For comparison with AMMC1, Table 12 is also shown. In the case of AMMC2, the presence of Fe can be seen, which is not present in AMMC1. This is since the aluminium that makes up the matrix of the AMMC2 is made from recycled material in which Fe is present as an inclusion. Elements such as Cu and Ba, on the other hand, are present in higher quantities on the AMMC2 than on the AMMC1. On the other hand, an element that is less present on the AMMC2 than on the AMMC1 is O.

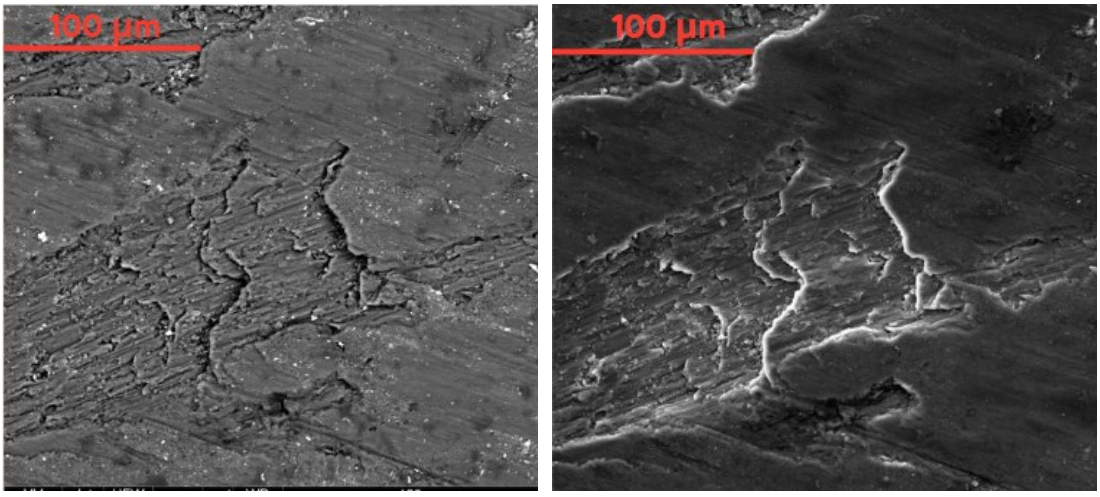

a) b)

Figure 46- SEM images of AMMC2 pin on the track with 1000x magnification: a) BSE mode, b) SE mode.

Table 25- Chemical composition of AMMC2 pin on the worn surface with 108 N as applied load [wt.%].

	C	O	Mg	Al	Si	S	K	Ca	Fe	Cu	Ba
AMMC2	13,85	12,41	0,75	53,94	10,4	0,88	0,28	0,95	0,42	3,1	2,90

Table 12- Chemical composition of AMMC1 plate on the worn surface with 108 N as applied load [wt.%].

	C	O	Mg	Al	Si	S	K	Ca	Fe	Cu	Ba
AMMC1	8,47	17,21	0,28	53,52	17,97	0,39	-	0,39	-	0,55	1,22

Again, the COF was derived. Figure 47 shows the COF trend for an AMMC2 pin against a BP plate. For the AMMC1 and GCI, similar trends are obtained as for the previous configurations with a higher average COF for the GCI than for the AMMC1. The COF of the AMMC2, on the other hand, is lower than that of the AMMC1, presenting similar behavior. The maximum COF value was obtained with the GCI with a value very similar to that of Configuration 1. The same result also applies to AMMC1; AMMC2, on the

other hand, was found to behave very similarly to AMMC1. In this case, a value of 22.28 % was used to calculate the density of the AMMC2 for the percentage of reinforcement previously measured with the LAS X software. The other parameters, except for the load, which returns to 108 N, remain unchanged. For the weight losses, the data in Table 24 were used. Table 26 shows different COF and K values for the metal pins used during this configuration. It can be seen, that the results for AMMC1 and GCI are very similar to those of Configuration 1, although the plates and pins are reversed. AMMC1 always has a K that is an order of magnitude lower than the GCI. AMMC2, on the other hand, has the lowest K value of the three materials in the configuration, slightly lower than AMMC1.

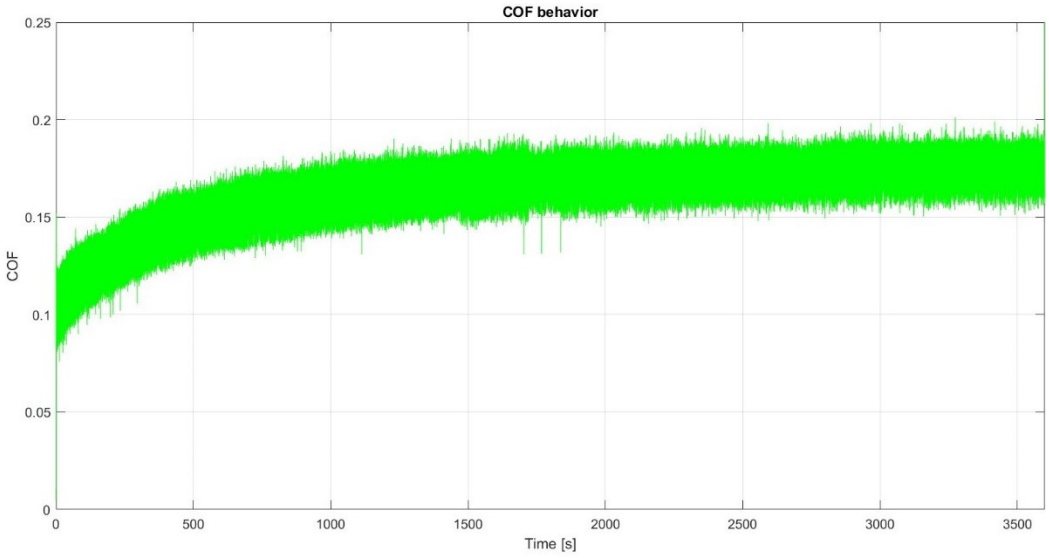

Figure 47- COF behavior for an AMMC2 pin.

Table 26- Different COF and K values for metallic pins in Configuration 3.

	Average COF	Maximum COF	K
AMMC1	0,103	0,269	1,32 E^{-9}
AMMC2	0,093	0,270	4,41 E^{-10}
GCI	0,121	0,354	1,57 E^{-8}

After the test, LAS X software was used to compare the pins of AMMC1 and AMMC2.

Figure 48 relates the pin matrix of AMMC1, on the left, and AMMC2, on the right, used in Configuration 3. The main difference between the two pins is in the shape the eutectic took at the end of the test. In the case of AMMC1, the eutectic appears more jagged, while in the second case, it appears more agglomerated. In both cases, the presence of Fe can be found, due to the BP plate. The alpha phases in both composites remained unchanged.

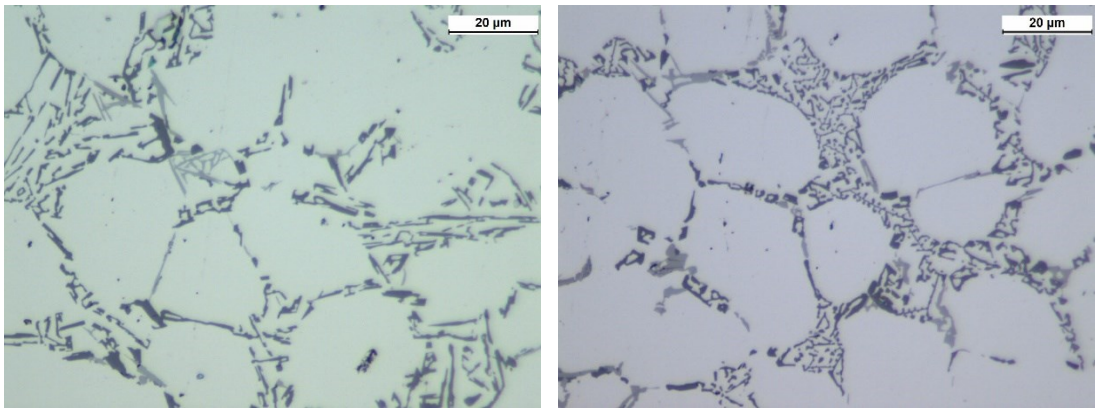

a) b)

Figure 48- Pin matrix comparisons in Configuration 3: a) AMMC1 matrix, b) AMMC2 matrix.

Figure 49 shows the wear tracks obtained with Configuration 1 under a load of 108 N. The images were made with the "Panorama" function of the Olympus optical microscope. Figure 50 instead, shows the worn surface of the metal pins used in Configuration 3. Again, the images were obtained with the same function as before. It can be seen, especially in the case of the AMMC1 and AMMC2, that the track is not present on the entire pin surface. In particular, only one part of the surface has been subjected to wear, leaving the other part unconsumed. This may be due to the contact surface between the pin and plate. It is possible that the surface was not entirely flat, thus creating preferential contact zones between the materials.

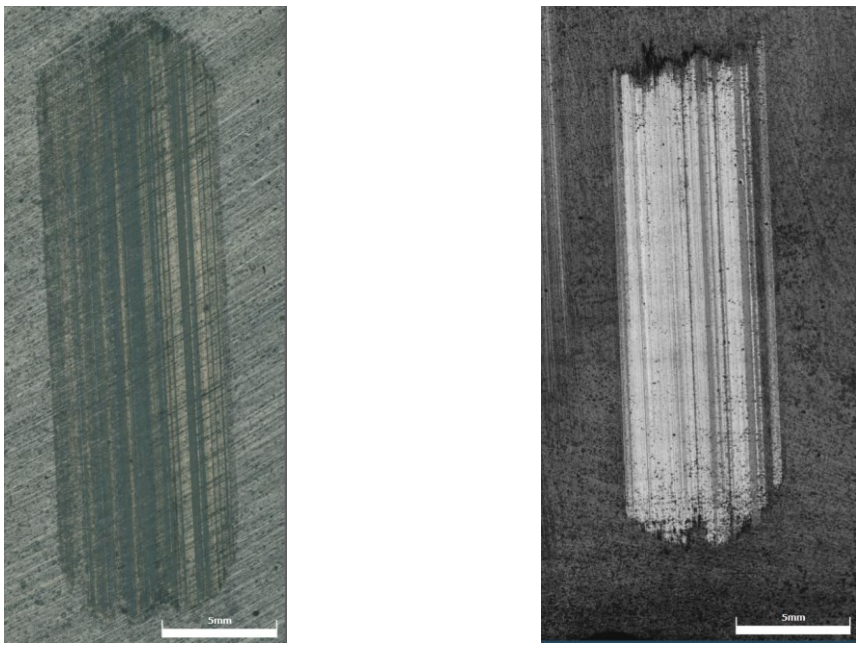

a) b)

Figure 49- Configuration 1 wear track: a) on AMMC1 plate, on GCI plate.

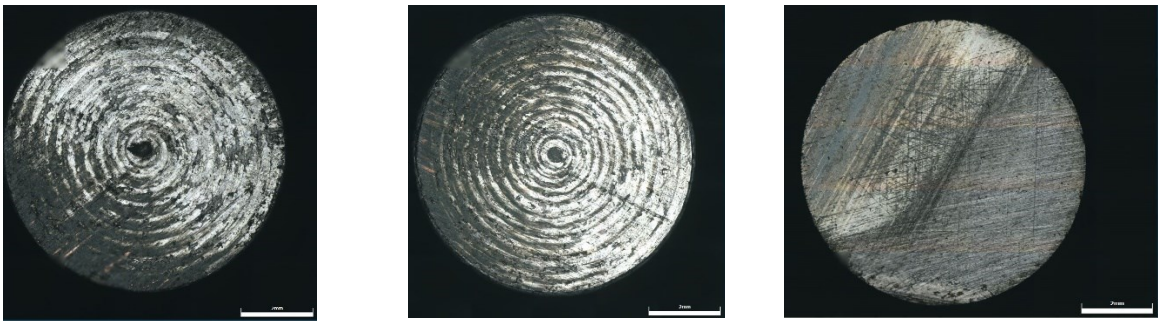

a) b) c)

Figure 50- Configuration 3 wear track: a) on AMMC1 pin, b) on AMMC2 pin, c) on GCI pin.

4.3 Life cycle assessment

This section analyses the data obtained as a result of the LCA study in terms of energy consumed and CO2 emitted. The results of the GCI, AMMC1 and AMMC2 are presented for the different phases that make up the stages of the product life cycle as described in Chapter 2 "Life Cycle Assessment". The two phases analyzed in more detail are "Material extraction" and "Use". The remaining phases, namely

"Manufacture", "Transport" and "Disposal" will not be analyzed in detail for the following reasons:

- There are no substantial differences between GCI, AMMC1 and AMMC2.
- These phases are responsible for only a small fraction of the CO2 emitted and energy consumed compared to the 'Material extraction' and 'Use' phases for all materials examined.

For each step, therefore, the energy consumed and emissions generated are reported. Starting with the study of the "Material extraction" phase, Table 27 shows the results obtained from the analysis.

Table 27- Material extraction phase data.

Material	Energy consumption (MJ)	CO_2 emissions (kg)
GCI	1130	85
AMMC1	2779	195
AMMC2	552	39

The energy used for the material extraction phase turns out to be higher for AMMC1 than for GCI. This result is a direct consequence of the aluminium production process, which is more energy-intensive than the process of producing GCI as shown in the Literature. Due to the high percentage of recycled material in AMMC2, this is more convenient in terms of sustainability than AMMC1. A recycling percentage of 80 % was set, which constitutes the aluminium matrix part, the other 20 % is the SiC reinforcement. The same reasoning can also be applied to CO_2 consumption.
The values obtained in Table 27 are independent of the country of use and the kilometers traveled. Figure 51 shows the results of the analysis.

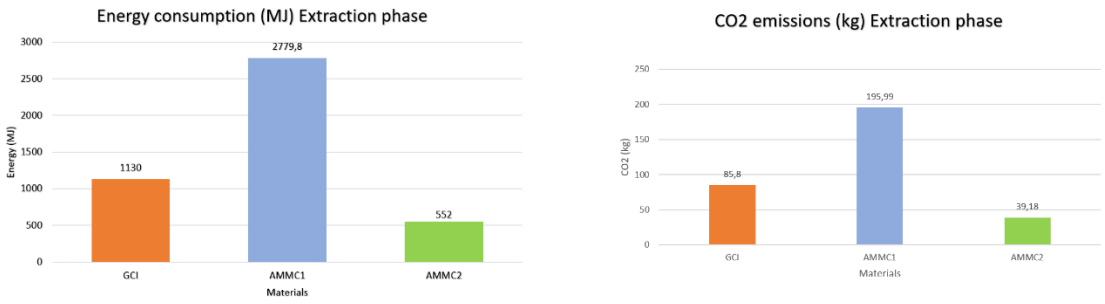

a) b)

Figure 51- Material extraction phase results: a) energy consumption (MJ), b) CO_2 emissions (kg). The graph uses data shown in table 27.

The difference between GCI and AMMC1 and AMMC2 is even more pronounced in the use phase. In this phase, parameters such as country of use and kilometers driven during the year using a medium-sized electric car were varied. Figure 52 shows the results of these analyses for different continents. It can be seen that GCI is the most disadvantaged in terms of both energy consumed and CO_2 emitted, again highlighting the benefits of AMMC1 and AMMC2. Speaking of energy consumed, it is important to observe the value assumed between the different countries, with Asia being the country with the most MJ consumed. As for CO_2 emitted, this also varies between countries of use, positioning America as the continent with the most CO_2 emitted. It should be noted that for the GCI, this is the phase that consumes the most energy and produces the most emissions, reaching more than 90 % of the energy consumed and more than 80 % of the emissions produced.

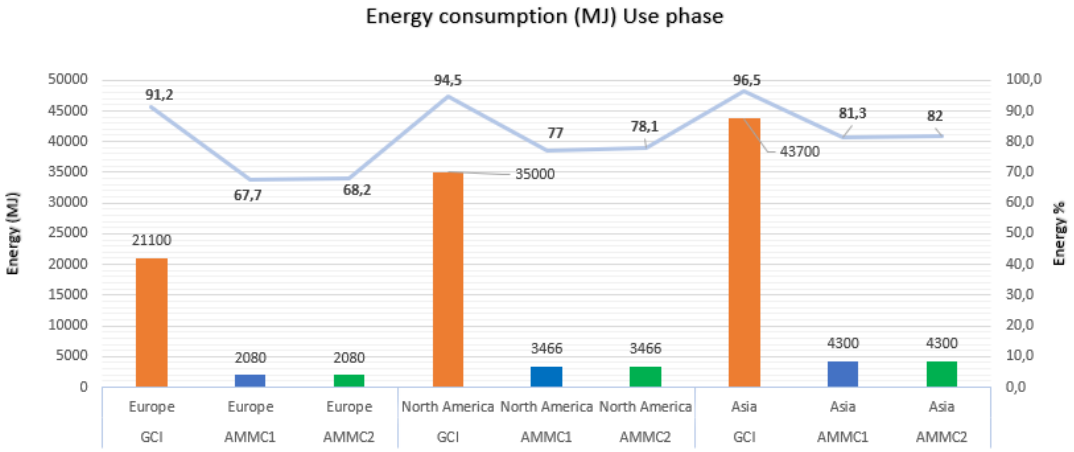

a)

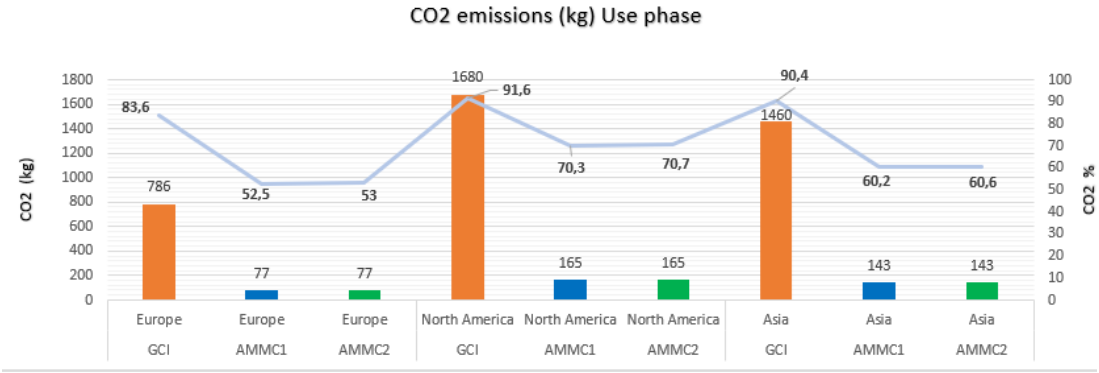

b)

Figure 52- Use phase results for different continents: a) energy consumption (MJ); b) CO_2 emissions (kg)

Analyses have shown that AMMC1 is only advantageous compared to GCI for the use phase. AMMC2, on the other hand, is suitable in terms of sustainability both in the use phase and also in the material extraction phase thanks to its fully recycled aluminium-based matrix. AMMC2 therefore proves to be the most suitable for brake production in terms of environmental impact. To reduce environmental impact, it is necessary to:

- Acting on the product's lifetime.
- Use a high percentage of recycled material to reduce the impact caused by the material extraction phase as much as possible.
- Decrease the mass by adopting lightweight design strategies to reduce the impact due to the use phase.

5. Conclusions

This chapter presents the conclusions of the thesis work, summarising the results obtained and comparing them with the literature.

- Roughness: Changing from 50 N to 108 N load did not change the roughness behavior of the AMMC1. In both cases, the BP pin decreased the roughness peaks by halving the values of both Sa and Ra. In the case of the GCI, there was a different behavior when switching to a higher load. With the 50 N test, there was a severe decrease in roughness and the BP pin decreased the roughness peaks. Going to 108 N, on the other hand, the BP pin dug into the material, especially in the central area of the GCI sample, thus causing a greater removal of material while keeping the roughness unchanged. Regarding AMMC2, on the other hand, this was only tested with a load of 108 N. This material exhibits the same behavior as AMMC1; after the test, the roughness was halved.
- Weight losses: By changing the load from 50 N to 108 N, the weight losses for AMMC1 decreased by an order of magnitude. This result is opposite to that reported by *Manikonda et al* [49]. In this case, weight losses increased as the load increased. The different percentages of SiC used for the experiments must be taken into account. For the experiments in this thesis, the volumetric fraction of SiC is 21 % while that used by Manikonda et al is 5 %. The different percentages of SiC could have influenced the different behavior of the weight losses. The situation is the opposite regarding the GCI. The increase in load led to an increase in weight losses. The increase in weight losses related to the increase in applied load is a phenomenon already found in the literature *Abdou et al* [51]. AMMC2, on the other hand, reports the same weight loss values as AMMC1, again showing that there are no particular differences between the two materials.
- Wear behavior: GCI and AMMC1 exhibited different types of wear. On the worn surface of the GCI for the 50 N test, parallel grooves can be seen, which indicate abrasive-type wear. In contrast, AMMC1 with the same load shows pits and voids at low magnifications (1000x magnification) and cracks at higher magnifications (8000x magnification). The presence of these elements indicates that delamination and abrasion wear have occurred. As reported by *Idusuyi et al* delamination wear is predominant at high loads but in the base alloy. A typical phenomenon is abrasive wear, which is found on the worn surface of materials [71]. The percentage of O detected using Pathfinder

software is higher on the worn surface of the GCI than that of the AMMC1. Surface oxidation was therefore one of the main wear mechanisms in the GCI in the mild wear regime, as also reported by *Riahi et al* [63]. By increasing the load, the same types of wear can be seen, but more pronounced. Particularly in the case of the AMMC1, the crack size was found to be larger with increasing load. The percentage of O for AMMC1 from 50 N to 108 N remained unchanged at around 14%, while for GCI it increased, remaining higher than for AMMC1 in both cases. AMMC2, on the other hand, showed smearing wear. The oxidation level is the same as AMMC1. Figure 53 shows the wear maps for the GCI* and AMMC. The red crosses indicate where the results obtained in this thesis work are located. In the case of the GCI, a mild wear regime is confirmed for both the 108 N and 50 N tests. Increasing the sliding speed would lead to severe wear. In the case of the AMMC, on the other hand, abrasive wear with even traces of delamination on the surface occurs as shown in the maps.

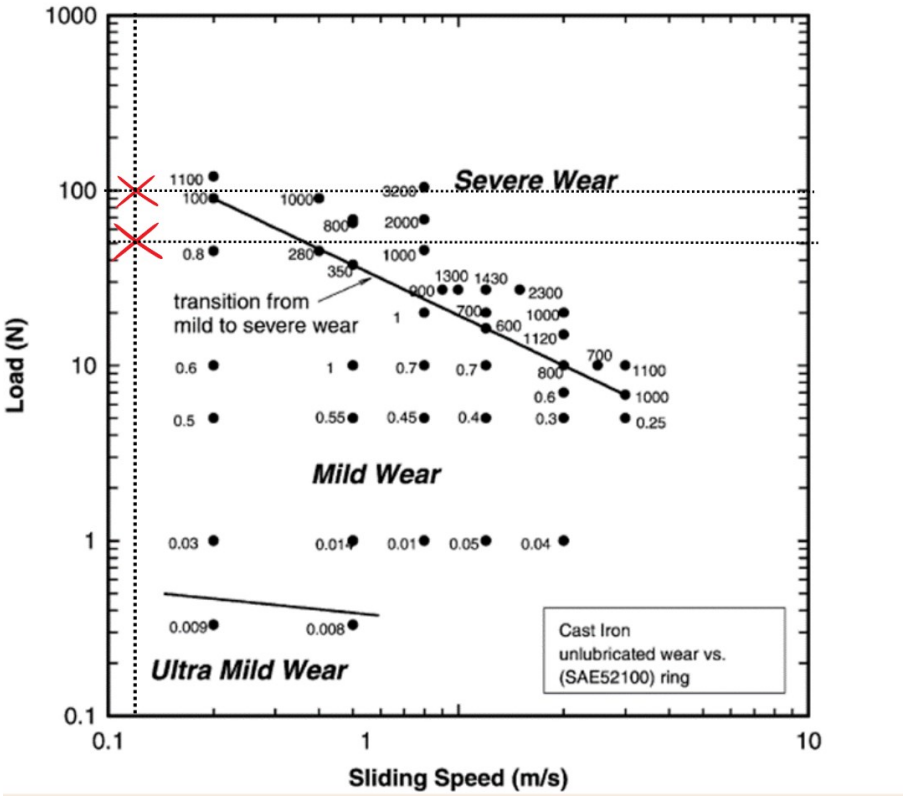

a)

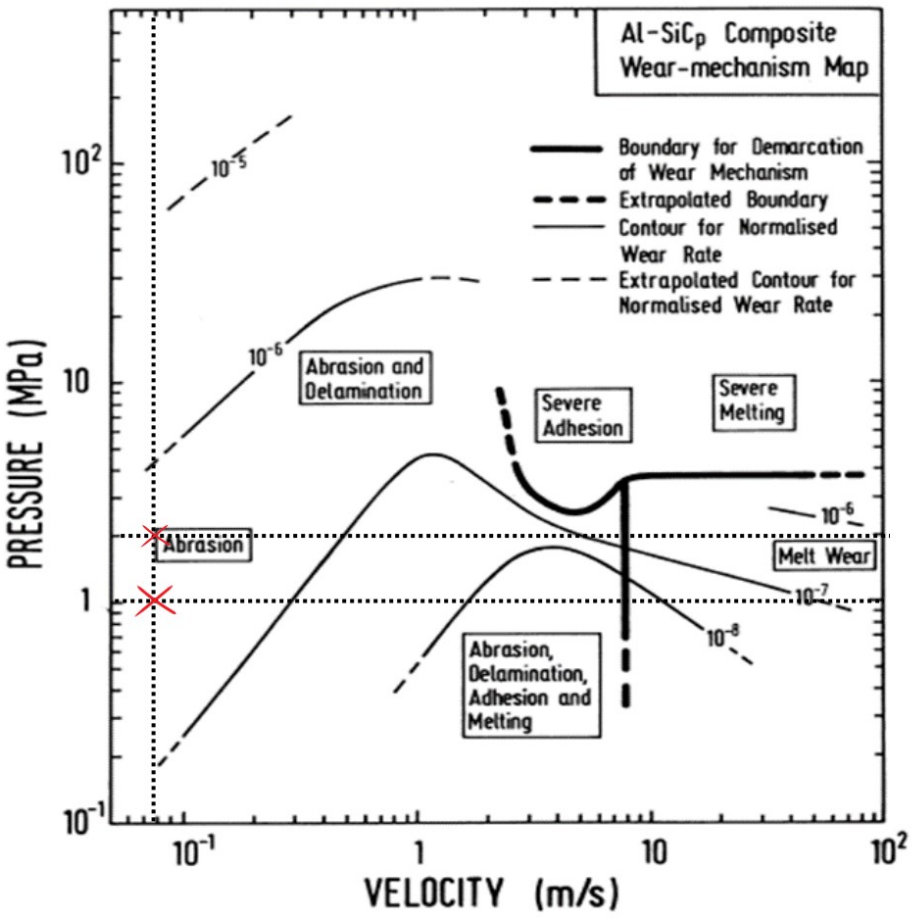

b)

Figure 53- Wear maps used for: a) GCI, b) AMMC. The red crosses in the maps indicate where the results of this thesis are located.

* In the case of the GCI, a sliding speed of 0.1 m/s was set, although a speed of 0.05 m/s was used in the thesis. This reason is related to the values assumed by the horizontal axis in the map.

- Material Transfer: At 50 N load, no material transfer occurred for both GCI and AMMC1. This phenomenon only occurred by increasing the load to 108 N. Both materials in this case show traces of Ba, Ca and S from the chemical composition of BP on the worn surface. Quantitative analysis using the Pathfinder software showed that the percentage of Ba and Ca present on the worn surface of the GCI is higher than that on the AMMC1. This may indicate that more material transfer occurred in the BP pin and GCI plate configuration rather than BP pin and AMMC1 plate. Concerning AMMC2, a strong presence of Ba can be seen on the worn surface trace. This strong presence could be

related to the change in configuration. In this case, BP as a plate and AMMC2 as a pin were used.

- Debris collected: The debris was only collected and analyzed using the 108 N test. The chemical composition of the debris is different for GCI and AMMC1. In the case of GCI, the debris is composed of elements that can be traced back to the BP pin such as Ca, Ba and Al, as well as elements belonging to the GCI such as C and Fe. In the case of AMMC1, on the other hand, the debris consists only of elements from the BP pin such as Ba, Cu, S, and Ca. This means that during the test, the BP pin was consumed the most with AMMC1, leaving the plate unmarked, whereas in the case of GCI, the plate was also consumed. This also confirms the fact that there was material removal in the case of the GCI.
- COF behavior: Increasing the load from 50 N to 108 N increases the COF of AMMC1, in contrast to *Manikonda et al* [49], who used a volumetric percentage of SiC of 5% as opposed to the 21% used in this thesis. It is important to note that in this thesis work, as the load increased, COF increased and weight losses decreased, in Manikonda's work, COF decreased but weight losses increased. The COF of the GCI for the 50 N test is higher than that of the AMMC1, showing that the friction force exerted against the GCI is higher. By increasing the load, the COF of the GCI increases as also reported by *Cueva et al* [50] The COF of the AMMC2 is slightly lower than that of the AMMC1.
- Specific wear rate: At 50 N, the specific wear rate for the GCI and AMMC1 is very similar. The value of the specific wear rate of the GCI appears to be an order of magnitude higher than that reported by *Dizdar et al* with 0,6 MPa as applied pressure, and 2 m/s as sliding speed for a total sliding distance of 14400 m [45]. As the load increases, however, the specific wear rate of the GCI increases as a direct consequence of weight losses increase as reported by *Abdou et al* [51]; while that of the AMMC1 decreases significantly. At 50 N, AMMC1 exhibits a specific wear rate of the same order of magnitude as reported by [72] with a volumetric reinforcement rate of 10 % and a test duration of 10 minutes. At high loads, the wear rate is milder for the AMMC1 than for the GCI.
- Energy consumption and CO_2 emissions: The analysis with Granta software highlighted the energy loads used for the production of disc brakes. AMMC1 is more suitable than GCI for the use phase, while for the material extraction phase, AMMC1 has higher values for energy consumption and emissions compared to GCI. AMMC2, on the other hand, proves to be the best material for both the use phase and the material extraction phase due to the high use of recycled material. The extraction phase consists only of the production of SiC

particles. The phases with the least consumption were manufacture, transport, and disposal.

6. Future work

This chapter briefly mentions elements that may be useful for future work. These elements derive from the section in Chapter 2 'Delimitations and Problems' and the experience acquired during the experimental part.

- Changing the duration test: In this thesis work, a duration of 1 h was set for the test. It may be useful to increase the test duration by performing longer tests. Increasing the duration also increases the sliding distance, which influences the special wear rate (K), as shown in Equation 5. At a fixed sliding velocity, the wear rate increased linearly as the sliding distance increased. The clustering of the reinforcing SiC particles and non-uniform blending with the aluminium matrix was said to have been the reason for this trend [73]. Previous tests with Pin-on-Plate configuration were carried out with a total duration of 4 hours.
- Focus on brake pad: This thesis work focuses only on the study of disc brake wear, and the wear behavior of brake pads is not analyzed. The only analysis conducted concerns the material transfer that occurred between the plate and the pin. For future analysis, the type of wear occurring in brake pads should also be investigated to obtain a more complete analysis of the wear mechanisms for the disc and pad apparatus.
- High-temperature tests: It would be appropriate for future analysis to investigate the behavior at high temperatures during wear tests. Increasing the operating temperature may lead to different wear mechanisms. In addition, working with high temperatures would represent an operating situation more similar to the real situation. A possible temperature to perform wear tests can be 420 °C. This is the maximum operable temperature for reference materials, which the disc manufacturer AC Floby tested. After this temperature, disc brakes no longer exhibit the optimal braking characteristics required.
- Focus on all types of electric vehicles: As stated in Chapter 2 "Delimitations and Problems", the thesis focuses on the LCA study on medium-sized electric vehicles, as they are estimated to be the first to enter the market. An analysis could also be conducted on heavy-size vehicles by studying the wear behavior of brakes and conducting an LCA analysis as done in this thesis work for medium-size vehicles.

7. References

[1] S. A. Awe, "Developing Material Requirements for Automotive Brake Disc", doi: 10.33552/MCMS.2020.02.000531.

[2] "What Are the Main Parts of a Braking System? | Firestone Complete Auto Care." Accessed: Apr. 12, 2023. [Online]. Available: https://www.firestonecompleteautocare.com/blog/brakes/parts-of-the-braking-system/#

[3] S. N. Nagesh, C. Siddaraju, S. V. Prakash, and M. R. Ramesh, "Characterization of Brake Pads by Variation in Composition of Friction Materials," *Procedia Materials Science*, vol. 5, pp. 295–302, 2014, doi: 10.1016/j.mspro.2014.07.270.

[4] "Drum Brakes | Brakes for Automobiles | Product | Products and Technologies | Akebono Brake Industry Co., Ltd." Accessed: Oct. 12, 2023. [Online]. Available: https://www.akebono-brake.com/english/product_technology/product/automotive/drum/

[5] "Drum brake components and parts." Accessed: Apr. 12, 2023. [Online]. Available: https://blog.frenkit.es/en/drum-brake-parts-and-elements

[6] "When to replace brake discs and pads | CHAMPION." Accessed: Oct. 12, 2023. [Online]. Available: https://www.championautoparts.com/en-gb/news/when-to-replace-brake-pads-discs.html

[7] "How Do Brake Discs Work? | MAT Foundry Group." Accessed: Apr. 13, 2023. [Online]. Available: https://www.matfoundrygroup.com/blog/how-do-brake-discs-work

[8] "Slotted vs Drilled vs Vented Rotors - What's The Difference? | BuyBrakes Blog." Accessed: Apr. 13, 2023. [Online]. Available: https://www.buybrakes.com/help/slotted-drilled-vented-rotor-differences/

[9] "Cast iron | Definition, Composition, History, & Facts | Britannica." Accessed: Apr. 12, 2023. [Online]. Available: https://www.britannica.com/technology/cast-iron

[10] Prof. R. K. Pohane, Dr. S. C. Kongare, and Prof. S. P. Daf, "Mechanical Property Which Affect the Performance of Disk Brake Material," *International Journal of Engineering Research & Technology*, vol. 4, no. 30, Apr. 2018, doi: 10.17577/IJERTCONV4IS30076.

[11] "Frenata rigenerativa: come funziona il recupero di energia in frenata." Accessed: Apr. 16, 2023. [Online]. Available: https://www.partsweb.it/la-frenata-rigenerativa-spiegata-da-delphi-technologies/

[12] "Brakes - Mech Content." Accessed: Oct. 12, 2023. [Online]. Available: https://mechcontent.com/category/brakes/?utm_content=cmp-true

[13] "Aluminum and Aluminum Alloys Introduction and Overview," 2001, doi: 10.1361/autb2001p351.

[14] "7 Things to Consider When Choosing an Aluminum Grade | Metal Supermarkets." Accessed: Oct. 12, 2023. [Online]. Available: https://www.metalsupermarkets.com/7-things-consider-choosing-aluminum-grade/

[15] P. T. Tang, J. Fugl, L. Uriarte, G. Bissacco, and H. N. Hansen, "Indirect tooling based on micromilling, electroforming and selective etching," *4M 2006 - Second International Conference on Multi-Material Micro Manufacture*, pp. 183–186, 2006, doi: 10.1016/B978-008045263-0/50042-8.

[16] O. S. I. Fayomi, P. A. L. Anawe, and A. Daniyan, "The Impact of Drugs as Corrosion Inhibitors on Aluminum Alloy in Coastal-Acidified Medium," *Corrosion Inhibitors, Principles and Recent Applications*, Apr. 2018, doi: 10.5772/INTECHOPEN.72942.

[17] "Megatrend / Trend / Driver / Issue – European Foresight Platform." Accessed: Apr. 16, 2023. [Online]. Available: http://foresight-platform.eu/community/forlearn/how-to-do-foresight/methods/analysis/megatrend-trend-driver-issue/

[18] "Alternative Fuels Data Center: Electric Vehicle (EV) Definition." Accessed: Apr. 16, 2023. [Online]. Available: https://afdc.energy.gov/laws/12660

[19] M. Kah, S. Lang, J. Chiu, and H. X. Wong, “FORECASTS OF ELECTRIC VEHICLE PENETRATION AND ITS IMPACT ON GLOBAL OIL DEMAND,” 2022. [Online]. Available: www.sipa.columbia.edu
[20] “Electric Vehicles: Market Data Analysis & Forecast INDUSTRIES & MARKETS,” 2022.
[21] “Aluminum Market Size, Growth Report, Trends, 2022-2030.” Accessed: Apr. 19, 2023. [Online]. Available: https://www.precedenceresearch.com/aluminum-market
[22] “Secondary Aluminum Alloy Market Size, Share And Future Insight, 2021-230.” Accessed: Apr. 19, 2023. [Online]. Available: https://www.researchnester.com/reports/secondary-aluminum-alloy-market/3578
[23] “Euro 1 to Euro 6 – find out your vehicle’s emissions standard | RAC Drive.” Accessed: Apr. 16, 2023. [Online]. Available: https://www.rac.co.uk/drive/advice/emissions/euro-emissions-standards/
[24] “Normativa Euro 7: quando entra in vigore e cosa prev - Rattix - Ratti Auto.” Accessed: Apr. 16, 2023. [Online]. Available: https://www.rattiauto.it/it-it/blog/automotive/normativa-auto-euro-7
[25] “Euro 7: cosa vuol dire, normativa, diesel, quando entrerà in vigore.” Accessed: Apr. 16, 2023. [Online]. Available: https://www.quotidianomotori.com/automobili/euro-7-emissioni-auto/
[26] “Emissions in the automotive sector.” Accessed: Apr. 16, 2023. [Online]. Available: https://single-market-economy.ec.europa.eu/sectors/automotive-industry/environmental-protection/emissions-automotive-sector_it
[27] “Circular economy: definition, importance and benefits | News | European Parliament.” Accessed: Apr. 16, 2023. [Online]. Available: https://www.europarl.europa.eu/news/en/headlines/economy/20151201STO05603/circular-economy-definition-importance-and-benefits
[28] “Circular economy: definition, importance and benefits | News | European Parliament.” Accessed: Apr. 16, 2023. [Online]. Available: https://www.europarl.europa.eu/news/en/headlines/economy/20151201STO05603/circular-economy-definition-importance-and-benefits?&at_campaign=20234-Economy&at_medium=Google_Ads&at_platform=Search&at_creation=RSA&at_goal=TR_G&at_audience=circular%20economy&at_topic=Circular_Economy&at_location=SE&gclid=CjwKCAjwue6hBhBVEiwA9YTx8FCtoildwI9yR-d_4awGbURlqWbVW0q1lDjJCF5wG2tXu21kEcahoRoCKXkQAvD_BwE
[29] “Cast-Iron: Manufacture, Composition, Types, Properties and Uses | Engineering.” Accessed: Apr. 24, 2023. [Online]. Available: https://www.engineeringenotes.com/metallurgy/cast-iron/cast-iron-manufacture-composition-types-properties-and-uses-engineering/46725
[30] “cast-iron-we-just-need-to-get-better-at-telling-our-story”.
[31] H. Fidvi and A. Langde, “Relevance of Using Cupola Furnace in Current Scenario of Technological Advancements,” *Int J Sci Res Sci Technol*, 2018, doi: 10.32628/NCAEAS4349.
[32] “Machinability study on GCI brake discs MASTER THESIS DIVISION OF PRODUCTION AND MATERIALS ENGINEERING DEPARTMENT OF MECHANICAL ENGINEERING.”
[33] “Distribution map of global bauxite resource reserves in 2020. (He 2015) | Download Scientific Diagram.” Accessed: Oct. 12, 2023. [Online]. Available: https://www.researchgate.net/figure/Distribution-map-of-global-bauxite-resource-reserves-in-2020He-2015_fig1_359476933
[34] “How aluminium is produced.” Accessed: Apr. 22, 2023. [Online]. Available: https://www.aluminiumleader.com/production/how_aluminium_is_produced/
[35] W. Tang, M. Khavarian, and A. Yousefi, “Red Mud,” *Sustainable Concrete Made with Ashes and Dust from Different Sources: Materials, Properties and Applications*, pp. 577–606, Jan. 2022, doi: 10.1016/B978-0-12-824050-2.00013-9.

[36] Y. Yao and J. Bao, “State and Parameter Estimation in Hall-Héroult Cells using Iterated Extended Kalman Filter∗,” Elsevier B.V., Jan. 2018, pp. 36–41. doi: 10.1016/j.ifacol.2018.09.389.
[37] E. Balomenos, D. Panias, and B. Friedrich, “Carbothermic reduction of alumina: A review of developed processes and novel concepts Certificates of Achievements, Accomplishments and Awards View project ecoLiga-Recycling and resynthesis of carbon materials from lithium batteries: Recovery, processing, reuse and adapted cell design View project,” 2011. [Online]. Available: https://www.researchgate.net/publication/234107917
[38] W. T. Choate and B. A. Incorporated John S Green, “U.S. Energy Requirements for Aluminum Production Historical Perspective, Theoretical Limits and Current Practices,” 2007.
[39] “Sustainability – Recycling | Aluminum Association.” Accessed: Apr. 19, 2023. [Online]. Available: https://www.aluminum.org/Recycling
[40] W. Wei, “Energy Consumption and Carbon Footprint of Secondary Aluminum Cast House Master Thesis.”
[41] “Tribology Testing Services| Friction and Wear| Mechaction.” Accessed: Oct. 12, 2023. [Online]. Available: https://www.mechaction.com/friction-and-wear
[42] “Sa (Arithmetical Mean Height) | Area Roughness Parameters | Introduction To Roughness | KEYENCE America.” Accessed: Jul. 23, 2023. [Online]. Available: https://www.keyence.com/ss/products/microscope/roughness/surface/parameters.jsp
[43] “Average Roughness basics - Michigan Metrology.” Accessed: Jul. 23, 2023. [Online]. Available: https://michmet.com/average-roughness-basics/
[44] “09636935130220040 1”.
[45] S. Dizdar, Y. Lyu, C. Lampa, and U. Olofsson, “Grey Cast iron brake discs laser cladded with nickel-tungsten carbide-Friction, wear and airborne wear particle emission,” *Atmosphere (Basel)*, vol. 11, no. 6, Jun. 2020, doi: 10.3390/atmos11060621.
[46] F. Bonollo, L. Giordano, A. Tiziani, and A. Zambon, “A study on wear Behaviour of Al- Matrix Composites,” Padova.
[47] F. Bonollo and A. Tiziani, “Evaluation of microstructural homogeneity in Aluminiu-matrix composites”.
[48] A. Mazahery and M. O. Shabani, “Microstructural and abrasive wear properties of SiC reinforced aluminum-based composite produced by compocasting,” *Transactions of Nonferrous Metals Society of China (English Edition)*, vol. 23, no. 7, pp. 1905–1914, Jul. 2013, doi: 10.1016/S1003-6326(13)62676-X.
[49] R. Deepika Manikonda, S. Kosaraju, and A. Raj, “Wear Behavior Analysis of Silica Carbide Based Aluminum Metal Matrix Composites,” 2018. [Online]. Available: www.sciencedirect.comwww.materialstoday.com/proceedings2214-7853
[50] G. Cueva, A. Sinatora, W. L. Guesser, and A. P. Tschiptschin, “Wear resistance of cast irons used in brake disc rotors,” *Wear*, vol. 255, no. 7–12, pp. 1256–1260, 2003, doi: 10.1016/S0043-1648(03)00146-7.
[51] S. Abdou, A. Elkaseer, H. Kouta, and J. Abu Qudeiri, “Wear behaviour of grey cast iron with the presence of copper addition,” *Advances in Mechanical Engineering*, vol. 10, no. 10, Oct. 2018, doi: 10.1177/1687814018804741.
[52] “What is a Composite Material? (A Definitive Guide) - TWI.” Accessed: Apr. 21, 2023. [Online]. Available: https://www.twi-global.com/technical-knowledge/faqs/what-is-a-composite-material
[53] F. Nturanabo, L. Masu, and J. B. Kirabira, “Novel Applications of Aluminium Metal Matrix Composites.” [Online]. Available: www.intechopen.com
[54] P. Chakrapani and T. S. A. Suryakumari, “Mechanical properties of aluminium metal matrix composites-A review,” in *Materials Today: Proceedings*, Elsevier Ltd, 2020, pp. 5960–5964. doi: 10.1016/j.matpr.2020.09.247.
[55] P. S. Reddy, R. Kesavan, and B. Vijaya Ramnath, “Investigation of Mechanical Properties of Aluminium 6061-Silicon Carbide, Boron Carbide Metal Matrix Composite,” *Silicon*, vol. 10, no. 2, pp. 495–502, Mar. 2018, doi: 10.1007/s12633-016-9479-8.

[56] F. Bonollo, L. Ceschini, L. Garagnani, G. Palombarini, and A. Zambon, “Discontinuosly reinforced aluminium composites sliding against steel: study on wear behaviour ”.
[57] P. Yadav, A. Ranjan, H. Kumar, A. Mishra, and J. Yoon, “A contemporary review of aluminium mmc developed through stir-casting route,” *Materials*, vol. 14, no. 21. MDPI, Nov. 01, 2021. doi: 10.3390/ma14216386.
[58] A. Karthik, R. Karunanithi, A. S. Selvakumar, and S. A. Srinivasan, “The Impact of Squeeze Casting in AMMC—Review,” in *Lecture Notes in Mechanical Engineering*, Springer Science and Business Media Deutschland GmbH, 2021, pp. 253–259. doi: 10.1007/978-981-33-6428-8_19.
[59] S. Senthil, M. Raguraman, and D. T. Manalan, “Manufacturing processes & recent applications of aluminium metal matrix composite materials: A review,” in *Materials Today: Proceedings*, Elsevier Ltd, 2020, pp. 5934–5938. doi: 10.1016/j.matpr.2020.08.792.
[60] A. Devaraju, “Article ID: IJMET_06_11_009 Cite this Article: Dr. A. Devaraju. A Critical Review on Different Types of Wear of Materials,” *International Journal of Mechanical Engineering and Technology*, vol. 6, no. 11, pp. 77–83, 2015, [Online]. Available: http://www.iaeme.com/IJMET/index.asp77http://www.iaeme.com/IJMET/issues.asp?JType=IJMET&VType=6&IType=11http://www.iaeme.com/currentissue.asp?JType=IJMET&VType=6&IType=11
[61] S. Wilson and A. T. Alpas, “WEAR Wear mechanism maps for metal matrix composites,” 1997.
[62] A. Misra and I. Finnie, “SOME OBSERVATIONS ON TWO-BODY ABRASIVE,” Elsevier Sequoia S.A, 1981.
[63] A. R. Riahi and A. T. Alpas, “Wear map for grey cast iron,” *Wear*, vol. 255, no. 1–6, pp. 401–409, 2003, doi: 10.1016/S0043-1648(03)00100-5.
[64] S. C. Lim, “Recent developments in wear-mechanism maps,” 1998.
[65] “life cycle assessment — European Environment Agency.” Accessed: Apr. 20, 2023. [Online]. Available: https://www.eea.europa.eu/help/glossary/eea-glossary/life-cycle-assessment
[66] “An Introduction to LCA methods by.” [Online]. Available: www.lightright.eu
[67] “Life Cycle Assessment Best Practices of ISO 14040 Series Ministry of Commerce, Industry and Energy Republic of Korea Asia-Pacific Economic Cooperation Committee on Trade and Investment,” 2004.
[68] “Sa (arithmetical mean height) | Area Roughness Parameters | What is area roughness? | Solving the questions about profile and surface roughness measurements! Introduction to ‘Roughness’ | KEYENCE International Belgium.” Accessed: May 23, 2023. [Online]. Available: https://www.keyence.eu/ss/products/microscope/roughness/surface/parameters.jsp
[69] I. R. Sola, “Meccanica dei materiali compositi.”
[70] “Barite for Brake Linings | Başer Mining.” Accessed: Sep. 02, 2023. [Online]. Available: https://basermining.com/products/friction
[71] N. Idusuyi and J. I. Olayinka, “Dry sliding wear characteristics of aluminium metal matrix composites: A brief overview,” *Journal of Materials Research and Technology*, vol. 8, no. 3. Elsevier Editora Ltda, pp. 3338–3346, May 01, 2019. doi: 10.1016/j.jmrt.2019.04.017.
[72] K. K. Singh, S. Singh, and A. K. Shrivastava, “Study of Tribological Behavior of Silicon Carbide Based Aluminum Metal Matrix Composites under Dry and Lubricated Environment,” *Advances in Materials Science and Engineering*, vol. 2016, 2016, doi: 10.1155/2016/3813412.
[73] M. Singla, L. Singh, and V. Chawla, “Study of Wear Properties of Al-SiC Composites,” 2009.

ha formattat

ha formattat